CR 151337

THE UNIVERSITY OF TEXAS AT AUSTIN

EFFECTS OF SURFACE COOLING AND OF ROUGHNESS ON THE HEATING (INCLUDING TRANSITION) TO THE WINDWARD PLANE-OF-SYMMETRY OF THE SHUTTLE ORBITER

John J. Bertin, Ed S. Idar, III, and
Stanley R. Galanski

Aerospace Engineering Report 77002

This work was supported by
the Johnson Space Center
through NASA Contract NAS 9-13680

April 1977

Department of Aerospace Engineering and Engineering Mechanics

EFFECTS OF SURFACE COOLING AND OF ROUGHNESS ON THE HEATING (INCLUDING TRANSITION) TO THE WINDWARD PLANE-OF-SYMMETRY OF THE SHUTTLE ORBITER*

by John J. Bertin, Ed S. Idar, III, and
Stanley R. Galanski

Aerospace Engineering Report 77002

*This work was supported
by the Johnson Space Center
through Contract NAS 9-13680

Department of Aerospace Engineering and
Engineering Mechanics

The University of Texas at Austin

April 1977

ACKNOWLEDGEMENTS

This research was supported by the Johnson Space Center (NASA) through contract NAS 9-13680. The authors acknowledge the considerable efforts of Dr. W. D. Goodrich in providing technical assistance and guidance to the effort. The authors would also like to thank Mrs. Pat Kleinert for cheerfully typing the numerous drafts of the manuscript.

TABLE OF CONTENTS

INTRODUCTION

In order to predict the convective heat-transfer distribution for the windward surface of the Space Shuttle entry configuration, one must develop engineering correlations for the three-dimensional, compressible boundary-layer. Since the aerodynamic heating rates generated by a turbulent boundary-layer may be several times greater than those for a laminar boundary-layer at the same flight condition, the correlations must include a transition criteria suitable for the complex flow fields. Because the windward surface of the Orbiter is composed of a large number of thermal protection tiles, the transition criteria must include the effect of the distributed roughness arising from the joints and possible tile misalignment.

During tests in which a ring of spherical roughness elements were located in a supersonic flow past a cone, Van Driest and Blumer (ref. 1) observed variations in the relative roles played by the disturbances in the basic flow field and those resulting from the presence of roughness elements. For some conditions, the disturbances associated with the basic flow field were predominant in establishing transition, whereas for other flows, the roughness elements dominated the transition process.

However, the correlation for the effect of roughness is complicated when other transition-related parameters interact. Morisette (ref. 2) found that although the effective roughness Reynolds number increases significantly in the presence of a favorable pressure gradient near the centerline, much smaller roughness was required to promote transition near the shoulder of an Orbiter configuration, where again there was a favorable pressure gradient (this one associated with cross flow). McCauley et al

(ref. 3) found that the spherical roughness elements required to trip the boundary layer on sphere noses were several times larger than the boundary-layer thickness, whereas the trips required for a cone were within the boundary layer. Heat-transfer data (ref. 4) obtained in Tunnel B of the Arnold Engineering Development Center (AEDC) for an 0.04-scale Orbiter indicated that a ring of spherical trips, which were 0.079 cm. (0.031 in.) in diameter and were 0.11L from the nose, caused the transition location to move considerably upstream of the natural transition location (i.e., that for a smooth body). In the same test program (ref. 4), a simulated interface gap between two insulation materials, which was 0.102 cm. (0.040 in.) wide by 0.203 cm. (0.080 in.) deep and was located at x = 0.02L, had no measurable effect on boundary-layer transition at $\alpha = 40°$ and $Re_{\infty,L} = 8.6 \times 10^6$. In a series of tests using delta-wing Orbiter models (ref. 5), premature boundary-layer transition was observed on a model having simulated heat-shield panels with raised joints. Slot joints, however, did not cause premature transition of the boundary layer. The former model featured a series of transverse panels 0.635 cm. (0.250 in.) wide separated by a raised retaining strip 0.025 cm. (0.010 in.) wide by 0.0025 cm. (0.001 in.) high. The panels on the model with slotted joints were 0.635 cm. (0.250 in.) square separated by slots 0.020 cm. (0.008 in.) wide by 0.005 cm. (0.002 in.) deep. The Reynolds number ($Re_{\infty,L}$) for these tests ranged from 6.5×10^6 to 9.0×10^6 using a model 0.403 m. (1.321 ft.) long.

The stability of laminar boundary-layers has been found to be significantly affected by heating or by cooling (usually indicated parametrically by a temperature ratio, or enthalpy ratio, such as T_w/T_r or T_w/T_e). Lees (ref. 6) found that heat-transfer from the fluid to the wall

stabilized a laminar boundary layer for two-dimensional disturbances and that, if there is a sufficient amount of cooling, the boundary layer on a hydrodynamically, smooth configuration could be completely stabilized. Reshotko (ref. 7) presents data supporting the trend toward complete stabilization. Using the flight data of Rumsey and Lee (ref. 8), Reshotko observed that, for conditions outside the predicted region of complete stabilization, transition did occur (as expected), but at relatively high Reynolds numbers.

However, the unqualified prediction that cooling stabilizes the boundary layer cannot be made since transition reversal has been observed by numerous workers as the model is "cooled" (e.g., refs. 9 and 10). As a result of cooling the boundary layer, there is a relative increase in the magnitude of the disturbance due to a fixed roughness (ref. 11). A further complication is associated with wind tunnel data. Since a low value of T_w/T_r may be obtained either by cooling the wall or by heating the test gas, alternative effects may arise. Using data from a single tunnel, Wagner et al (ref. 12) noted that reducing T_w/T_r by heating the flow significantly decreased $Re_{s,tr}$, possibly because of nonuniform mixing of the supply gas in the stagnation chamber.

Data from an experimental program which was conducted to investigate what effect tile misalignment representative of a reasonable manufacturing tolerance has on heat transfer and transition criteria in the plane-of-symmetry of the Shuttle Orbiter have been analyzed (e.g., ref. 13). The vertical tile misalignment simulated on the 0.0175-scale model was approximately 0.1451 cm. (0.0571 in.) full-scale. Furthermore, the surface temperature for the Tunnel B tests was essentially constant at $0.42T_t$. As

noted in ref. 13, the presence of tile misalignment did not significantly affect the transition locations over the range of test conditions considered. Another test program was conducted in Tunnel F where the windward surface was roughened by a grit blasting technique. The surface temperature for the Tunnel F tests varied from $0.14T_t$ to $0.28T_t$. At the higher Reynolds numbers of the Tunnel F tests, the transition location moved near the nose. The roughness elements became large relative to the boundary layer and became effective as tripping elements. However, there were not sufficient parametric variations to establish suitable correlations.

The present report presents calculations which indicate the effect that variations in the flow-field model would have on correlation of wind-tunnel data. The theoretical heat-transfer distributions are compared with experimental heat-transfer distributions obtained in Tunnel B at the Arnold Engineering Development Center (AEDC) using a 0.0175 scale model of the Space Shuttle Orbiter Configuration for which the first 80% of the windward surface was roughened by a simulated tile misalignment. The experimental heat-transfer data were used to determine the transition locations. Data were obtained for a Mach number of 8 over a Reynolds number range (based on model length) from 1.862×10^6 to 7.091×10^6 with surface temperatures from $0.114T_t$ to $0.435T_t$. with tile-misalignment heights of 0.0025 cm. (0.0010 in.) and of 0.0051 cm. (0.0020 in.).

NOMENCLATURE

C_p	pressure coefficient (eqn 1); or specific heat for a constant pressure process (eqn 2)
h	metric scale-factor used to represent the radius of an equivalent body-of-revolution (see Fig. 7); or the local heat transfer coefficient, $\dot{q}/(T_r-T_w)$
H	stagnation enthalpy
$h_{t,ref}$	heat-transfer coefficient for the stagnation point of the reference sphere
k	height of the misaligned tiles
L	axial model length, 0.5734 m. (1.881 ft)
M	Mach number
p	local static pressure
$\dot{q}$	local heat-transfer rate
R	gas constant
r_{ref}	radius of the reference sphere, 0.00533 m. (0.0175 ft.)
Re_{ns}	Reynolds number based on flow conditions behind a normal shock (eqn 6)
Re_s	Reynolds number based on local flow properties integrated along the wetted distance along a streamline (eqn 4)
Re_θ	Reynolds number based on local flow properties and the momentum thickness
$Re_{\infty,L}$	Reynolds number based on free-stream flow properties and the model length (eqn 5)
s	entropy (eqn 2); or wetted distance along a streamline (eqn 4)

T	temperature
T_{init}	temperature used in correlation of transition location (see eqn 14b)
T_r	recovery temperature
U	streamwise component of the velocity
x	axial coordinate
y	coordinate measured normal to the model surface
α	angle of attack
δ^*	displacement thickness
θ	momentum thickness
μ	viscosity
ρ	density
ξ_1	relative transition location defined in eqn 17
ξ_2	relative transition location defined in eqn 18

Subscripts

e	evaluated at the edge of the boundary layer
i	evaluated at the particular run of interest (see eqn 17)
ns	evaluated downstream of a normal shock wave
tr	evaluated at the transition location
w	evaluated at the wall
∞	evaluated at the free-stream conditions

EXPERIMENTAL PROGRAM

A primary objective of the present investigation was to determine what effect tile misalignment representative of a reasonable manufacturing tolerance has on the heat-transfer distribution in the plane of symmetry of the Shuttle Orbiter. To do this, the heat-transfer data from three test programs conducted in Tunnel B of the AEDC were studied. The data were obtained at a free-stream Mach number of 8 over a range of free-stream Reynolds number (based on model length) from 1.862×10^6 to 7.091×10^6. The surface temperature was varied from $0.114T_t$ to $0.435T_t$. The data presented in the present report were obtained at angles-of-attack of 30° and 40°. The test conditions for these data are summarized in Table 1.

Models

The basic model used in the test programs (see the sketch of Fig. 1) was a 0.0175-scale model of the Space Shuttle configuration defined by Rockwell drawing VL70-000139 and designated Model 29-0. Twenty seven coaxial surface thermocouples were used to obtain the heat-transfer-rate distribution for the windward plane-of-symmetry. The locations of the heat-transfer gages in the windward plane-of-symmetry are indicated in Fig. 1. To study the effect of tile misalignment, selected tiles were precisely etched (or deposited, as discussed in ref. 14, depending on the misalignment height) on the windward surface, so that they were slightly above the model surface. The misaligned tiles formed a herringbone pattern (symmetric about the plane of symmetry) covering the windward surface of the Orbiter model up to the tangent line of the chines from x = 0.02L to 0.80L. The raised tiles, which were selected randomly, represented 25% of the tiles in the area of interest, as shown in the photograph of Fig. 2. The selected tiles were 0.267 cm. (0.105 in.) square. The model surface for each of the three test programs is summarized below.

OH4A test program. - For the OH4A tests, the surface of the 0.0175-scale Orbiter model was smooth. Thus, the transition locations determined from the heat-transfer distributions serve as the reference, or smooth-body, transition locations. The reader is referred to ref. 15 for the basic data and for additional information regarding these tests.

MH2A test program. - For the MH2A tests, the misaligned tiles were deposited to a height of approximately 0.0025 cm. (0.0010 in.). The vertical misalignment, thus simulated, was 0.1451 cm. (0.0571 in.) full-scale. Thus, the nondimensionalized tile height (k/L) for this model was 4.43×10^{-5}. The basic data for this tile misalignment height (designated k_1 in the present report) are presented in ref. 16. An analysis of the heat-transfer data and the transition locations was presented in ref. 13.

MH2B test program. - For the MH2B tests, the surface surrounding the tiles was removed until the misaligned tiles were approximately 0.0051 cm. (0.0020 in.) in height. This misalignment, which is designated k_2 in the present report, corresponds to a full-scale vertical misalignment of 0.2903 cm. (0.1143 in.). For the k_2 misalignment, k was 8.86×10^{-5}L. Additional information about the model and the basic data for the MH2B test program is presented in ref. 17.

THEORETICAL FLOW FIELDS

Theoretical solutions for a nonsimilar, laminar boundary-layer were generated for the pitch plane of the Orbiter model at angles-of-attack of 30° and of 40°. These theoretical boundary-layer solutions were computed using a modified version of the code described in ref. 18. Required as input for the code are the flow conditions at the edge of the boundary layer, the radius of the "equivalent" body-of-revolution, and the wall-temperature distribution. The metric scale-factor describing the streamline divergence was used to represent the radius of the equivalent body-of-revolution in the axisymmetric analogue for a three-dimensional boundary-layer. Two different flow-field models were used to generate the required inviscid solution for the plane of symmetry. The pressure distribution and the streamline-divergence characteristics for the first flow model, designated "Mod-Newt NSE", represent modified Newtonian flow. For this flow model, it was assumed that the fluid at the edge of the boundary layer was that which had passed through the normal portion of the bow shock wave and had accelerated isentropically from the stagnation point to the local static pressure which was defined by:

$$C_p = C_{p_t} \sin^2 \theta \qquad (1)$$

The streamwise distributions of the static pressure, of the entropy at the edge of the boundary-layer, and of the cross-sectional radius for the equivalent body-of-revolution for the second flow model, designated "Var Ent", were computed using the code described in ref. 19. Because the bow shock-wave is curved, the entropy varies throughout the shock layer (the magnitude of the entropy change across the shock wave depending upon the

free-stream Mach number). The entropy at the edge of the boundary layer depends not only on the streamwise location but on the local boundary-layer thickness and, hence, on the Reynolds number. However, the variation of the local entropy at the edge of the boundary layer due to the variations in the boundary-layer thickness was believed to be of second order importance for the present study. Therefore, the local entropy was assumed to be that obtained in the theoretical solution for $Re_{\infty,L} \approx 1.9 \times 10^6$ at the Orbiter surface.

Surface static-pressure distributions for the plane of symmetry are presented in Fig. 3. For $\alpha = 30°$, the theoretical distributions for the two flow models are compared with the experimental pressures presented in ref. 20. The theoretical values for the "Var Ent" flow model are in very good agreement with the experimental values. The theoretical pressures for the "Mod-Newt NSE" are significantly below the experimental values.

Once the local static pressure and the local entropy have been defined, the local Mach number at the edge of the boundary layer can be calculated using the following relations:

$$\frac{T_e}{T_t} = \exp\left\{\frac{1}{C_p}\left[(s_e - s_{t2}) + R \ln \frac{p}{p_{t2}}\right]\right\} \tag{2}$$

$$U_e = \sqrt{2 H_e \left(1 - \frac{T_e}{T_t}\right)} \tag{3}$$

Note, that in all calculations, the air has been assumed to behave as a perfect gas. The Mach number distributions presented in Fig. 4 clearly indicate that the "Var Ent" flow model provides a more realistic representation of the actual flow field than does the "Mod-Newt NSE" model Although experimental values were not available for $\alpha = 40°$, extrapolation of the data for $\alpha = 30°$ and for $\alpha = 35°$ indicates that the "Var Ent" flow model should pro-

vide a reasonable representation of the actual flow field at an angle-of-attack of 40°.

The Mach number distribution across the laminar boundary-layer is presented in Fig. 5. The theoretical distribution obtained using the University's NONSIMBL code is in excellent agreement with that obtained using the BLIMP code as calculated by Goodrich et al (e.g., refer to ref. 19). Experimental values of the Mach number which were obtained at similiar test conditions (ref. 21) are included for comparison. The experimental values are in fair agreement with the two sets of theoretical calculations.

Streamwise distributions of the theoretical value of the Reynolds number at the edge of the boundary layer are presented in Fig. 6. The local values of Re_s, where

$$Re_s = \int_0^s \frac{\rho_e U_e}{\mu_e} ds \tag{4}$$

have been divided by the free-stream Reynolds number based on model length. The local Reynolds numbers were calculated using the local entropy distribution for the "inviscid" flow-field for $Re_{\infty,L} = 1.9 \times 10^6$. Since the entropy is evaluated at the edge of the local boundary layer, which is a function of the free-stream conditions, the value of the local entropy would also depend on $Re_{\infty,L}$. If we had accounted for the entropy variation normal to the surface, the nondimensionalized Reynolds number at the edge of the boundary layer would have depended on the free-stream Reynolds number. This Reynolds-number effect was neglected for the purposes of the present report. Note that the local Reynolds number which was calculated using the Var Ent flow model is roughly twice the corresponding value for the Mod-Newt NSE flow model (refer to Fig. 6a). Thus, both the local Mach number (refer to Fig. 4) and the

local Reynolds number are significantly greater for the Var Ent flow field model.

The metric which represent the cross-sectional radius of the equivalent body-of-revolution is presented as a function of the axial coordinate in Fig. 7. The metric coefficients were calculated using the relations described by De Jarnette (ref. 22) and by Rakich and Mateer (ref. 23). The streamlines near the plane of symmetry diverge much more rapidly for the Var Ent flow model.

With the exception of the Mach number profiles for a laminar boundary-layer which were presented in Fig. 5, the theoretical values presented thus far describe the inviscid flow field (specifically, conditions at the edge of the boundary layer). Since the streamwise distributions for the entropy at the edge of the boundary layer and for the static pressure were provided by Dr. W. D. Goodrich of the Johnson Space Center (JSC), NASA, one would expect that the values of parameters such as the edge Mach number generated using the NONSIMBL code would correlate well with the values calculated by others. Thus, to substantiate correlations based on the viscous portion of the code, the heat-transfer-rate distribution calculated using the University's NOMSIMBL code for one of the test conditions was compared with the distribution calculated at the JSC using the BLIMP code. As shown in Fig. 8, the rates calculated using the NONSIMBL code are within 15%, or less, of the values calculated using the BLIMP code.

The effect of surface temperature on the heat-transfer rates in the plane of symmetry is illustrated by the calculations presented in Fig. 9. The results are presented as the local heat-transfer coefficient divided by the heat-transfer coefficient for the stagnation point of a 0.00533 m. (0.0175 ft.) radius sphere as calculated using the theory of Fay and Riddell (ref.

24). For the present report, the recovery factor r has been set equal to unity. Distributions of the dimensionless heat-transfer-coefficient ratio, $h/h_{t,ref}$, are presented for each of the flow models for the extreme values of wall temperature covered in the experimental program. For each case, the surface temperature was assumed to be constant along the entire length of the model. For each of the three flow models, the nondimensionalized heating was slightly greater for the colder surface. This should be expected since the boundary layer is thinner at the lower surface temperature, the velocity gradients and, hence, the energy generated within the boundary layer by viscous dissipation are greater.

Because of the streamwise variation in the heat-transfer, the surface temperature did not remain constant during an experimental run as was assumed in the calculations presented in Fig. 9. Therefore, the theoretical heat-transfer distribution which was calculated assuming the wall temperature to be constant ($T_w = 0.423\ T_t$) was compared in Fig. 10 with that calculated using the experimentally-determined surface temperatures (the surface temperatures varied from $T_w = 0.450\ T_t$ to $T_w = 0.429\ T_t$). These theoretical heat-transfer distributions are compared with the corresponding experimental heat-transfer coefficients. However, the improvement is relatively small. Therefore, subsequent solutions for the laminar boundary-layer assume the surface temperature to be constant along the entire length of the model. The values used in computing theoretical solutions will represent "nominal" values from the experimental program.

EXPERIMENTAL DATA

The heat-transfer measurements are presented as a dimensionless ratio of heat-transfer coefficients, $h/h_{t,ref}$, which involves the ratio of the measured, local heat-transfer rate to the theoretical heat-transfer rate to the stagnation point of a 0.00533 m. (0.0175 ft.) radius sphere as calculated using the theory of Fay and Riddell (ref. 24). For purposes of data presentation, the recovery factor has been set equal to unity. Other parameters used in the data correlations include the free-stream Reynolds number based on model length, $Re_{\infty,L}$, where

$$Re_{\infty,L} = \frac{\rho_\infty U_\infty L}{\mu_\infty} \tag{5}$$

and L is the model length, 0.5734 m. (1.881 ft.). The Reynolds number behind a normal shock Re_{ns} is

$$Re_{ns} = \frac{\rho_{ns}\, U_{ns}\, r_{ref}}{\mu_{ns}} \tag{6}$$

where r_{ref} = 0.00533 m. (0.0175 ft.).

Heat-Transfer Distributions for α = 30°

The effect of the height of the misaligned tiles on the heat-transfer distribution for the plane-of-symmetry when the Orbiter is at an α of 30° is illustrated in the data presented in Fig. 11. Data are presented from tests where the surface temperature of the model was approximately 300°K (540°R). For the geometries tested in the wind tunnel and for this wall temperature, tile misalignment did not significantly affect the heat-transfer rates in regions where the boundary layer was either laminar or turbulent.

Furthermore, the boundary layer remained laminar along the entire length of the model for the lower Reynolds number, i.e., $Re_{\infty,L} \approx 1.92 \times 10^6$. At the higher Reynolds number, i.e., $Re_{\infty,L} \approx 7.03 \times 10^6$, the heat-transfer measurements for the model with $k = 4.43 \times 10^{-5}L$ departed from the laminar distribution at approximately the same location as observed for the smooth body. Increasing the tile misalignment height to $k = 8.86 \times 10^{-5}L$ caused the transition location to move slightly upstream and caused a more rapid streamwise increase in heating, i.e., the heating increased very rapidly with distance in the transitional flow regime.

Theoretical heat-transfer distributions for a laminar boundary layer when $T_w = 0.416\ T_t$ and $Re_{\infty,L} = 3.67 \times 10^6$ are included in Fig. 11 for comparison with the experimental distribution. Since (as has been noted already) the variations in the local entropy at the edge of the boundary layer due to the variations in the boundary-layer thickness had been neglected, the theoretical value for the dimensionless ratio of the local heat-transfer coefficient was independent of the test Reynolds number. Solutions are presented for both flow models, i.e., the "Var Ent" and the "Mod-Newt NSE" flow models. For $x > 0.2L$, the Var Ent model provides a better prediction of the laminar measurements. It is interesting to note that whereas the theoretical solution describes the laminar boundary layer adjacent to a smooth surface, it provides a reasonable prediction of the heating rates to the tile-roughened surface.

The data presented in Fig. 11 are from tests for which the model surface was at room temperature. Thus, the wall temperature was approximately 42 percent of the stagnation temperature of the tunnel flow. This is significantly higher than the values for the ratio T_w/T_t which would be encountered in flight. Therefore, to more nearly simulate the flight values, the model

was cooled by exhausting liquid nitrogen over the model prior to injecting it into the free stream. Cooling the model (and, hence, the boundary layer) causes the boundary-layer thickness to decrease. Theoretical Mach-number profiles are presented for the various surface temperatures of the test program in Fig. 12 for $Re_{\infty,L} \approx 1.9 \times 10^6$ and in Fig. 14 for $Re_{\infty,L} \approx 7.1 \times 10^6$. Shadowgraphs of the corresponding flow fields are presented in Figs. 13 and 15. At the lower Reynolds number, the theoretical solutions (which neglect any perturbation of the flow due to the presence of the misaligned tiles) indicate that the tile is submerged within the subsonic portion of the boundary layer. Although weak waves generated by the tiles appear in each shadowgraph (see Fig. 13), they only become easily visible for the coldest surface temperature, i.e., $T_w = 0.128\ T_t$, for which the boundary layer is thinnest. Although the presence of the perturbation waves indicates at least a weak flow-field disturbance, the heat-transfer rates in the laminar region do not appear to be significantly affected by the tile misalignment (see Fig. 16a). However, whereas the boundary layer remained laminar along the entire length of the model for $T_w = 0.423\ T_t$ and for $T_w = 0.340\ T_t$, the heat-transfer distribution indicates that the boundary layer becomes transitional for $x > 0.70L$ when T_w was decreased to $0.128\ T_t$. Thus, as a result of cooling the boundary layer, there is a relative increase in the magnitude of the disturbance due to a fixed roughness. The effect is obviously a nonlinear function of surface temperature.

The Mach number profiles at the higher Reynolds number, i.e., $Re_{\infty,L} \approx 7.1 \times 10^6$, indicate that the misaligned tiles would protude into the sonic regions of an unperturbed boundary layer at $x = 0.255L$ (see Fig. 14). Thus, one would expect that the presence of the misaligned tiles would alter the basic flow field. That the misaligned tiles significantly perturb

the flow field is verified in the shadowgraphs of Fig. 15. Easily visible waves emanate from the tiles at all surface temperatures. At the lower surface temperatures, the highly vortical flow which results when the turbulent boundary layer bounces over the misaligned tiles can be seen in the photographs, see Fig. 15(c) and 15(d). As a result, transition occurs well upstream on the fuselage, as evident in the heat-transfer distributions of Fig. (16c). For $T_w = 0.231\ T_t$, the heating increases from x = 0.08L to x = 0.10L, and then decreases nearly following the laminar theory for the gage at x = 0.15L. Downstream of x = 0.15L, the heating increases rapidly with distance as the boundary layer becomes fully turbulent. The presence of a strongly favorable pressure gradient may have innibited the transition process in the region 0.10L < x < 0.15L. For $T_w = 0.171\ T_t$, the heat-transfer measurements depart from the laminar distribution at x = 0.07L. However, there is little difference in the transition location for $T_w = 0.401\ T_t$ and that for $T_w = 0.313\ T_t$. These data indicate that the primary impact of cooling was to shorten the transition length for these two test conditions. Thus, again any correlation between the transition location and the surface temperature would be nonlinear.

The effect of surface temperature on the heat-transfer distribution is illustrated in the data of Fig. 16. The theoretical solutions indicate that thinning the boundary layer by surface cooling increased the nondimensionalized value of the local heat-transfer coefficient. The heating increase is attributed to the increased gradients and viscous dissipation which result when the boundary layer thickness is decreased. At a given location, the nondimensionalized heat-transfer coefficient measured for the coldest surface temperature was more than for the highest surface temperature, as predicted by theory. However, the values obtained at the intermediate surface temperatures did not fall between these extremes. Thus, although

there are considerable differences in the experimental values in the laminar region for the various surface temperatures, there is no consistent trend with surface temperature. However, the coaxial surface thermocouple gages used to measure the heating rates were not calibrated to show variations of this magnitude.

Heat-Transfer Distribution for $\alpha = 40°$

The effect of the height of the misaligned tiles on the heat-transfer distibution for the plane-of-symmetry when the Orbiter is at an α of 40° is illustrated in the data presented in Fig. 17. The measurements are taken from tests where the surface temperature of the model was approximately 300°K (540°R). For the geometries tested in the wind tun l and for this wall temperature, tile misalignment did not significantly affect the heat-transfer rates in regions where the boundary layer was either laminar or turbulent. Increasing the tile misalignment height to $k = 8.86 \times 10^{-5} L$ caused the transition location to move only slightly upstream and caused a more rapid streamwise increase in heating, i.e., the heating increased very rapidly with distance in the transitional flow regime.

The decrease in the boundary-layer thickness due to cooling the model is illustrated by the theoretical Mach number profiles presented in Fig. 18. At this Reynolds number, the theoretical solutions (which neglect any perturbation of the flow due to the presence of the misaligned tiles) indicate that the tile is submerged within the subsonic portion of the boundary layer. However, as the wall temperature is decreased, the velocity profile is such that the flow is transonic near the top of the tile. Shadowgraphs of the corresponding flow fields are presented in Fig. 19. Although weak waves generated by the tiles appear in each shadowgr·ph, they only become easily visible for the coldest surface temperature, i.e., $T_w = 0.138\ T_t$, for which the boundary layer is thinnest.

The effect of surface temperature on the heat-transfer distribution is illustrated by the data presented in Fig. 20. As was the case for the $\alpha = 30°$ measurements, these heat-transfer gages did not verify the theoretical trend with surface temperature. There is a definite effect on the transition location. For both values of the free-stream Reynolds number, the transition location moves rapidly upstream as the surface is cooled, since there is an increase in the relative magnitude of the disturbance.

Transition Correlations

The heat-transfer distributions were used to determine the point at which boundary-layer transition occurred in the plane of symmetry. The experimentally-determined transition location was that "point" at which the heat transfer first deviated from the laminar distribution. The transition locations, thus determined, are presented in Fig. 21 and in Table 1. The transition location is a function of the angle of attack, the free-stream conditions (specifically, the Reynolds number, since the Mach number is essentially constant for these Tunnel B tests), the surface temperature, and the misalignment height. Thus, for a given angle of attack, the transition location is a function of the dimensionless variables: Re_{ns}, k/L, and T_w/T_t, i.e.,

$$\frac{x_{tr}}{L} \left(Re_{ns}, \frac{k}{L}, \frac{T_w}{T_t} \right) \tag{7}$$

Although the use of a local Reynolds number would be desirable, Re_{ns} was chosen because it was both simple to calculate and yet could account for the variations in the free-stream Mach number. Since data were obtained (1) for the smooth body over a range of Reynolds number, (2) over a range of tile height for a single surface temperature, and (3) over a range of surface temperature with a fixed tile height, it was possible to develop an empirical correlation for the transition location as a product:

$$\left(\frac{x_{tr}}{L}\right)_{corr} = \text{(Smooth-Body Correlation) (Roughness Factor) (Temperature Factor)} \quad (8)$$

This empirical correlation is developed in the following paragraphs using the data for an angle-of-attack of 30°.

Smooth-body correlation. - Referring to the experimentally-determined transition locations for the smooth-body Orbiter model, i.e., k_o, with $T_w \approx 0.42\ T_t$ at an angle-of-attack of 30°, it is clear that:

$$\text{Smooth-Body Correlation} = a_o + a_1 \log_{10} Re_{ns} \quad (9)$$

A least-squares fit of the data yields the numerical values for a_o and a_1:

$$\text{Smooth-Body Correlation} = 4.3131 - 0.9858 \log_{10} Re_{ns} \quad (10)$$

Equation (10) provides a good correlation of the data, as can be seen in Fig. 22.

Roughness factor. - As was discussed in reference 13 and as is illustrated in the data of Fig. 21, the transition locations for a tile-roughened model where $k = 4.43 \times 10^{-5}$ L were essentially the same as those recorded for a smooth body. However, when the heights of the misaligned tiles were 8.86×10^{-5} L, the transition locations moved forward approximately 0.05 L, which is the distance between adjacent heat-transfer gages. Using another set of data obtained in Tunnel B, Hube (ref. 25) observed that, "Projecting tiles were effective boundary-layer trips". The height k of the transition-promoting tiles varied from 9.69×10^{-5} L to 48.45×10^{-5} L. This corresponds to a full-scale tile misalignment of 0.3175 cm. (0.1250 in.) to 1.5875 cm. (0.6250 in.). The effect of tile-misalignment height in promoting transition is clearly nonlinear.

The roughness factor which represents the forward shift in transition due to the misaligned tiles was assumed to be given by:

$$\text{Roughness Factor} = 1.0 - b_{oi} \left(\frac{k}{L}\right)^2 \qquad (11)$$

The boundary-layer perturbation due to tiles of a given height should increase as the boundary layer thins, i.e., as the Reynolds number increases. To represent this Reynolds-number dependence, b_{oi} was assumed to be a linear function of Re_{ns}. A least-squares fit of the experimentally-determined transition locations for $T_w \approx 0.42\ T_t$ and for the k_0, k_1, and k_2 surface finishes (which are given as the first eighteen test conditions of Table 1 for an angle-of-attack of 30°) was used to establish a value of b_{oi} for each of the Reynolds numbers tested. Another least-squares fit was used to correlate these values of b_{oi}. The resultant roughness-factor correlation is:

$$\text{Roughness Factor} = 1.0 - [9.3805 \times 10^6 + 174.94\ Re_{ns}] \left(\frac{k}{L}\right)^2 \qquad (12)$$

The transition locations given by equation (12) are compared with the experimental locations for $T_w \approx 0.42\ T_t$ in Fig. 23. The empirical correlation is in good agreement with the individual experimental values.

Temperature factor. - Data were obtained for the k_2 surface finish, i.e., $k = 8.86 \times 10^{-5}\ L$, over a range of surface temperature from $0.11\ T_t$ to $0.42\ T_t$. These data were used to determine the temperature factor, which represents the forward shift in transition due to cooling the boundary layer. Thus, the temperature factor represents the ratio of the transition location observed at the temperature of interest divided by the transition location observed at the reference temperature, which

is 0.42 T_t for the present tests. The temperature factor:

$$\left(\frac{x_{tr}}{L}\right)_{k_2, T_{wi}, Re_{ns}} \Big/ \left(\frac{x_{tr}}{L}\right)_{k_2, 0.42T_t, Re_{ns}}$$

is presented in Fig. 24 as a function of the surface temperature. Cooling the wall to 0.32 T_t did not significantly affect the transition locations. However, when the wall was cooled to 0.22 T_t or to 0.12 T_t matic forward movement of the transition location was observed. Furmore, the effect was very sensitive to Reynolds number. For the lower surface-temperatures, i.e., $T_w \approx 0.12\ T_t$ or 0.22 T_t, transition occurred very near the nose (depending on the Reynolds number), approaching a minimum transition length. Thus, the expression for the temperature factor should be such that:

(1) for large surface temperatures, i.e., as T_w approaches 0.42 T_t, the temperature factor approaches unity,

(2) for the lowest surface temperatures, the temperature factor approaches a minimum value, and

(3) the temperature factor changes rapidly with surface temperature once the temperature is below a critical minimum.

Data provided by Dr. Goodrich (ref. 26) indicated that cooling the wall from 0.42 T_t to 0.12 T_t had little effect on the transition location for the smooth body and had only a moderate effect on the transition location for the model with the k_1 surface finish. The general form of the proposed temperature factor is:

$$\text{Temperature Factor} = 1.0 - C_1\, e^{-\frac{C_2}{(k/L)}\left(\frac{T_w - T_{init}}{T_t}\right)} \qquad (13)$$

where T_{init} is the wall temperature at which the transition location reaches its upstream-most location. Decreasing the surface temperature below this value would not move transition forward. Because the tile-induced boundary-layer perturbation is a function of the height of the tile relative to the displacement thickness, the temperature-dependent parameter should reflect an interdependence on the Reynolds number. Thus, T_{init} is a function of the Reynolds number. A correlation of the experimentally-determined transition locations yields the following expression for the temperature factor:

$$\text{Temperature Factor} = 1.0 - 0.85\, e^{-\frac{3.322 \times 10^{-3}}{(k/L)}\left(\frac{T_w - T_{init}}{T_t}\right)} \qquad (14a)$$

where

$$T_{init} = 82.033 + 4.0573 \times 10^{-6} (Re_{ns})^2 \qquad (14b)$$

(see Fig. 24). The empirical correlation for the temperature factor is compared with the experimental data in Fig. 24. Although the least-squares expression for T_{init} fits the individual calculations quite well, there are significant differences between the correlation values and the individual experimental values for the temperature factor in the range $0.11\ T_t < T_w < 0.23\ T_t$. These differences will be reflected in the comparison between the experimental and the correlation values for the transition location.

Resultant correlation for the $\alpha = 30°$, Tunnel B data. - When the three factors, as given by equations (10), (12), and (14), are substituted into equation (8), the empirical correlation for the t ansition location for the tile-roughened Orbiter model at an angle of attack is 30° is:

$$\left(\frac{x_{tr}}{L}\right)_{corr} = (4.3131 - 0.9858 \log_{10} Re_{ns}) \left\{1.0 - [9.3805 \times 10^{6} + 174.94\, Re_{ns}] \left(\frac{k}{L}\right)^{2}\right\} \left\{1.0 - 0.85\, e^{-\frac{3.322 \times 10^{-3}}{(k/L)} \left(\frac{T_w - T_{init}}{T_t}\right)}\right\} \quad (15)$$

where $T_{init} = 82.033 + 4.0573 \times 10^{-6} (Re_{ns})^2$. The transition location moved significantly forward for a highly cooled surface, for high Reynolds numbers, and for relatively large tile-misalignment height. These parameters indicate that premature transition occurs when the height of the misaligned tiles was of the order of the displacement thickness. Note that the correlation uses only parameters which represent the test conditions, i.e., Re_{ns}, T_w/T_t, and k/L. It does not require knowledge of the local flow properties and, therefore, does not depend on the flow model used to calculate the local flow field.

The transition locations calculated using this empirical correlation are compared with the experimentally-determined transition locations in Table 1. For extreme test conditions, two limiting considerations were employed. For the highest surface temperature and for the k_o and the k_1 surface finishes, the correlation yields transition locations in excess of 1.00 at the lowest Reynolds number. Values in excess of unity, i.e., $x_{tr} > L$, were interpreted as representing wholly laminar boundary-layers. For that case where T_w was less than T_{init} (refer to Fig. 24 and note the hexogonal symbol), the temperatur actor was assumed to be equal to its lower limit, 0.15. This avoided the error which would result if the actual temperatures were used, since the exponent would then be positive and the correlation of Fig. 24 violated.

In addition, the difference between the empirical value and the experimental value of the transition location for a given test condition is presented in Fig. 25 as a function of Re_{ns}. For the majority of the test conditions, the two values are within 0.05 L of each other. Since the heat-transfer gages were 0.05 L apart over most of the fuselage (see Fig. 1), the difference is approximately equal to the ability to define the transition location. The greatest differences result in those tests where the surface had been cooled considerably. For these tests, the transition location was very sensitive to Re_{ns}, T_w/T_t, and k/L and, thus, reflected the sensitivity of the displacement thickness relative to the tile height on these parameters. As noted earlier, even though the least-squares expression for T_{init} fit the individual calculations quite well, there were significant differences in the values for the temperature factor at these conditions. Thus, the correlation is considered very good for these Tunnel B data.

Applicability of the correlation to other data. - When a correlation to predict the transition location for a particular configuration is developed using data from a single wind tunnel, one must ask how general is such a correlation? Thus, the correlation of the Tunnel B data, represented by equation (15), was compared with transition locations determined using heat-transfer distributions obtained on a similar model in Tunnel F (see refs. [27] and [28]). For the Tunnel F tests, the Mach number varied from 10.73 to 12.06 while the free-stream Reynolds number (based on model length) varied from 1.17×10^6 to 17.63×10^6. The surface temperature varied from 0.16 T_t to 0.27 T_t. The surface was roughened over the

80% of the windward surface using a grit-blasting technique. The average peak-to-valley distance for ten readings in a 0.25 cm. (0.10 in.) length as read from a photo-micrograph was 0.0041 cm. (0.0016 in.). As can be seen in the data presented in Fig. 26, surface roughness did not have a significant effect until the Reynolds number was sufficiently high to cause transition near the nose. At these high Reynolds numbers, the roughness elements became large relative to the boundary layer and became effective as tripping elements.

As can be seen in Fig. 26, the experimentally-determined transition locations for the smooth-body tested in Tunnel F fall significantly below the smooth-body correlation developed using the Tunnel B data, i.e., equation (10). However, by changing the value of the constant a_0, one obtains an approximate fit of the smooth-body Tunnel F data. Specifically, the relation

$$\frac{x_{tr}}{L} = 4.175 - 0.9858 \log_{10} Re_{ns} \qquad (16)$$

provides a reasonable correlation of the Tunnel F data. The "premature" transition of the boundary layer which occurred in the Tunnel F tests may have been due to tunnel noise, to nonuniform mixing of the relatively high-temperature flow, or to some other factor. It is also possible that a correlation of the transition location as a linear function of the $\log_{10} Re_{ns}$ is not appropriate for these data and that this parameter does not satisfactorily relate data from two different tunnels.

Thus, although the transition locations calculated using equation (15) are in good agreement with the individual experimental values from

Tunnel B, they do not agree with the Tunnel F data. Although the various factors, which are given in equations (10), (12), and (14), qualitatively describe the effect of the various parameters, caution should be used before applying equation (15) to predict the transition location for a Shuttle Orbiter exposed to significantly different flow conditions, i.e., those of another wind tunnel or of flight.

Correlations Based on Local Flow Properties

The Var Ent flow model was used to calculate the flow properties at the edge of the boundary layer and the momentum thickness at the experimentally-observed transition location. The ratio $(Re_\theta/M_e)_{tr}$, thus calculated, is presented in Fig. 27 as a function of the nondimensionalized transition location, x_{tr}/L. For those runs with the higher surface temperatures, i.e., 0.32 T_t or 0.42 T_t, the transition locations were not much different from the reference-temperature, smooth-body transition locations. For these runs

$$190 < \left(\frac{Re_\theta}{M_e}\right)_{tr} < 240$$

both for an angle-of-attack of 30° and of 40°. As often noted previously, cooling the surface increased the tile-induced flow perturbations and caused transition to move forward. As a result, the value of $(Re_\theta/M_e)_{tr}$ decreased continuously, approaching 100.

The previous discussion of the experimentally-determined transition locations has underlined the fact that the tile-induced flow perturbations become strongest when the height of the misaligned tiles is of the order

of the displacement thickness. The transition location moved significantly forward as surface cooling at the higher Reynolds numbers thinned the boundary layer. The transition location for the perturbed flows relative to the corresponding locations on the reference configuration are presented as a function of $\delta^*\sqrt{Re_s}/k$ in Figs. 28 through 30 and of δ^*/k in Figs. 31 through 33. Since smooth-body data were obtained only for angles-of-attack of 25°, 30°, and 35° (ref. 15), the reference transition-locations for an α of 40° were those for the k_1- tile-roughened model (ref. 16). Recall that there was no consistently measurable difference between the transition locations for the smooth-body (k_0) and those for the k_1- tile roughened model ($k = 4.43 \times 10^{-5}$ L) for an α of 30° (see Fig. 21). Thus, the relative transition locations for $\alpha = 30°$ are presented as the ratio ξ_1, where

$$\xi_1 = \frac{\left(\frac{x_{tr}}{L}\right)_{k_i, T_{wi}, Re_{ns}}}{\left(\frac{x_{tr}}{L}\right)_{k_o, 0.42T_t, Re_{ns}}} \tag{17}$$

For $\alpha = 40°$, the relative transition locations are presented as the ratio ξ_2, where

$$\xi_2 = \frac{\left(\frac{x_{tr}}{L}\right)_{k_i, T_{wi}, Re_{ns}}}{\left(\frac{x_{tr}}{L}\right)_{k_1, 0.42T_t, Re_{ns}}} \tag{18}$$

These nondimensionalized relative transition-locations represent the ratio of the experimentally-determined transition location at the tile misalign-

ment height of a particular run (k_i), at the surface temperature of that run (T_{wi}), and at the Reynolds number of that run divided by the transition location measured at the same Reynolds number but at the reference surface finish (either k_0 or k_1) and at the reference surface temperature (0.42 T_t).

The values of $\delta^*\sqrt{Re_s}/k$ and δ^*/k at $x \approx 0.1$ L and $x \approx 0.2$ L were calculated for a nonsimilar, laminar boundary layer. For some conditions, boundary-layer transition occurred upstream of these x-locations. Thus, the actual value of δ^* for these cases would be significantly different than the calculated value. Theoretical solutions were generated for the Mod Newt NSE flow model at $\alpha = 30°$, for the Var Ent flow model at $\alpha = 30°$ and for the Var Ent flow model at $\alpha = 40°$. As has been discussed, the theoretical flow models do not reflect tile-induced perturbations. All the test conditions of Table 1 are not represented in Figs. 28 through 33. Theoretical solutions were not generated for the Mod Newt NSE flow model for the $\alpha = 40°$ flow conditions or for the k_1-surface finish at an α of 30°. Furthermore, at the lowest surface temperature, i.e., $T_w \approx 0.12\ T_t$, the displacement thickness calculated at $x \approx 0.1$ L using the Mod Newt NSE flow model was often negative or very small (depending upon the Reynolds number). Thus, the relative transition location ξ_1 is represented by the range of values for these runs and is presented at an approximate value of δ^*/k. For a given surface temperature, the parameter $\delta^*\sqrt{Re_s}/k$ is essentially constant over the range of Reynolds number. Thus, for that surface temperature and a given surface roughness, the data tend to cluster in a group when this parameter is used as the abcissa (see Figs. 28 through 30).

For either nondimensionalized δ^*-parameter, the relative transition-location ξ is near unity (i.e., the tile-induced perturbations have a negligible effect on the transition location) at the highest values of the δ^*-parameter. As the δ^*-parameter is decreased (i.e., the boundary layer is cooled, the test Reynolds number is increased, or the tile-misalignment height is increased), transition moves gradually forward, i.e., ξ decreases slowly. In this region, i.e., $0.8 < \xi < 1.0$, the magnitude of ξ does not exhibit any dependence on the Reynolds number except through the value of the δ^*-parameter. Below a critical value of the δ^*-parameter, the relative transition location decreases rapidly (i.e., transition moves rapidly upstream toward the nose) as the boundary layer thins. Below the critical value of the δ^*-parameter, the Reynolds number has a strong effect on the magnitude of ξ. Note that the critical value of the δ^*-parameter evaluated at a given location is independent of the flow-field model used in the calculation of δ^* and Re_s and is independent of the angle-of-attack for these wind tunnel results.

The relative transition locations were correlated as a function of the theoretical, laminar values of δ^*/k at $x = 0.1L$ using a linear, least-squares fit of those data for which $\delta^* > 0.75$ k. The least-squares correlations are essentially identical for the $\alpha = 30°$ data. I.e., for the Mod Newt NSE model:

$$\xi_1 = 0.8404 + 0.0489 \left(\frac{\delta^*}{k}\right)_{x \approx 0.1L} \tag{19}$$

while for the Var Ent model:

$$\xi_1 = 0.8397 + 0.0517 \left(\frac{\delta^*}{k}\right)_{x \approx 0.1L} \tag{20}$$

The least-squares correlation for the $\alpha = 40°$ results is:

$$\xi_2 = 0.9017 + 0.0074 \left(\frac{\delta^*}{k}\right)_{x \approx 0.1L} \quad (21)$$

Recall that the heat-transfer distributions and, therefore, the transition locations were not measured for the smooth-bodv (k_0) at $\alpha = 40°$. It was assumed that the transition locations for the k_1-tile-roughened model would have been the same as those for the smooth bodv. Thus. they were used as the reference transition-location in evaluating the ξ_2 parameter. As a result, there were no measurements where ξ was unity, as had been the case for the $\alpha = 30°$ correlations (see Figs. 31 and 32). The absence of such points is the reason why eqn. (21) is significantly different than eqn (19) or eqn (20). Nevertheless, eqn (19) or eqn (20) would provide a reasonable correlation of the ξ_2 measurements for $\delta^* > 0.75$ which are presented in Fig. 33.

The relative transition locations for both angles-of-attack are presented in Fig. 34a as a function of the theoretical, laminar values of δ^*/k at $x \approx 0.1L$ for both flow models. Note that for $\delta^* \geq 0.75k$, the experimental values of $\xi \geq 0.81$, i.e., the roughness-perturbed transition locations are within 19% of the reference, smooth-body transition locations. At the lowest temperatures, δ^* was so thin, (i.e., $\delta^* < 0.75k$) that the presence of the misaligned tiles moved transition well upstream. Thus, 0.75k is the critical value of δ^* at $x \approx 0.1L$. Using a linear, least-squares fit of those data for which δ^* at $x \approx 0.1L$ was greater than 0.75k yields the correlation:

$$\xi = 0.8489 + 0.0468 \left(\frac{\delta^*}{k}\right)_{x \approx 0.1L} \quad (22)$$

The parameter ξ is used, since the correlation fits both the ξ_1- and the ξ_2-values presented in Figs. 31-33 and, therefore, is valid for both angles-

of-attack and for both flow models. Using this correlation, when the theoretical value of the displacement thickness at $x \simeq 0.1L$ is equal to 0.75k, $\xi = 0.884$. Thus, the "nominal" transition location moves upstream by just over 10% when δ^* at this station is of the order of the tile misalignment height.

The relative transition locations are presented in Fig. 34b as a function of the theoretical, laminar values of δ^*/k at $x \simeq 0.2L$ for both flow models. Note that for $\delta^* \geq 1.50k$, the experimental values of $\xi \geq 0.81$. The linear, least-squares fit of those data for which δ^* at $x \simeq 0.2L$ was greater than 1.50k yields the correlation:

$$\xi = 0.8500 + 0.0219 \left(\frac{\delta^*}{k}\right)_{x \simeq 0.2L} \tag{23}$$

Using this correlation, $\xi = 0.883$ when the theoretical value of the displacement thickness at $x \simeq 0.2L$ is equal to 1.50k.

The ratio of the laminar displacement thickness to the tile misalignment height is presented in Fig. 35 as a function of x/L. Note that

$$\left(\frac{\delta}{k}\right)_{x \simeq 0.2L} \simeq 2.0 \left(\frac{\delta}{k}\right)_{x \simeq 0.1L}$$

over the range of test Reynolds number at this surface temperature. Thus, it should not be surprising that, if the critical value of the displacement thickness at $x \simeq 0.1L$ is 0.75k, then the critical value of δ^* at $x \simeq 0.2L$ is 1.50k.

CONCLUDING REMARKS

The theoretical heat-transfer distributions are compared with experimental heat-transfer distributions obtained in Tunnel B at AEDC using a 0.0175 scale model of the Space Shuttle Orbiter Configuration for which the first 80% of the windward surface was roughened by a simulated tile misalignment. Data were obtained for a Mach number of 8 over a Reynolds number range (based on model length) from 1.862×10^6 to 7.091×10^6 with surface temperatures from 0.114 T_t to 0.435 T_t. For the geometries and for the flow conditions of the present wind-tunnel test programs, the following conclusions are made.

1. A study of the surface-pressure distributions, the Mach number at the edge of the boundary layer, and the heat-transfer distributions indicates that calculations based on the Var Ent flow model are in good agreement with the laminar data for $x \geq 0.2L$. For $x \leq 0.1L$, the calculations based on the Mod Newt NSE flow model are in reasonable agreement with the data.
2. The theoretical solutions indicate that thinning the boundary layer by surface cooling increased the nondimensionalized value of the local heat-transfer coefficient. The theoretical increase was due to the increased gradients and viscous dissipation which result when the boundary-layer thickness decreased. However, the coaxial surface thermocouples used to measure the heating rates were not calibrated to show the variations of the magnitude predicted by theory.
3. Tile misalignment did not significantly affect the heat-transfer rate in regions where the boundary layer was either laminar or turbulent.
4. The heat-transfer distributions were used to determine the transition

locations over a range of Reynolds number, surface cooling, and tile-misalignment height. The transition location moved significantly forward as surface cooling at the higher Reynolds number thinned the boundary layer. Furthermore, relatively large tile-misalignment heights were required to cause significant movement in the transition location. The tile-induced flow perturbations promoted transition only when the theoretical value of δ^* at $x = 0.1\ L$ was less than $0.75\ k$. This critical value of δ^*/k was independent of the flow-field model used to calculate δ^* and was independent of the angle-of-attack for these wind-tunnel tests. When δ^* at $x = 0.1\ L$ was equal to, or greater than, $0.75\ k$, the experimentally-determined transition locations for a tile-roughened, cooled model were within 20% of the reference, smooth-body transition location at the same free-stream conditions.

REFERENCES

1. van Driest, E.R., and Blumer, C.B., "Boundary-Layer Transition at Supersonic Speeds - Three-Dimensional Roughness Effects (Spheres)", Journal of the Aerospace Sciences, Aug. 1962, Vol. 29, No. 8, pp. 909-916.

2. Morrisette, E.L., "Roughness Induced Transition Criteria for Space Shuttle-Type Vehicles", Journal of Spacecraft and Rockets, Feb. 1976, Vol. 13, No. 2, pp. 118-120.

3. McCauley, W.D., Saydah, A.R., and Bueche, J.F., "Effect of Spherical Roughness on Hypersonic Boundary-Layer Transition", AIAA Journal, Dec. 1966, Vol. 4, No. 12, pp. 2142-2148.

4. Carver, D.G., "Heat-Transfer Tests on the Rockwell International Space Shuttle Orbiter with Boundary-Layer Trips (OH-54)", AEDC-TR-76-28, May 1976.

5. Seegmiller, H.L., "Effects of Roughness on Heating and Boundary Layer Transition, Part I - Effects of Simulated Panel Joints on Boundary-Layer Transition", Space Shuttle Aerothermodynamics Technology Conference, Volume II-Heating, NASA TM X-2507, February 1972.

6. Lees, L., "The Stability of the Laminar Boundary Layer in a Compressible Fluid", NACA Report No. 876, 1947.

7. Reshotko, E., "Transition Reversal and Tollmien-Schlichting Instability", Physics of Fluids, March 1963, Vol. 6, No. 3, pp. 335-342.

8. Rumsey, C.B. and Lee, D.B., "Measurements of Aerodynamic Heat Transfer and Boundary-Layer Transition on a 10° Cone in Free Flight at Supersonic Mach Numbers Up to 5.9", NASA TND-745, May 1961.

9. Diaconis, N.S., Jack, J.R. and Wisniewski, R.J., "Boundary-Layer Transition at Mach 3.12 as Affected by Cooling and Nose Blunting", NACA TN 3928, January 1957.

10. Richards, B.E. and Stollery, J.L., "Further Experiments on Transition Reversal at Hypersonic Speeds", AIAA Journal, December 1966, Vol 4, No. 12, pp. 2224-2226.

11. Potter, J.L. and Whitfield, J.D., "The Relation Between Temperature and the Effect of Roughness on Boundary-Layer Transition", Journal of the Aerospace Sciences, August 1961, Vol. 28, No. 8, pp. 663-664.

12. Wagner, R.D., Maddalon, D.V., Weinstein, L.M., and Henderson, A. Jr., "Influence of Measured Free-Stream Disturbances on Hypersonic Boundary-Layer Transition", AIAA Paper 69-704, presented at 2nd Fluid and Plasma Dynamics Conference, San Francisco, June 1969.

13. Bertin, J.J., Stalmach, D.D., Idar, E.S., Conley, D.B., and Goodrich, W.D., "Hypersonic Heat-Transfer and Transition Correlations for a Roughened Shuttle Orbiter", presented at the 13th Annual Meeting of the Society of the Engineering Sciences, Hampton, Virginia, November 1976.

14. Stalmach, C.J., Jr., and Goodrich, W.D., "Aeroheating Model Advancements Featuring Electroless Metallic Plating", presented at the AIAA 9th Aerodynamic Testing Conference in Arlington, Texas, June 1976.

15. Martindale, W.R., and Trimmer, L.L., "Test Results from the NASA/Rockwell International Space Shuttle Test (OH4A) Conducted in the AEDC-VKF Tunnel B", AEDC-DR-74-39, May 1974.

16. Siler, L.G., and Martindale, W.R., "Test Results from the NASA Space Shuttle Orbiter Heating Test (MH-2) Conducted in the AEDC-VKF Tunnel B", AEDC-DR-75-103, Oct. 1975.

17. Wannenwetsch, W.D., and Martindale, W.R., "Roughness and Wall Temperature Effects on Boundary-Layer Transition on a 0.0175 Scale Space Shuttle Orbiter Model Tested at Mach Number 8", AEDC-TR-77-19, to be published.

18. Bertin, J.J., and Byrd, O.E., Jr., "The Analysis of a Nonsimilar Boundary Layer - A Computer Code (NONSIMBL)", University of Texas at Austin, Aerospace Engineering Report 70002, Aug. 1970.

19. Goodrich, W.D., Li, C.P., Houston, C.K., Chiu, P., and Olmedo, L., "Numerical Computations of Orbiter Flow Fields and Heating Rates", AIAA Paper 76-359, presented at the AIAA 9th Fluid and Plasma Dynamics Conference, San Diego, Cal., July 1976.

20. Martindale, W.R., and Carter, L.D., "Flow-Field Measurements in the Windward Surface Shock Layer of Space Shuttle Orbiter Configurations at Mach Number 8", AEDC-TR-75-5, July 1975.

21. Adams, J.C., Jr., Martindale, W.R., Mayne, A.W., Jr., and Marchand, E.O., "Real Gas Scale Effects on Hypersonic Laminar Boundary-Layer Parameters Including the Effects of Entropy-Layer Swallowing", AEDC-TR-R-75-2, December 1975.

22. De Jarnette, F.R., "Calculation of Inviscid Surface Streamlines and Heat Transfer on Shuttle Type Configurations", NASA CR-11921, Aug. 1971 (prepared by North Carolina State University).

23. Rakich, J.V., and Mateer, G.G., "Calculation of Metric Coefficients for Streamline Coordinates", AIAA Journal, Vol. 10, No. 11, Nov. 1972, pp. 1538-1540.

24. Fay, J.A., and Riddell, F.R., "Theory of Stagnation Point Heat Transfer in Dissociated Air", Journal of the Aeronautical Sciences, Vol. 25, No. 2, Feb. 1958, pp. 73-85, 121.

25. Hube, H.K., "Simulated Thermal Protection Tile Roughness Effects on Windward Surface Heat Transfer on the Rockwell International Space Shuttle Orbiter", AEDC-TR-76-98, Jan. 1977.

26. Goodrich, W.D., Private transmittal of data, March 15, 1977.

27. Boudreau, A.H., "Test Results from the NASA/RI Shuttle Heating Test OH-11 in the AEDC-VKR Tunnel F", AEDC-DR-74-16, February 1974.

28. Siler, L.G., "Test Results from the NASA Space Shuttle Orbiter Heating Test (MH-1) Conducted in the AEDC-VKF Tunnel F", AEDC-DR-76-13, March 1976.

Table 1. - Test Conditions and Transition Correlations

(a) $\alpha = 30°$

Data Source Ref.	M_∞	$Re_{\infty,L}$ ($\times 10^{-6}$)	Re_{ns}	$\frac{k}{L}$ ($\times 10^{5}$)	$\frac{T_w}{T_t}$	$(\frac{x_{tr}}{L})_{exp}$	$(\frac{x_{tr}}{L})_{corr}$
15	7.94	1.970	1993	0.00	0.435	w.l.*	w.l.*
15	7.96	2.871	2933	0.00	0.417	0.95	0.895
15	7.97	3.655	3742	0.00	0.411	0.75	0.740
15	7.98	4.666	4757	0.00	0.412	0.70	0.688
15	8.00	5.619	5743	0.00	0.405	0.60	0.607
15	8.00	7.004	7191	0.00	0.400	0.50to0.55	0.511
16	7.94	1.887	1926	4.43	0.423	w.l.	w.l.
16	7.97	2.829	2886	4.43	0.416	0.95	0.878
16	7.98	3.652	3722	4.43	0.414	0.75	0.725
16	7.98	4.632	4736	4.43	0.411	0.70	0.674
16	7.99	5.625	5766	4.43	0.405	0.60	0.595
16	8.00	7.064	7244	4.43	0.402	0.50	0.500
17	7.94	1.894	1936	8.86	0.423	w.l.	0.991
17	7.97	2.846	2900	8.86	0.418	0.85	0.825
17	7.98	3.701	3768	8.86	0.416	0.70	0.682
17	7.98	4.673	4774	8.86	0.412	0.65	0.633
17	7.99	5.531	5772	8.86	0.406	0.55	0.557
17	8.00	7.040	7229	8.86	0.401	0.45	0.468
17	7.94	1.889	1925	8.86	0.340	w.l.	0.993
17	7.97	2.820	2875	8.86	0.324	0.90	0.825
17	7.98	3.653	3724	8.86	0.308	0.65to0.70	0.681
17	7.98	4.668	4762	8.86	0.317	0.65	0.632
17	7.99	5.653	5781	8.86	0.314	0.55	0.556
17	8.00	7.066	7244	8.86	0.313	0.45	0.457
17	7.98	3.661	3733	8.86	0.247	0.65	0.679
17	8.00	7.077	7255	8.86	0.231	0.08to0.15	0.224
17	8.00	1.868	1881	8.86	0.128	0.70	0.881
17	7.97	2.835	2893	8.86	0.114	0.50to0.55	0.540

*wholly laminar boundary-layer, i.e., transition did not occur.

(a) $\alpha = 30°$

Data Source Ref.	M_∞	$Re_{\infty,L}$ ($\times 10^{-6}$)	Re_{ns}	$\frac{k}{L}$ ($\times 10^5$)	$\frac{T_w}{T_t}$	$(\frac{x_{tr}}{L})_{exp}$	$(\frac{x_{tr}}{L})_{corr}$
17	7.98	3.661	3734	8.86	0.131	0.50	0.455
17	7.98	4.637	4743	8.86	0.135	0.35	0.152
17	7.99	5.616	5758	8.86	0.163	0.20	0.101
17	8.00	7.072	7252	8.86	0.171	0.07	0.070

(b) $\alpha = 40°$

	M_∞	$Re_{\infty,L}$ ($\times 10^{-6}$)	Re_{ns}	$\frac{k}{L}$ ($\times 10^5$)	$\frac{T_w}{T_t}$	$(\frac{x_{tr}}{L})_{exp}$
16	7.94	1.921	1955	4.43	0.427	w.l.
16	7.97	2.828	2888	4.43	0.415	0.95
16	7.98	3.655	3727	4.43	0.414	0.70
16	7.98	4.668	4766	4.43	0.413	0.60
16	7.99	5.571	5719	4.43	0.404	0.54
16	8.00	7.017	7202	4.43	0.401	0.47
17	7.94	1.917	1955	8.86	0.424	w.l.
17	7.97	2.837	2891	8.86	0.418	0.85
17	7.98	3.674	3418	8.86	0.414	0.67
17	7.98	4.656	4331	8.86	0.412	0.55
17	7.99	5.663	5268	8.86	0.407	0.46
17	8.00	7.038	6547	8.86	0.402	0.43
17	7.94	1.904	1940	8.86	0.341	w.l.
17	7.97	2.843	2901	8.86	0.331	0.82
17	7.98	3.661	3732	8.86	0.342	0.67
17	7.98	4.658	4760	8.86	0.356	0.56
17	7.99	5.616	5224	8.86	0.353	0.48
17	8.00	7.064	7244	8.86	0.360	0.43
17	7.98	3.667	3739	8.86	0.228	0.55
17	8.00	7.091	7262	8.86	0.258	0.225to0.300
17	8.00	1.862	1877	8.86	0.125	0.80

(b) $\alpha = 40°$

Data Source Ref.	M_∞	$Re_{\infty,L}$ $(\times 10^{-6})$	Re_{ns}	$\frac{k}{L}$ $(\times 10^{5})$	$\frac{T_w}{T_t}$	$(\frac{x_{tr}}{L})_{exp}$
17	7.97	2.828	2884	8.86	0.122	0.50
17	7.98	3.637	3710	8.86	0.138	0.44
17	7.98	4.675	4772	8.86	0.161	0.38
17	7.99	5.603	5747	8.86	0.169	0.225
17	8.00	7.040	7223	8.86	0.182	0.20

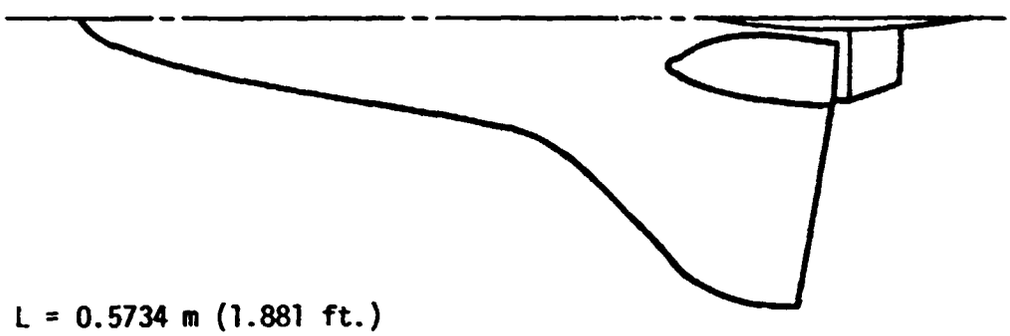

L = 0.5734 m (1.881 ft.)

Circles indicate locations of coaxial surface thermocouples in the plane of symmetry

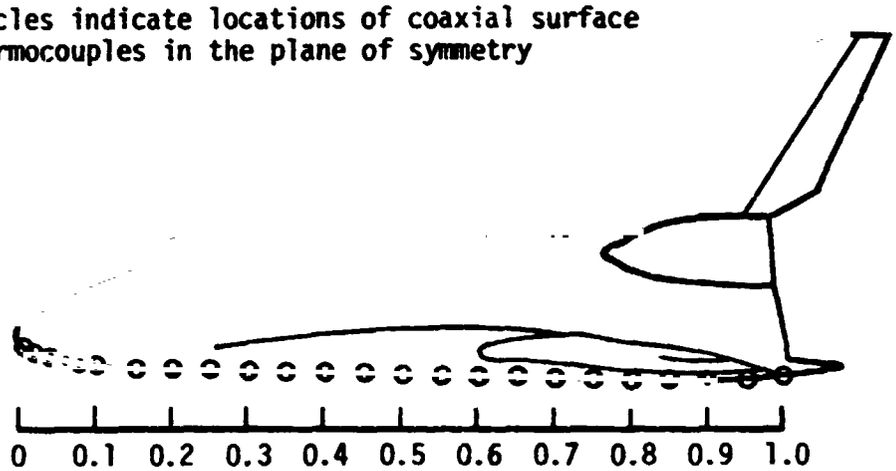

Figure 1. - Sketch of Space Shuttle Orbiter configuration (Rockwell Drawing VL70-000139) used in Tunnel B at AEDC.

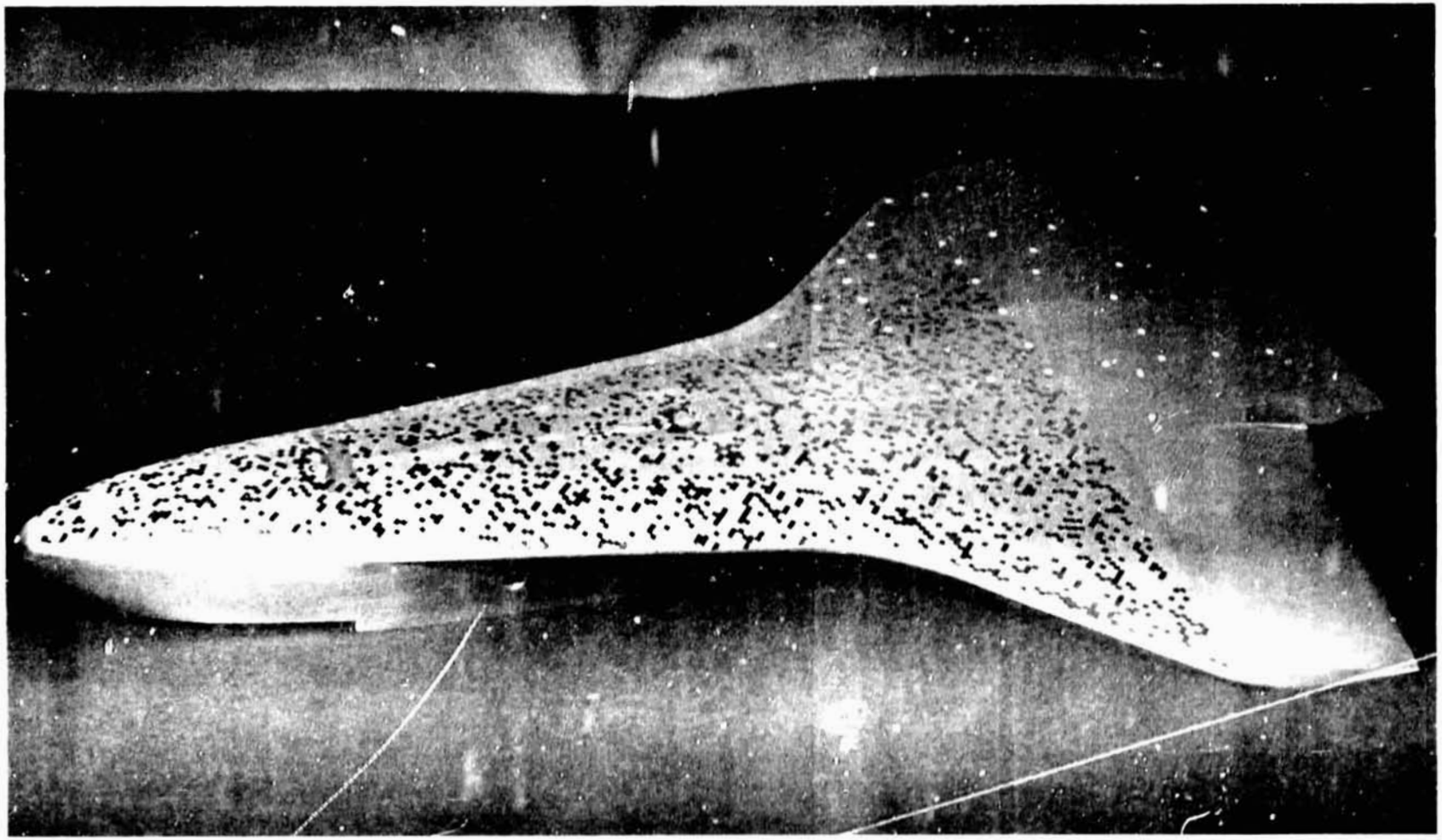

Figure 2. - Photograph of model showing randomly misaligned tiles.

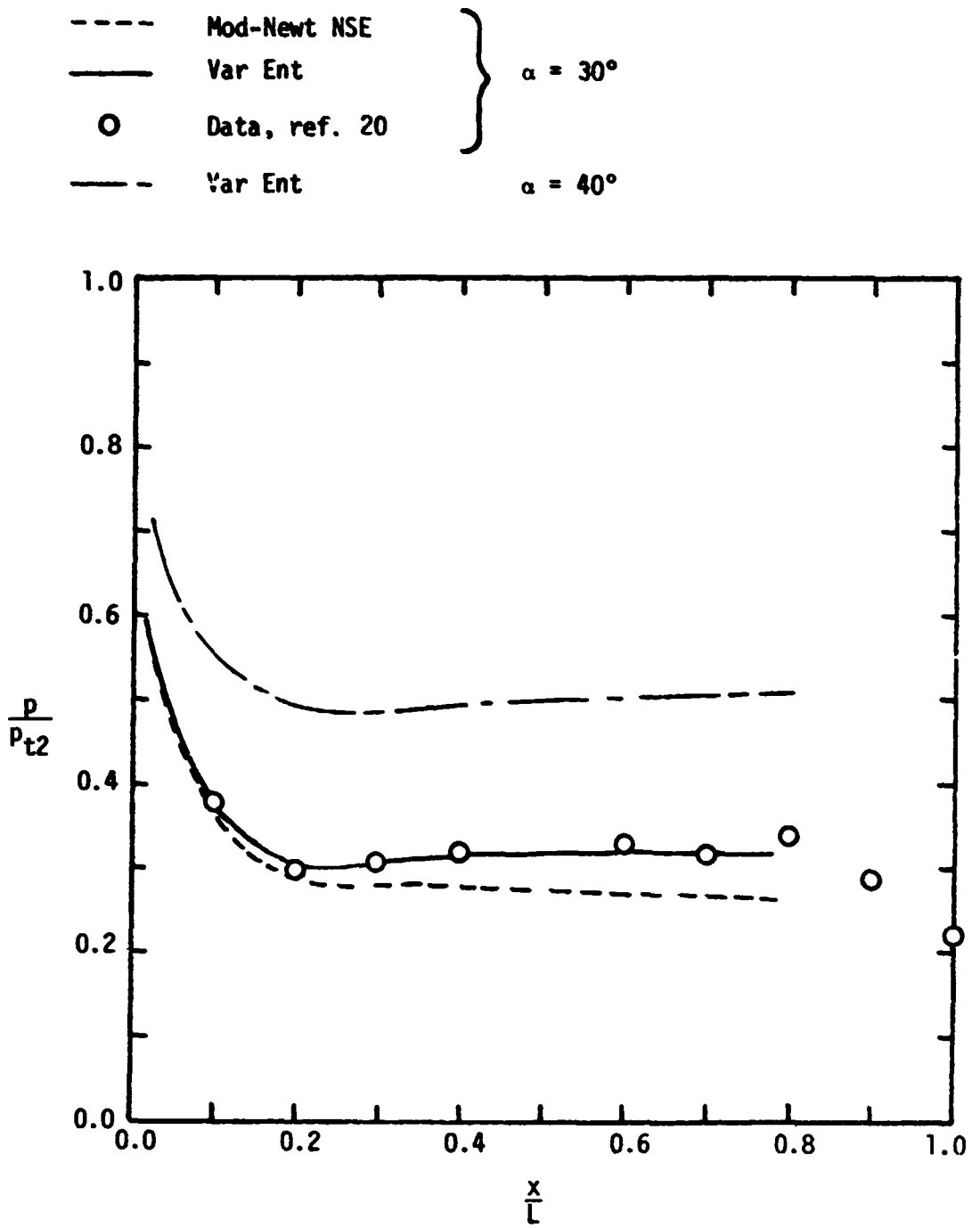

Figure 3. - Surface static-pressure distributions from the windward plane of symmetry for $\alpha = 30$ and for $\alpha = 40°$.

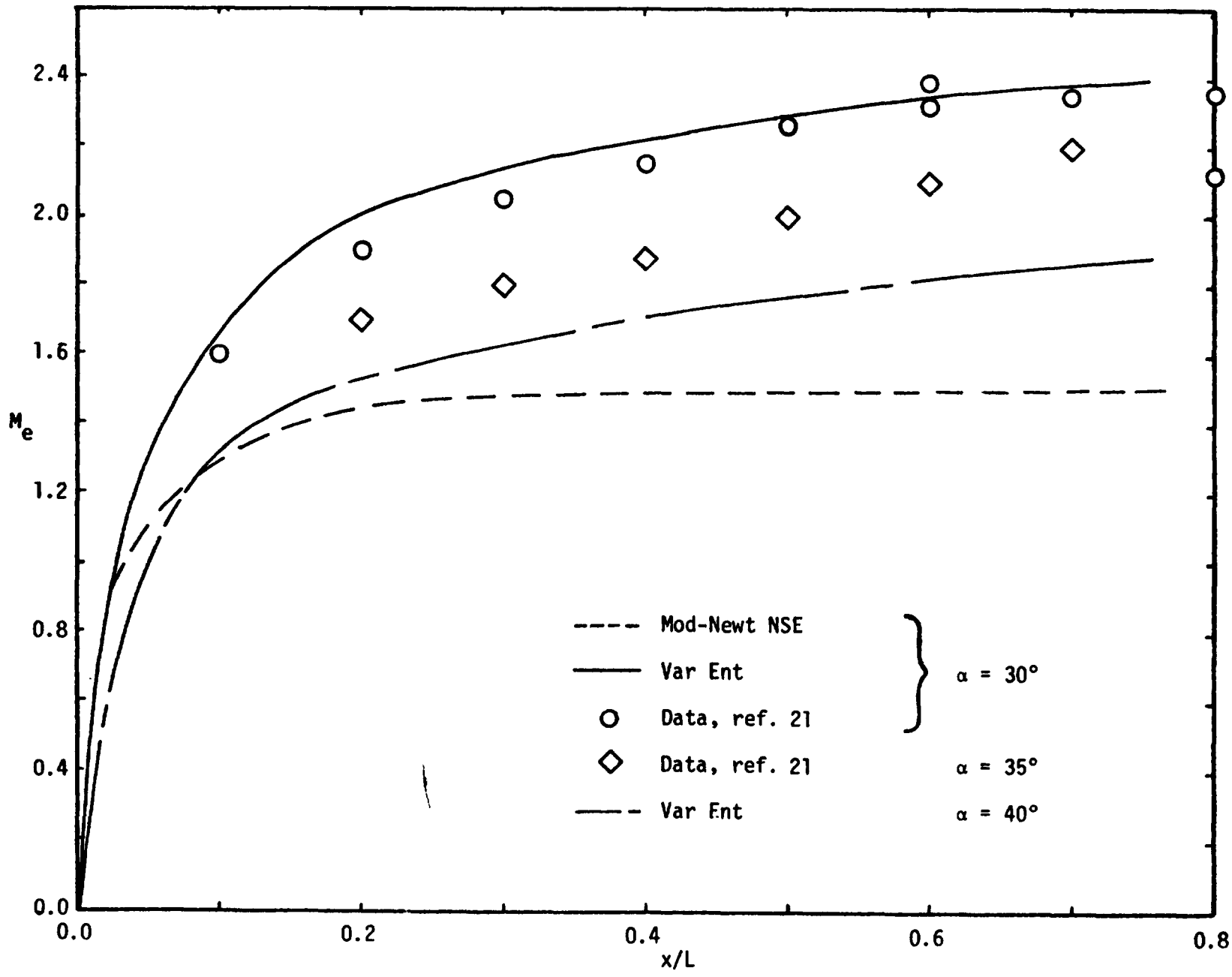

Figure 4. - Streamwise variation of the Mach number at the edge of the boundary layer.

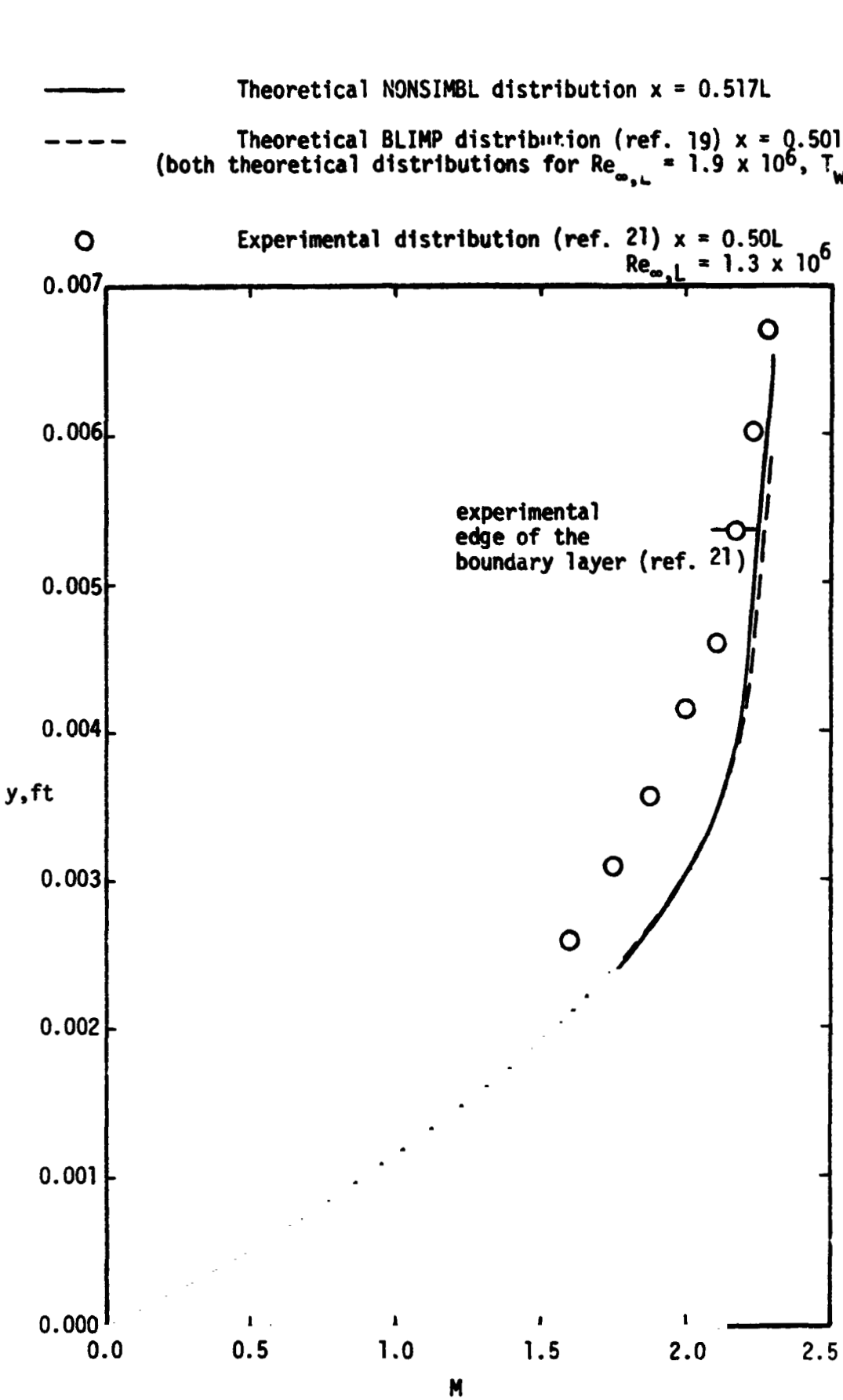

Figure 5. - Variation of the Mach number across the laminar boundary layer for x ≈ 0.5L, α = 30°.

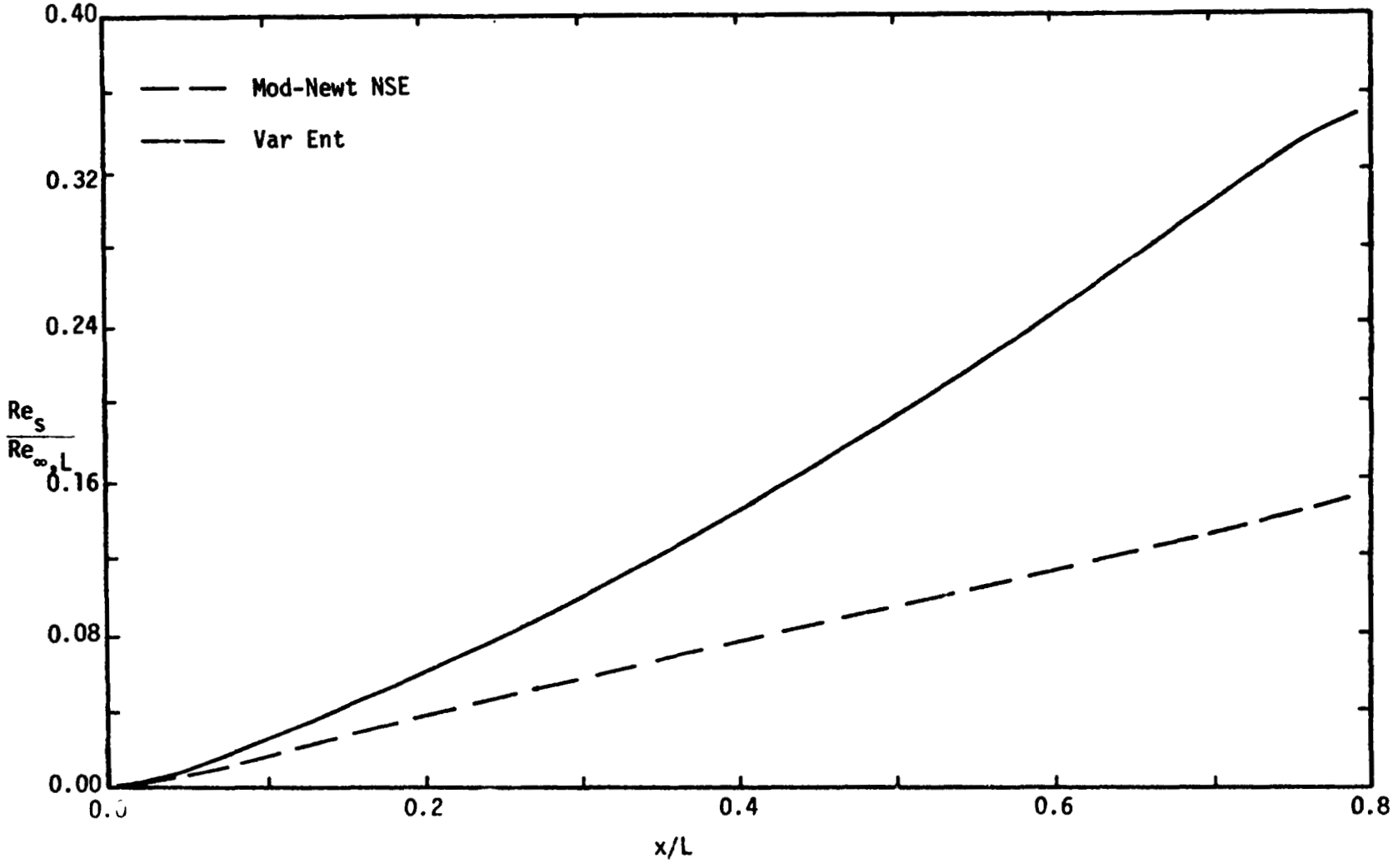

(a) $\alpha = 30°$

Figure 6. - Streamwise distribution of the Reynolds number at the edge of the boundary layer, $Re_{\infty,L} \approx 1.9 \times 10^6$.

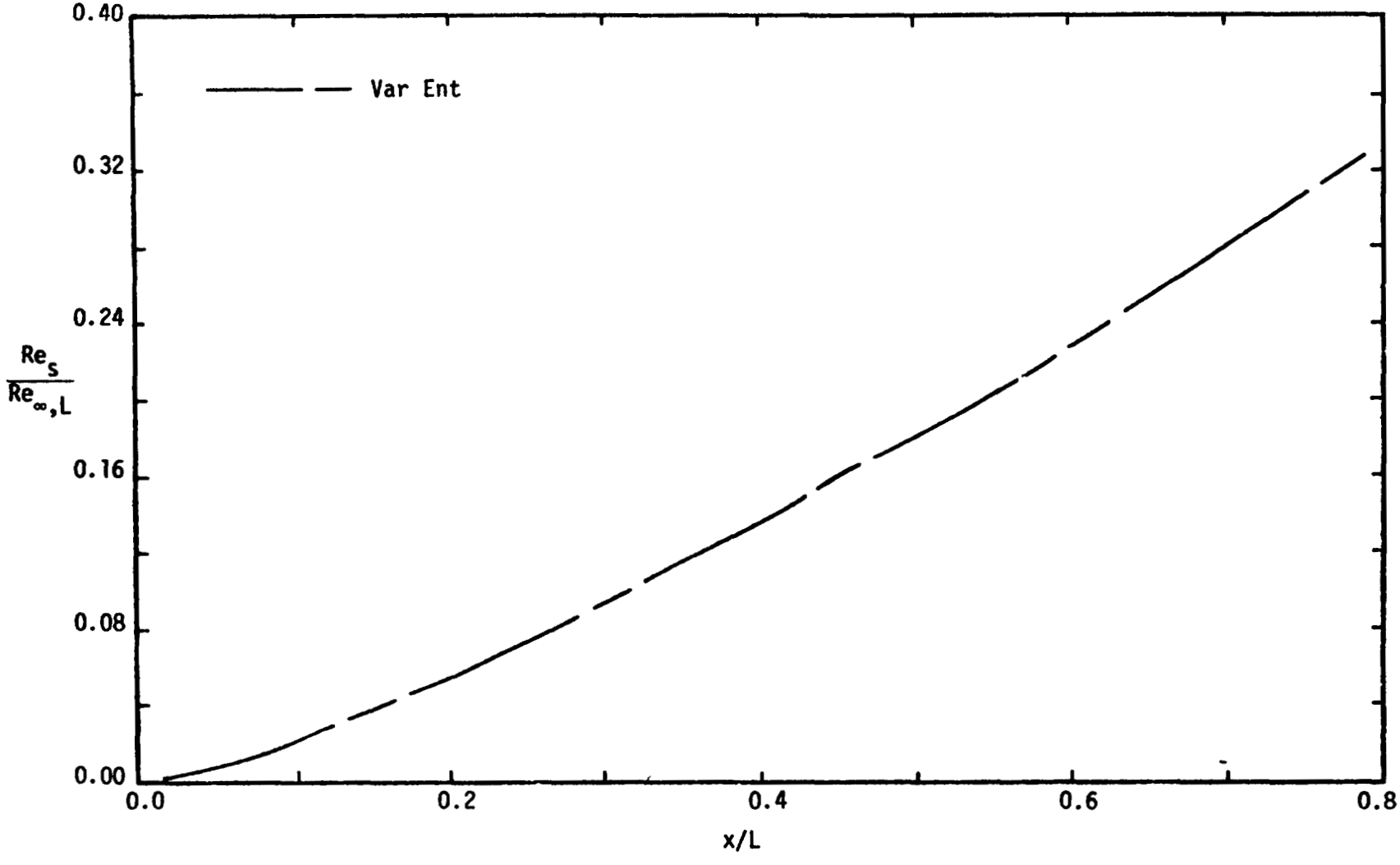

(b) $\alpha = 40°$

Figure 6. - Concluded.

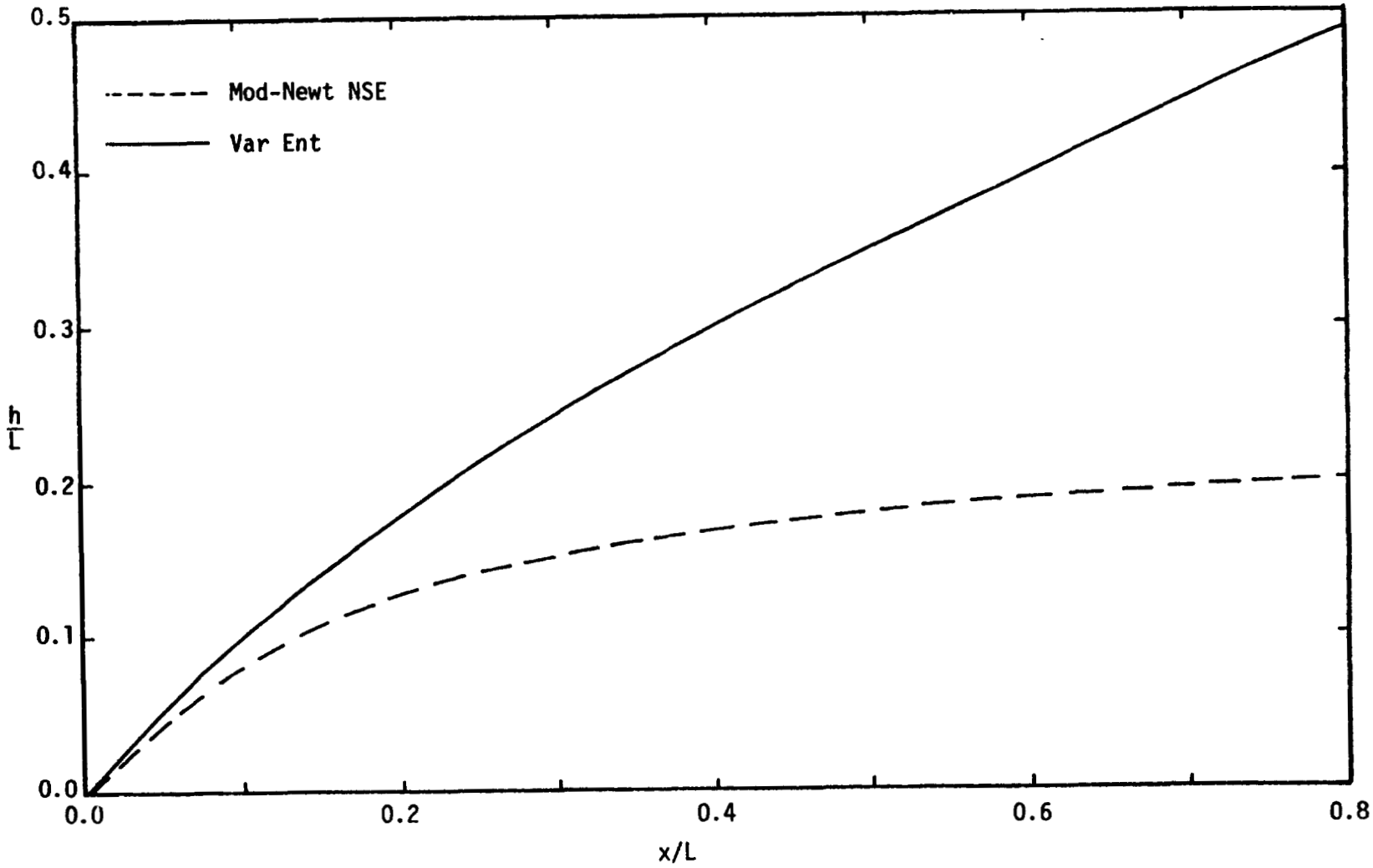

(a) $\alpha = 30°$

Figure 7. - Streamwise distribution of the radius of the "equivalent" body-of-revolution.

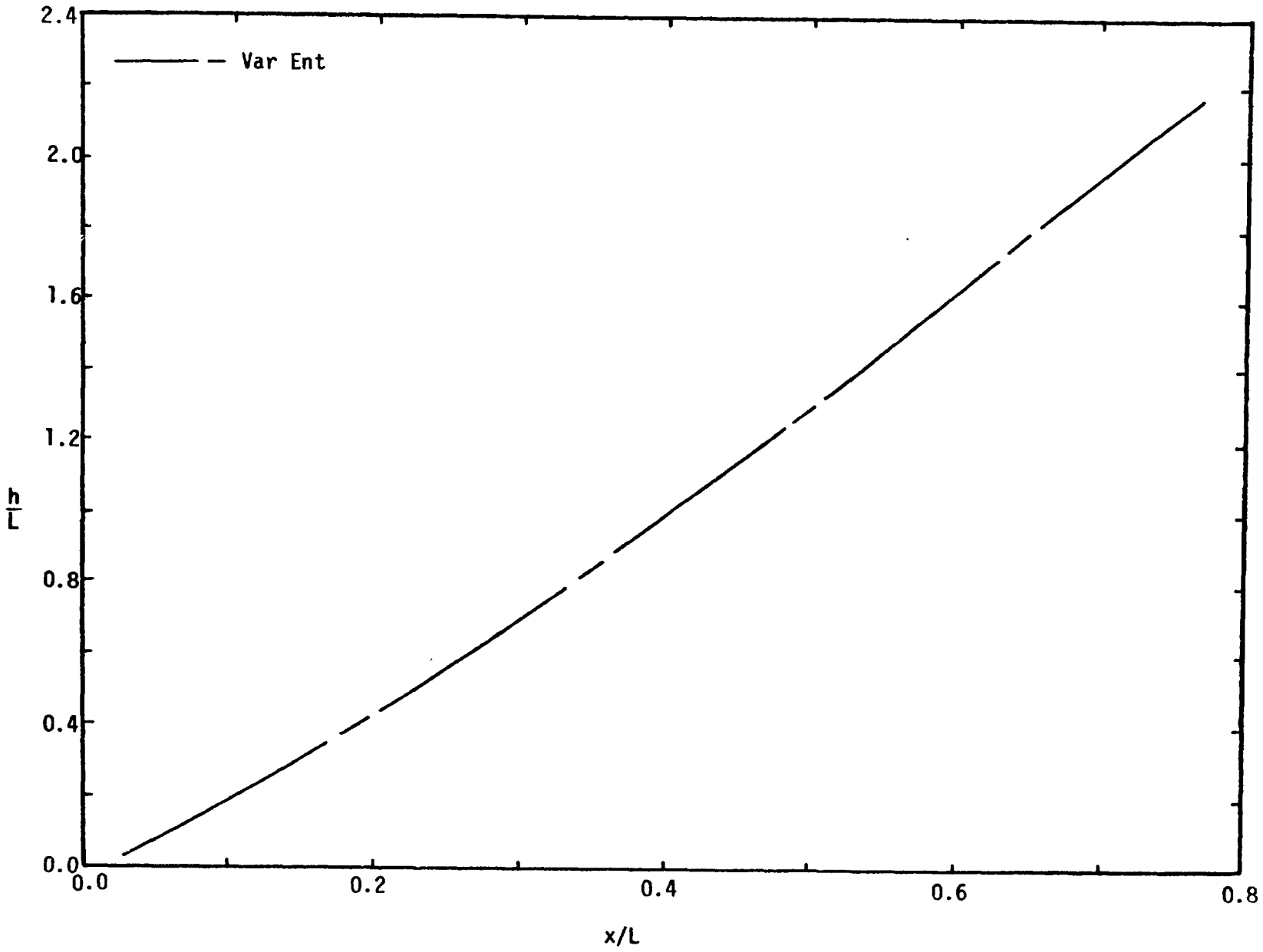

(b) $\alpha = 40°$

Figure 7. - Concluded.

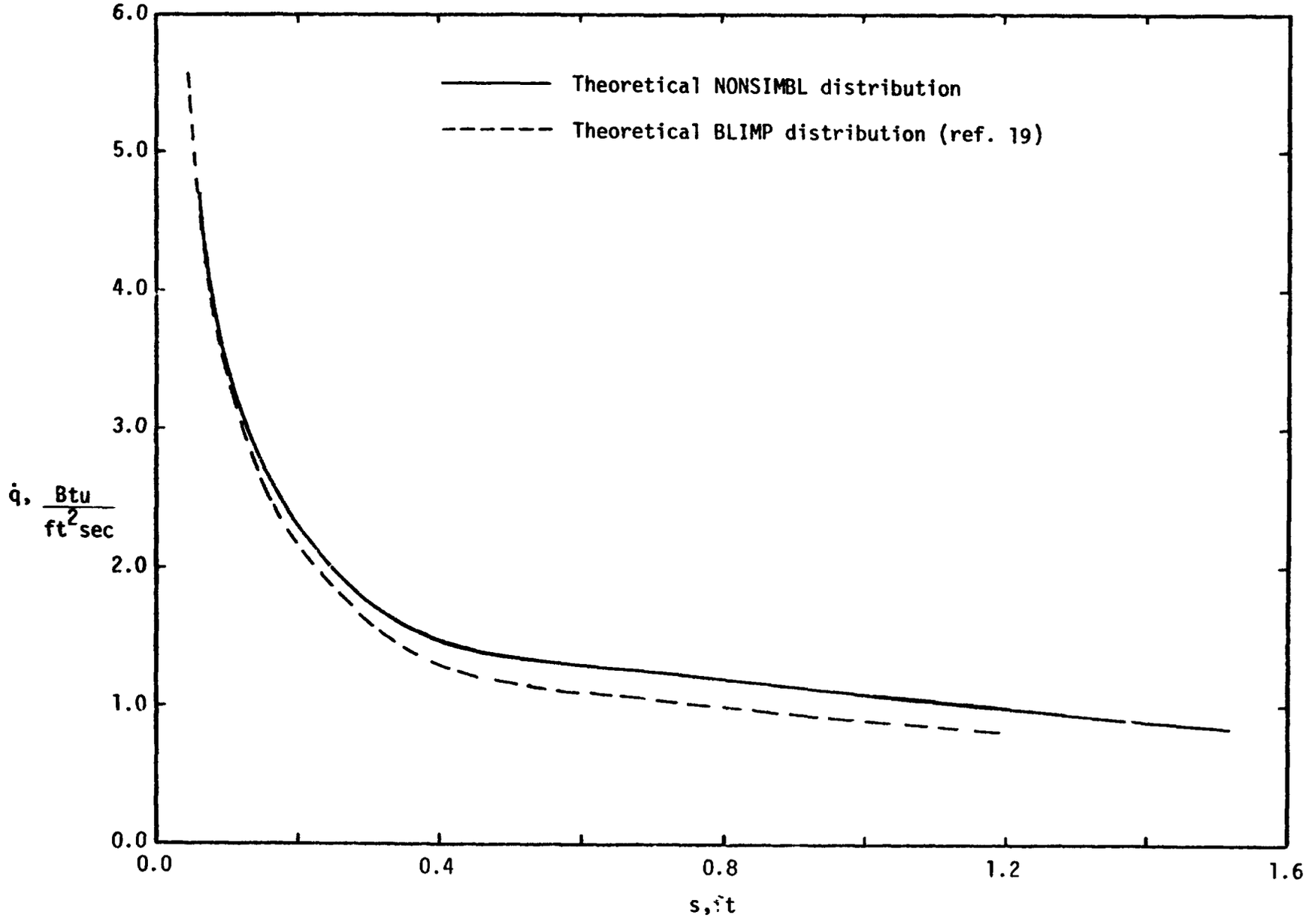

Figure 8. - Heat-transfer distribution for the plane-of-symmetry, $Re_{\infty,L} = 1.9 \times 10^6$, $T_w = 0.423\ T_t$, $\alpha = 30°$.

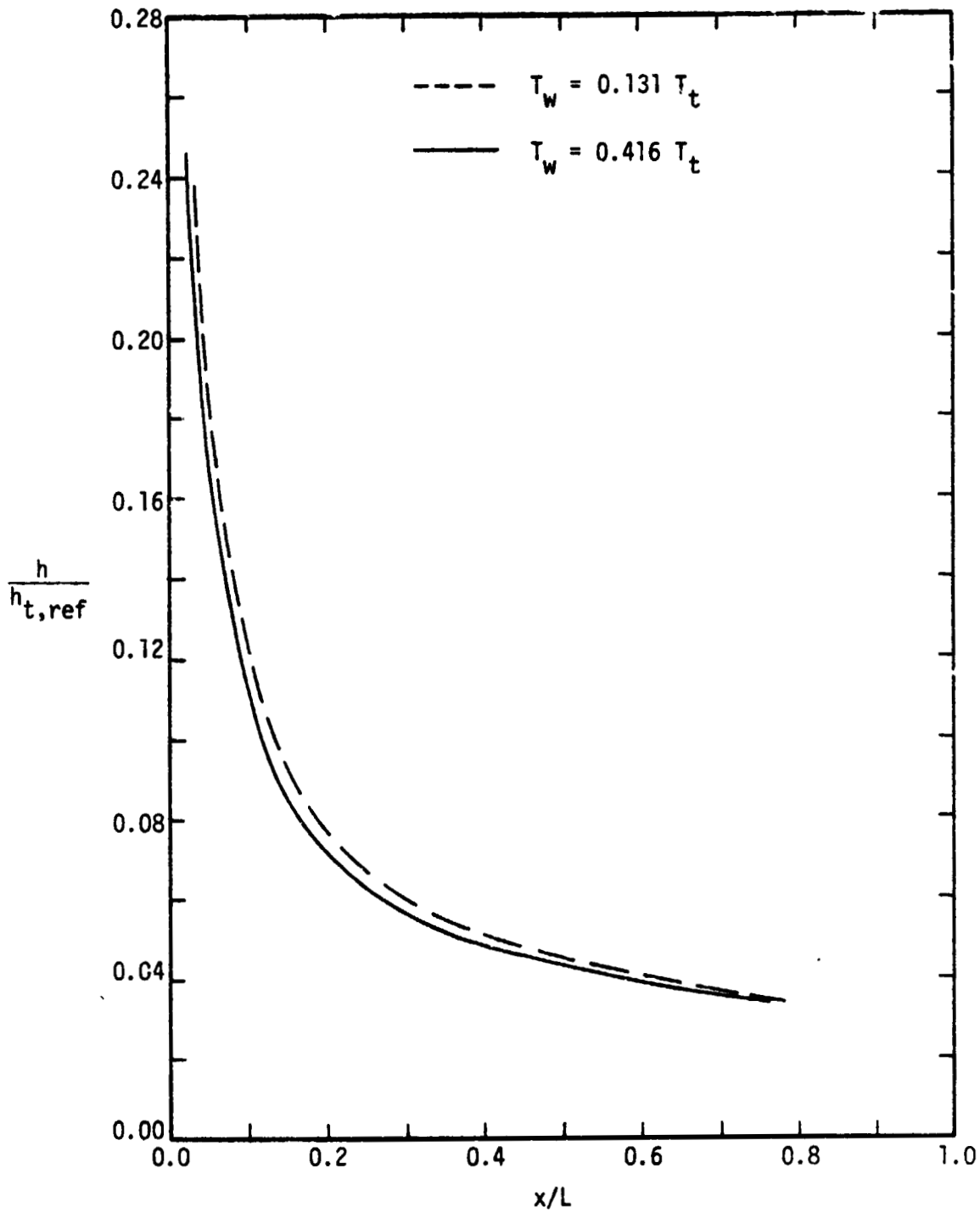

(a) Mod Newt NSE, $\alpha = 30°$

Figure 9. - The effect of the surface temperature (value independent of position) on the heat-transfer distribution for the plane of symmetry, $Re_{\infty,L} = 3.7 \times 10^6$.

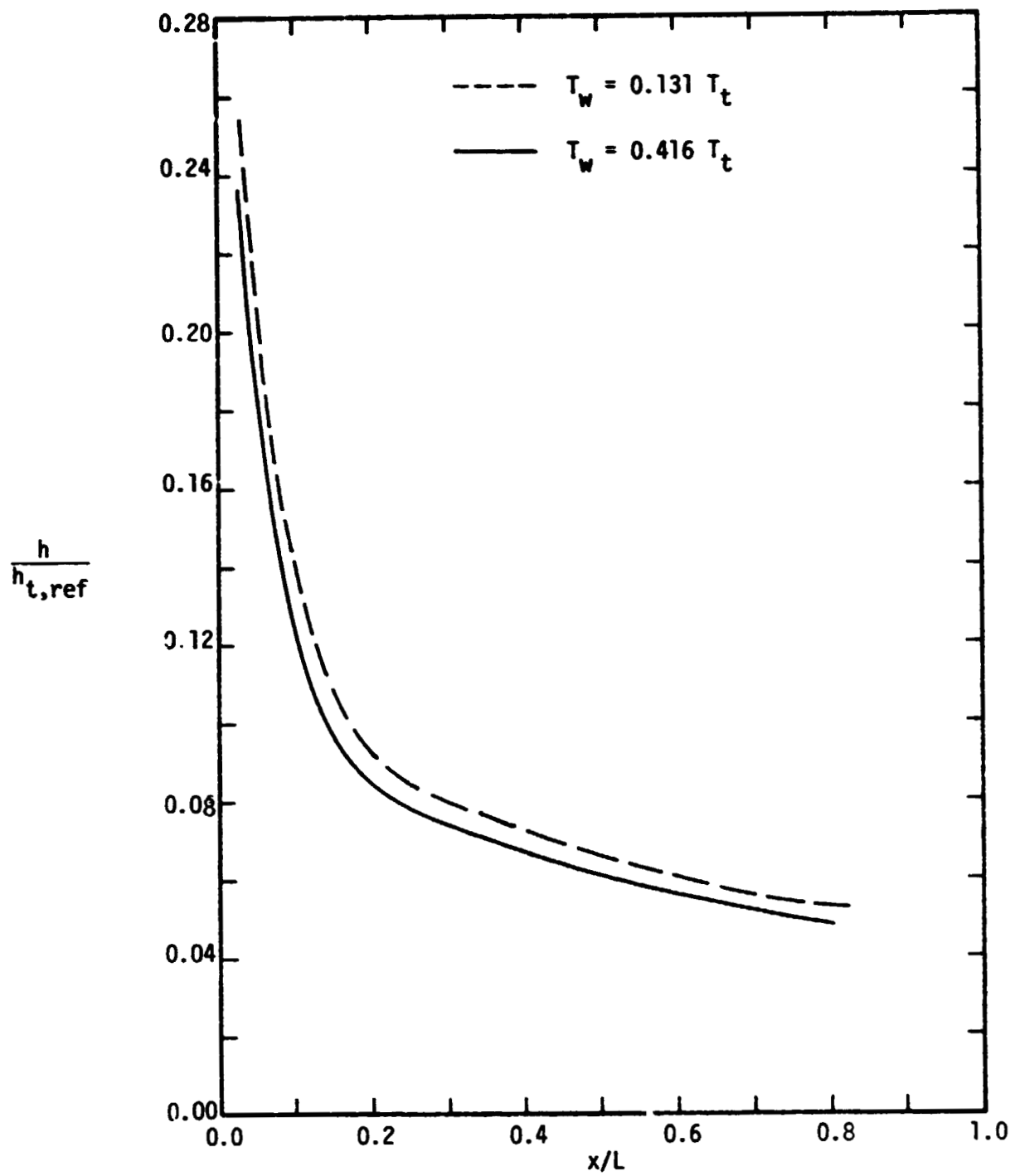

(b) Var Ent, $\alpha = 30°$

Figure 9. - Continued.

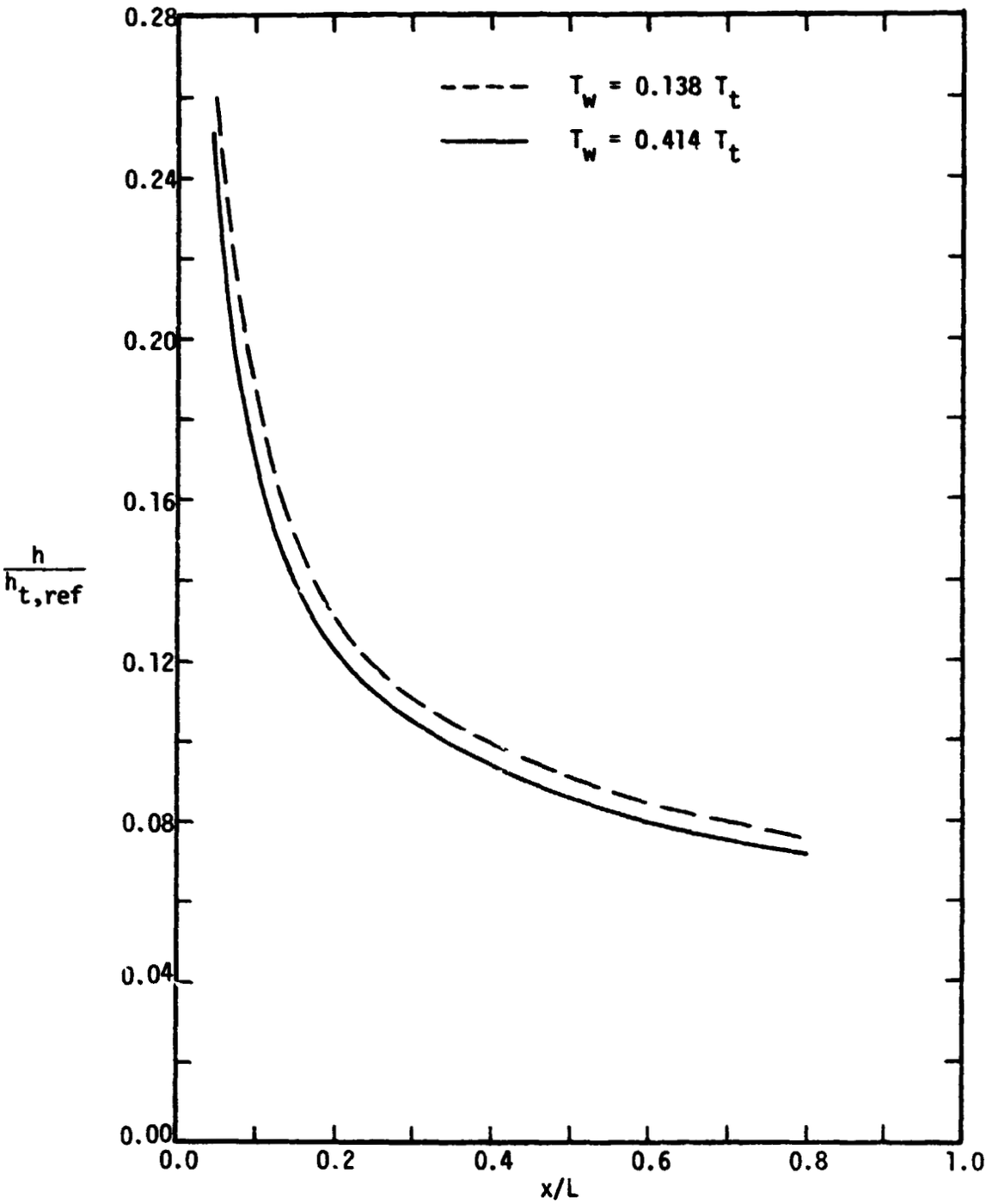

(c) Var Ent, $\alpha = 40°$

Figure 9. - Concluded.

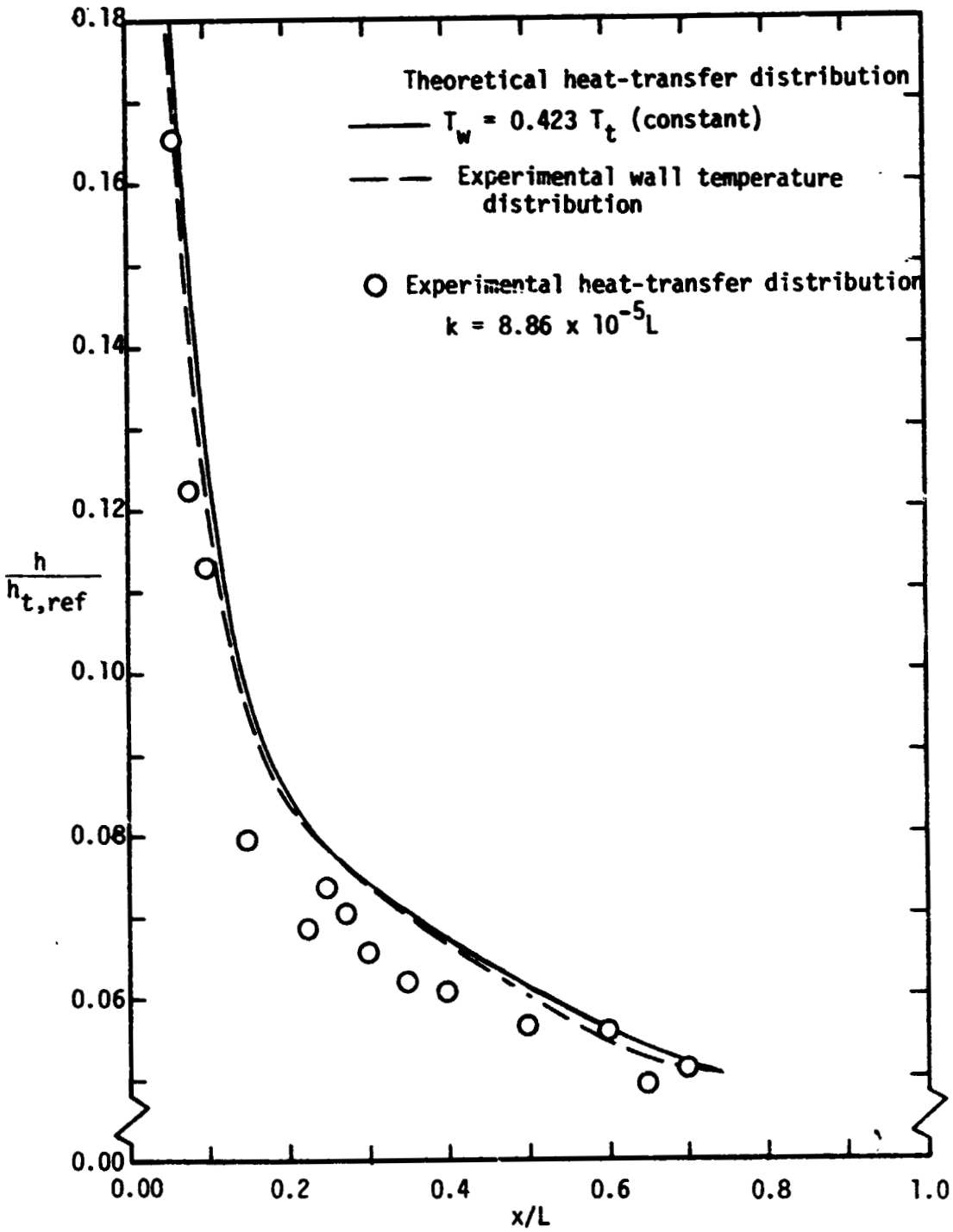

Figure 10. - The effect of the surface temperature distribution on the heat transfer distribution, $Re_{\infty,L} = 1.9 \times 10^6$, $\alpha = 30°$.

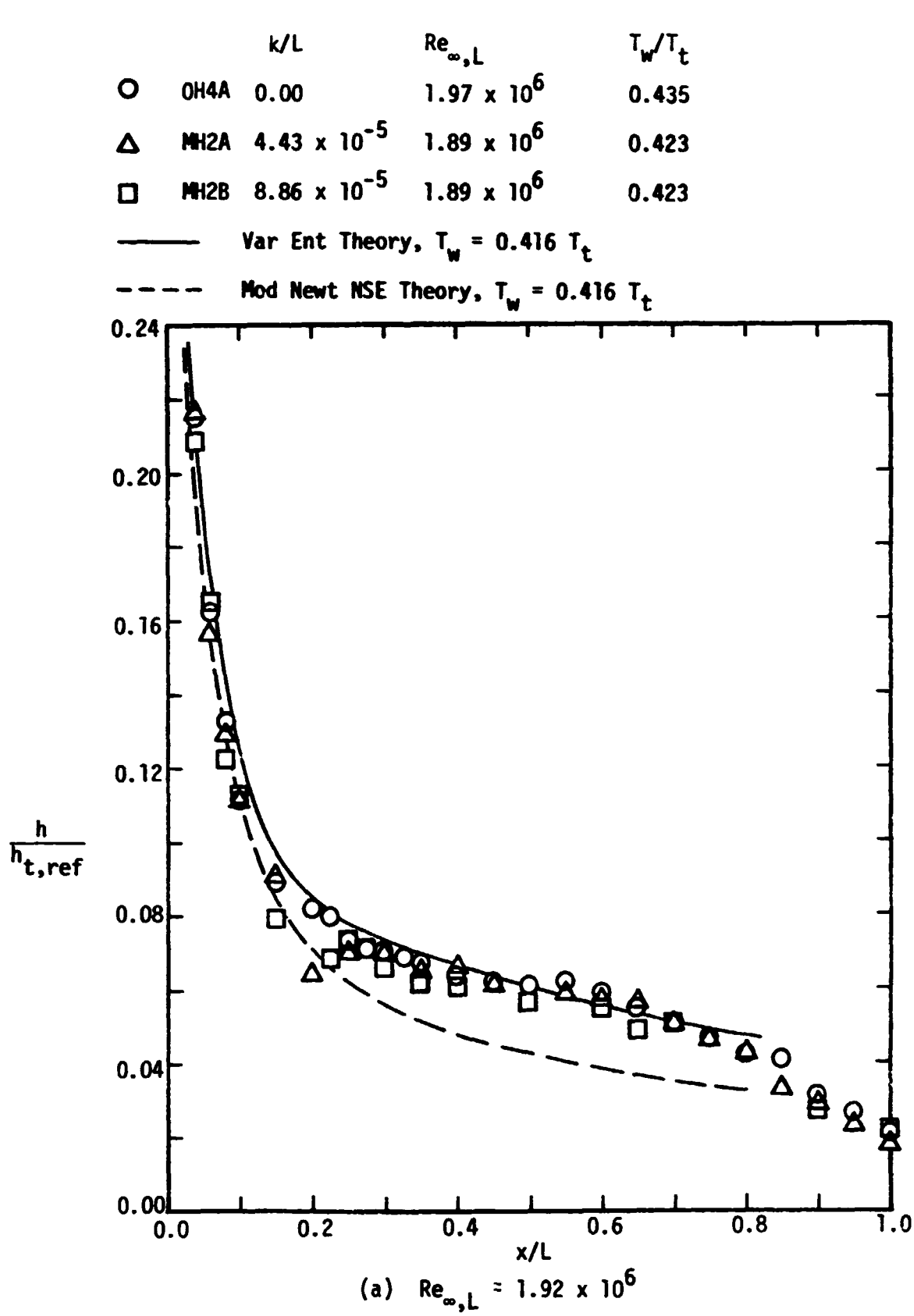

(a) $Re_{\infty,L} = 1.92 \times 10^6$

Figure 11. - The effect of tile misalignment height on the heat-transfer distribution for $\alpha = 30°$.

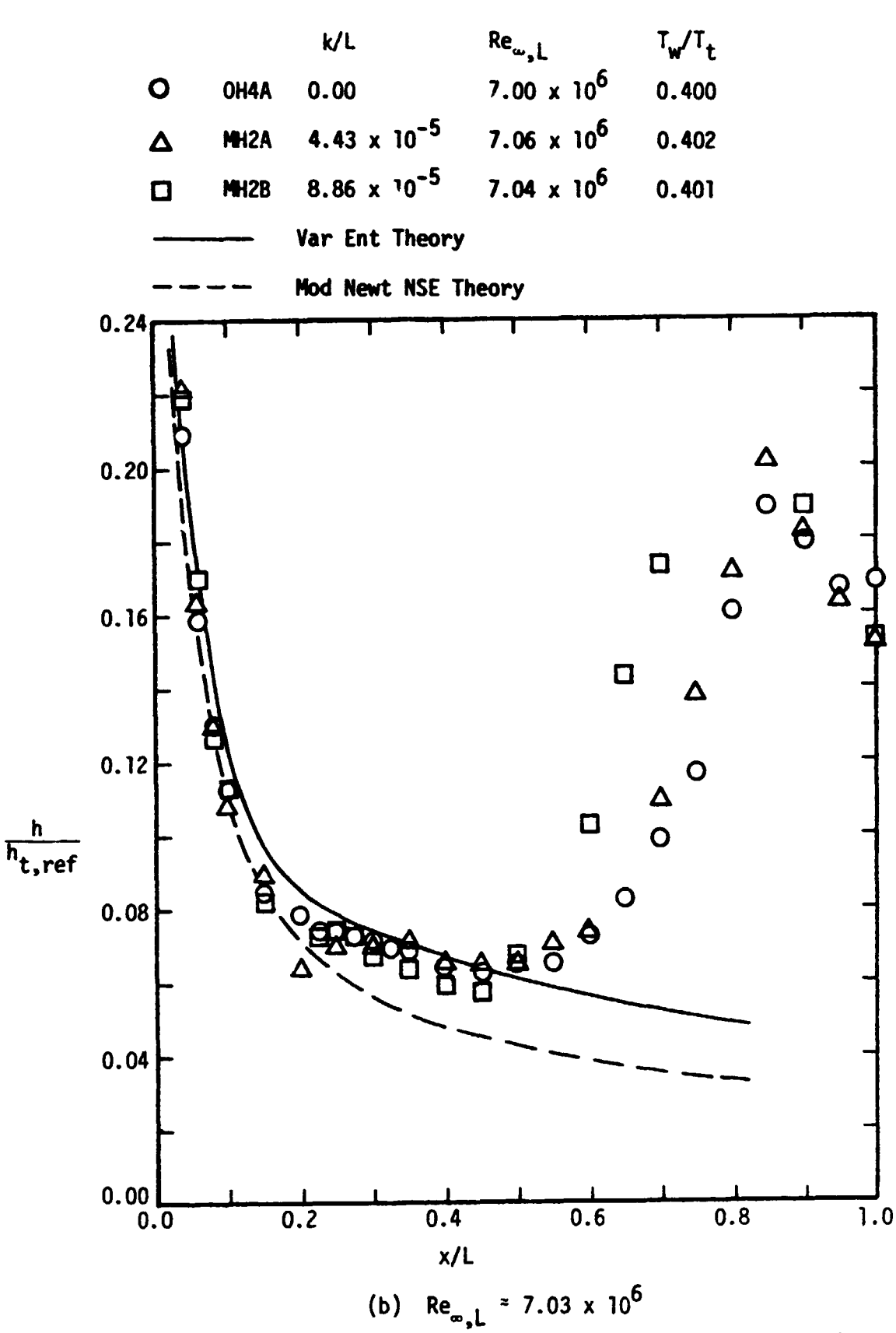

(b) $Re_{\infty,L} = 7.03 \times 10^6$

Figure 11. - Concluded.

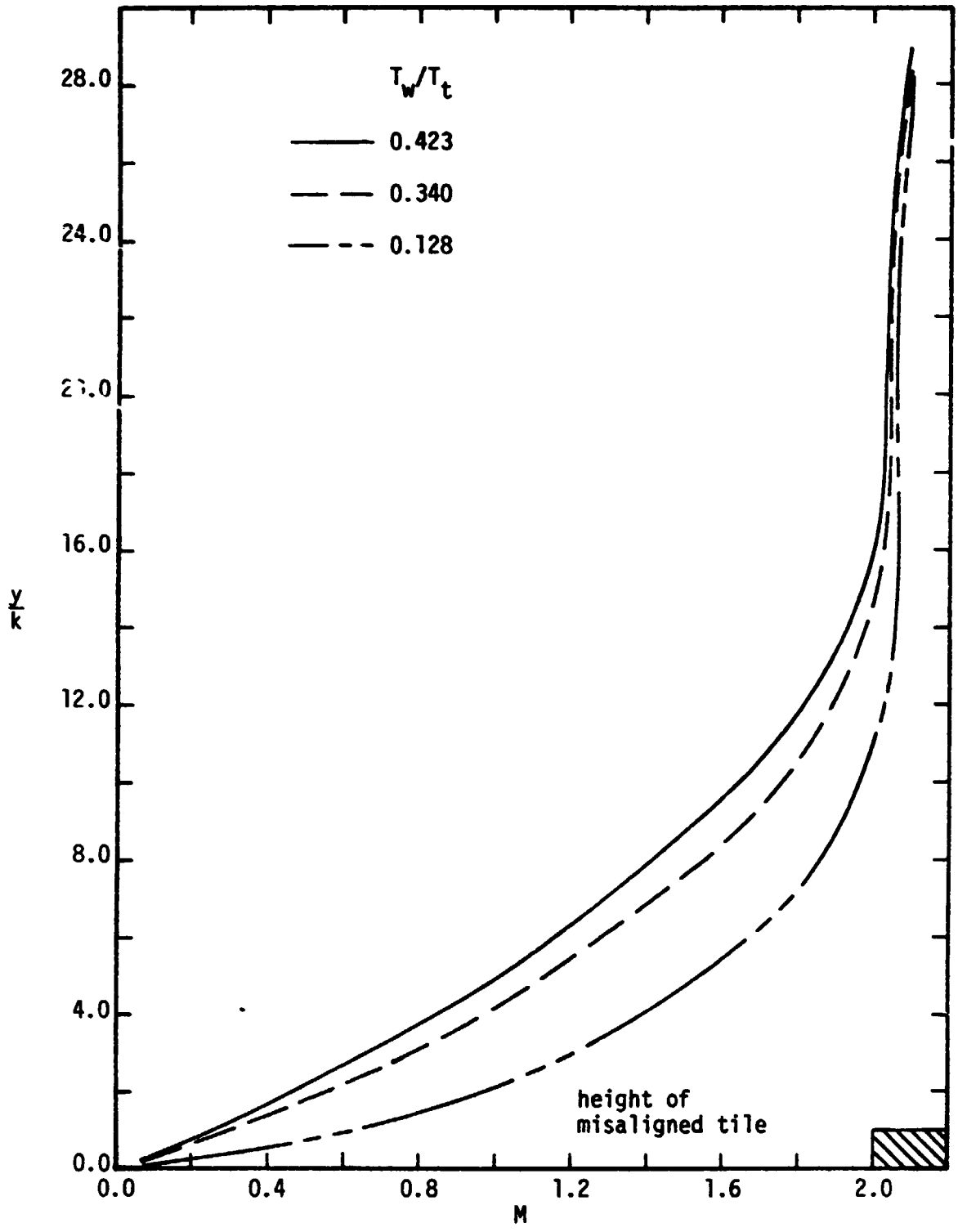

Figure 12. - The effect of surface temperature on the theoretical Mach-number distribution in a laminar boundary-layer at $\alpha = 30°$ for $Re_{\infty,L} = 1.9 \times 10^6$ at $x = 0.255L$.

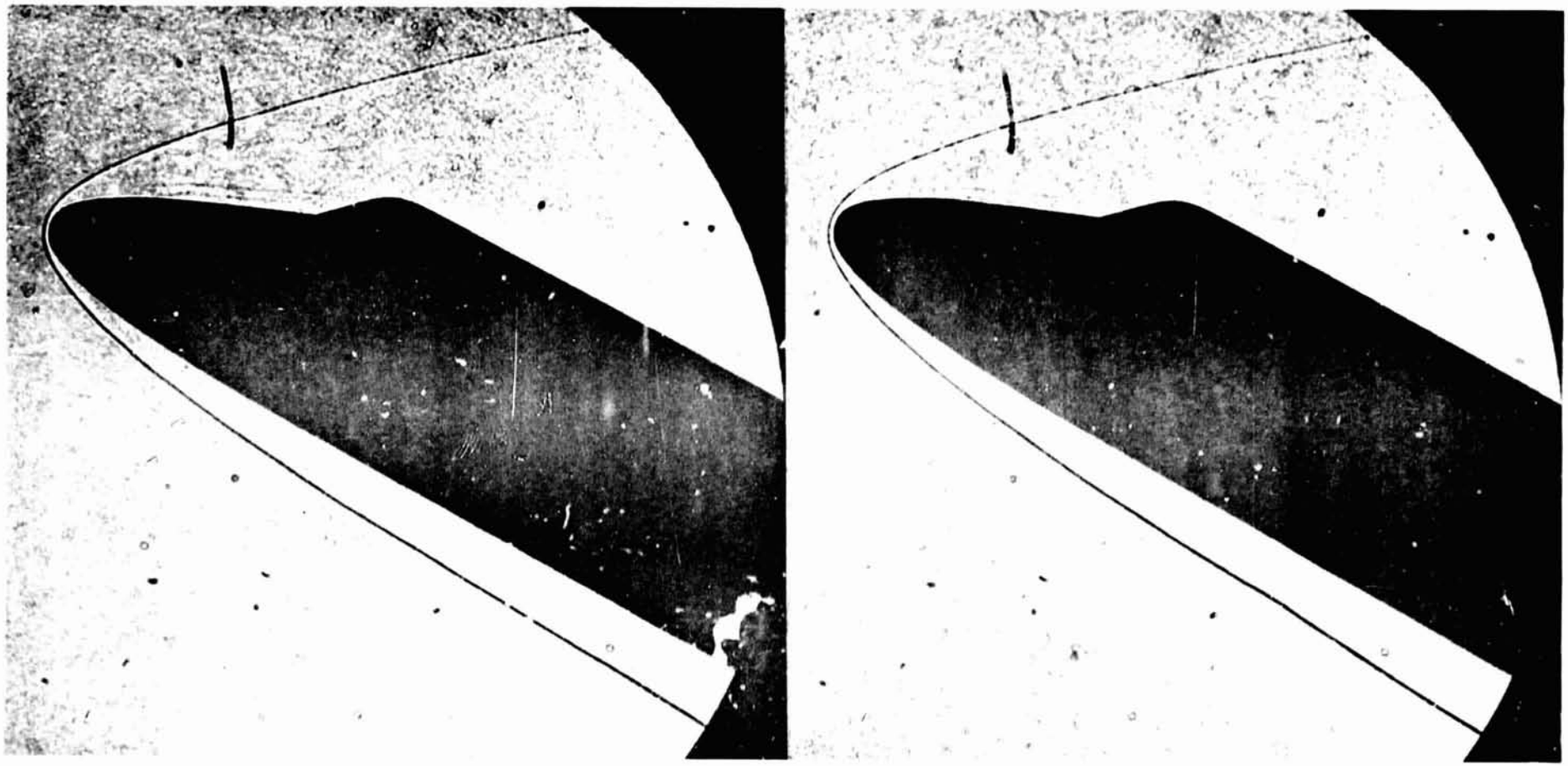

(a) $T_w = 0.423\ T_t$ (b) $T_w = 0.340\ T_t$

Figure 13. - Shadowgraphs for the MH2B Orbiter (i.e., $k = 8.86 \times 10^{-5} L$) at $\alpha = 30°$, $Re_{\infty,L} = 1.88 \times 10^6$

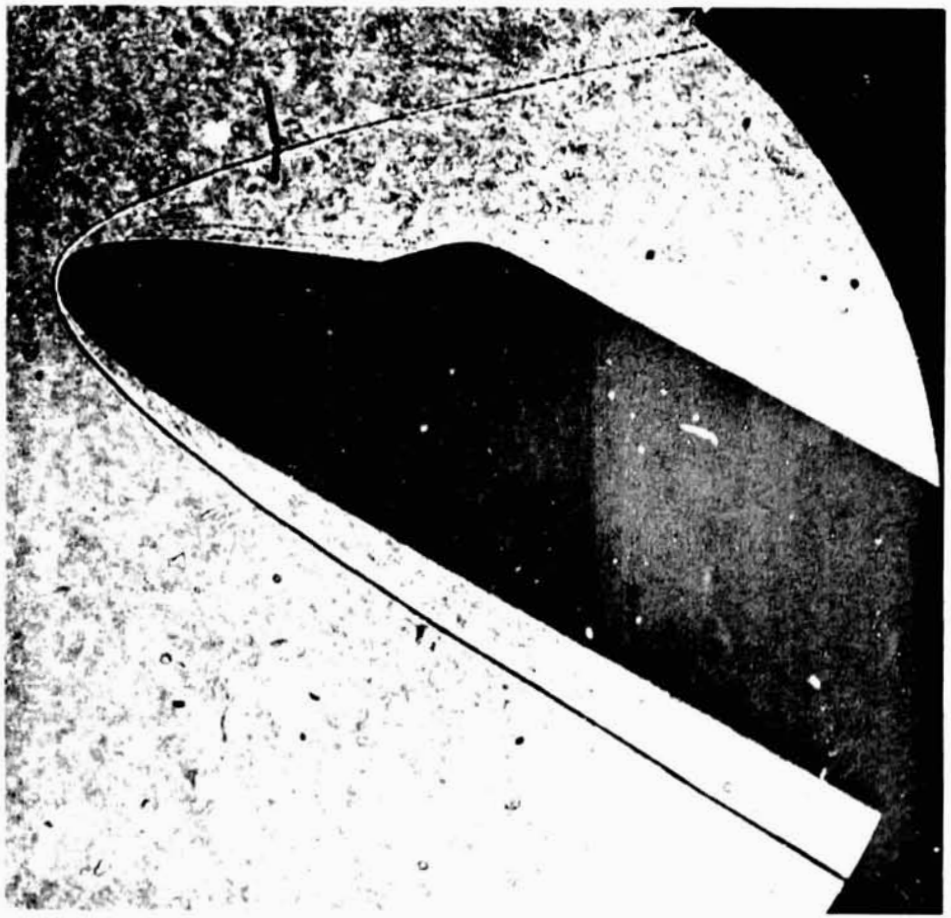

(c) $T_w = 0.128\ T_t$

Figure 13. - Concluded.

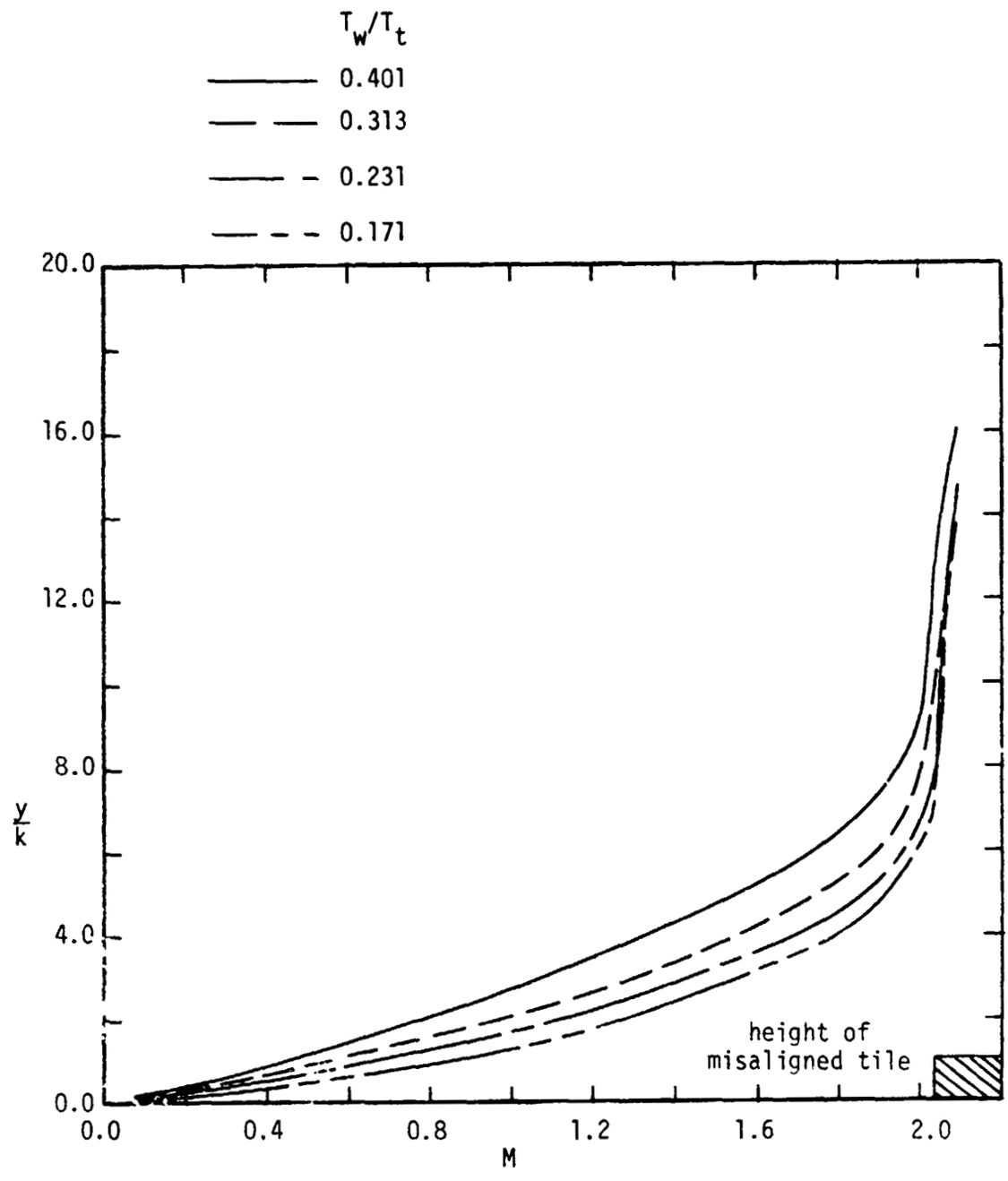

Figure 14. - The effect of surface temperature on the theoretical Mach-number distribution in a laminar boundary-layer at $\alpha = 30°$ for $Re_{\infty,L} \approx 7.1 \times 10^6$ at $x = 0.255L$.

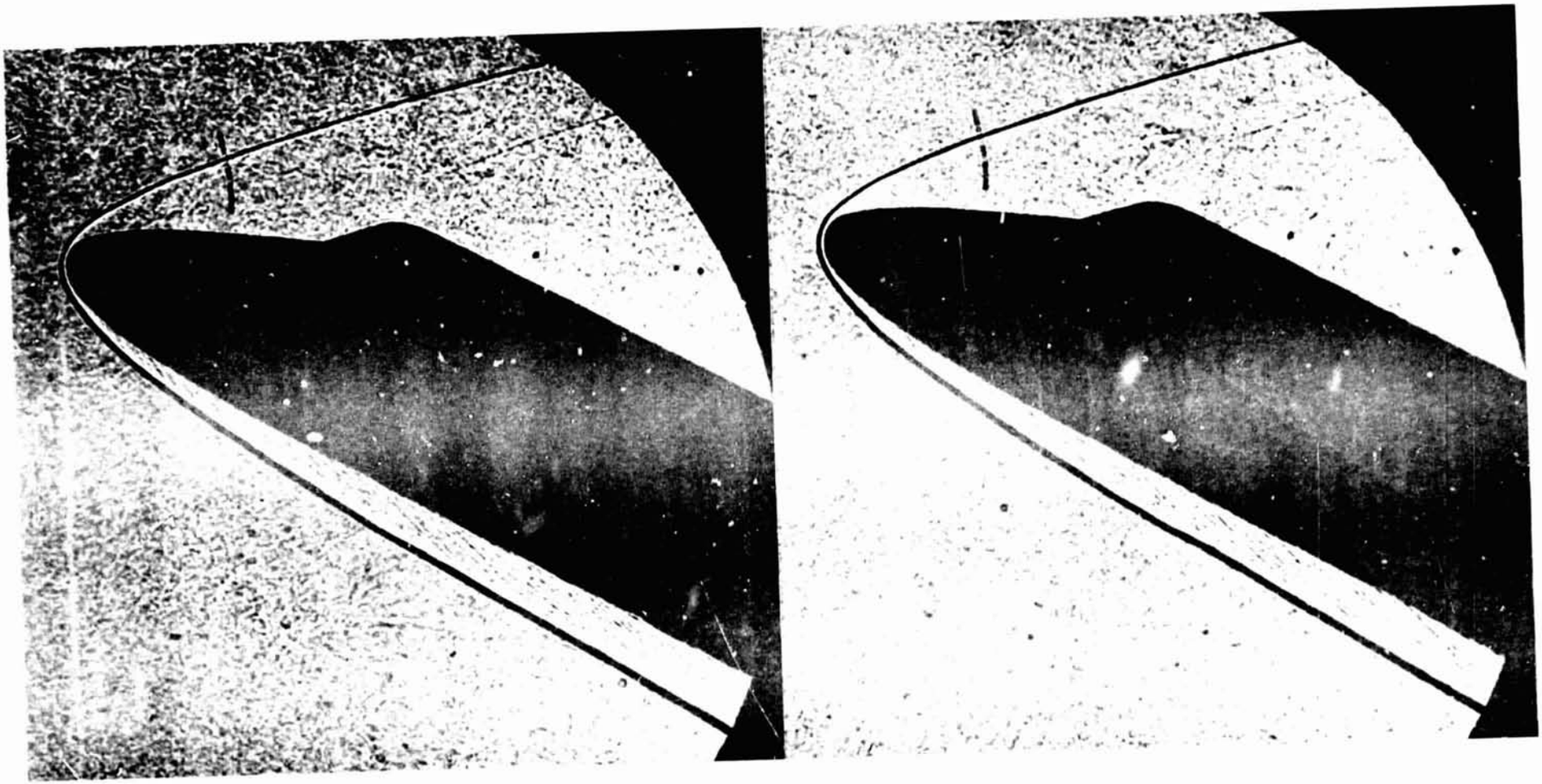

(a) $T_w = 0.401\ T_t$

(b) $T_w = 0.313\ T_t$

Figure 15. - Shadowgraphs for the MH2B Orbiter (i.e., $k = 3.86 \times 10^{-5} L$) at $\alpha = 30°$ $Re_{\infty,L} \approx 7.07 \times 10^6$.

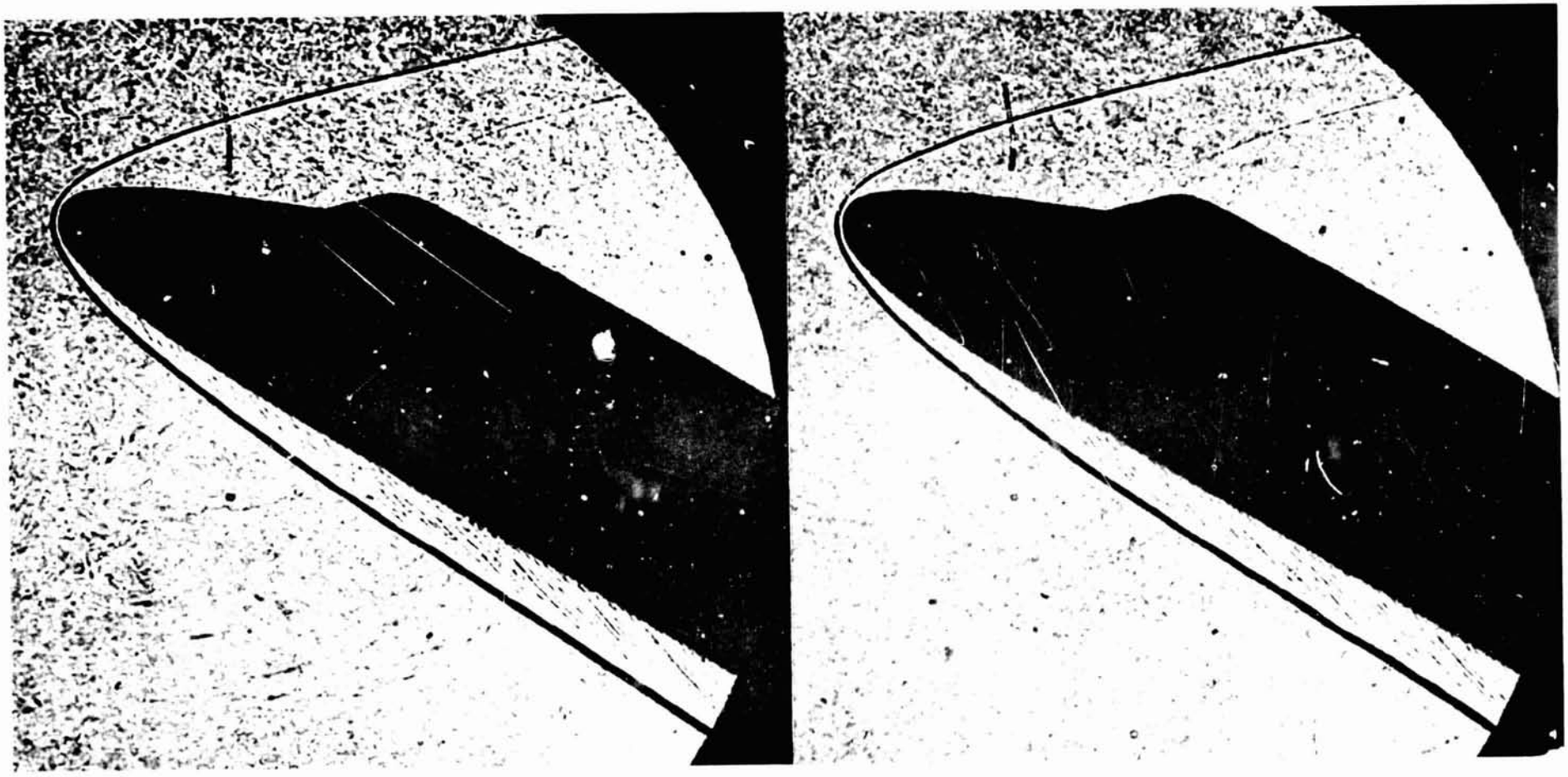

(c) $T_w = 0.231\ T_t$

(d) $T_w = 0.171\ T_t$

Figure 15. - Concluded.

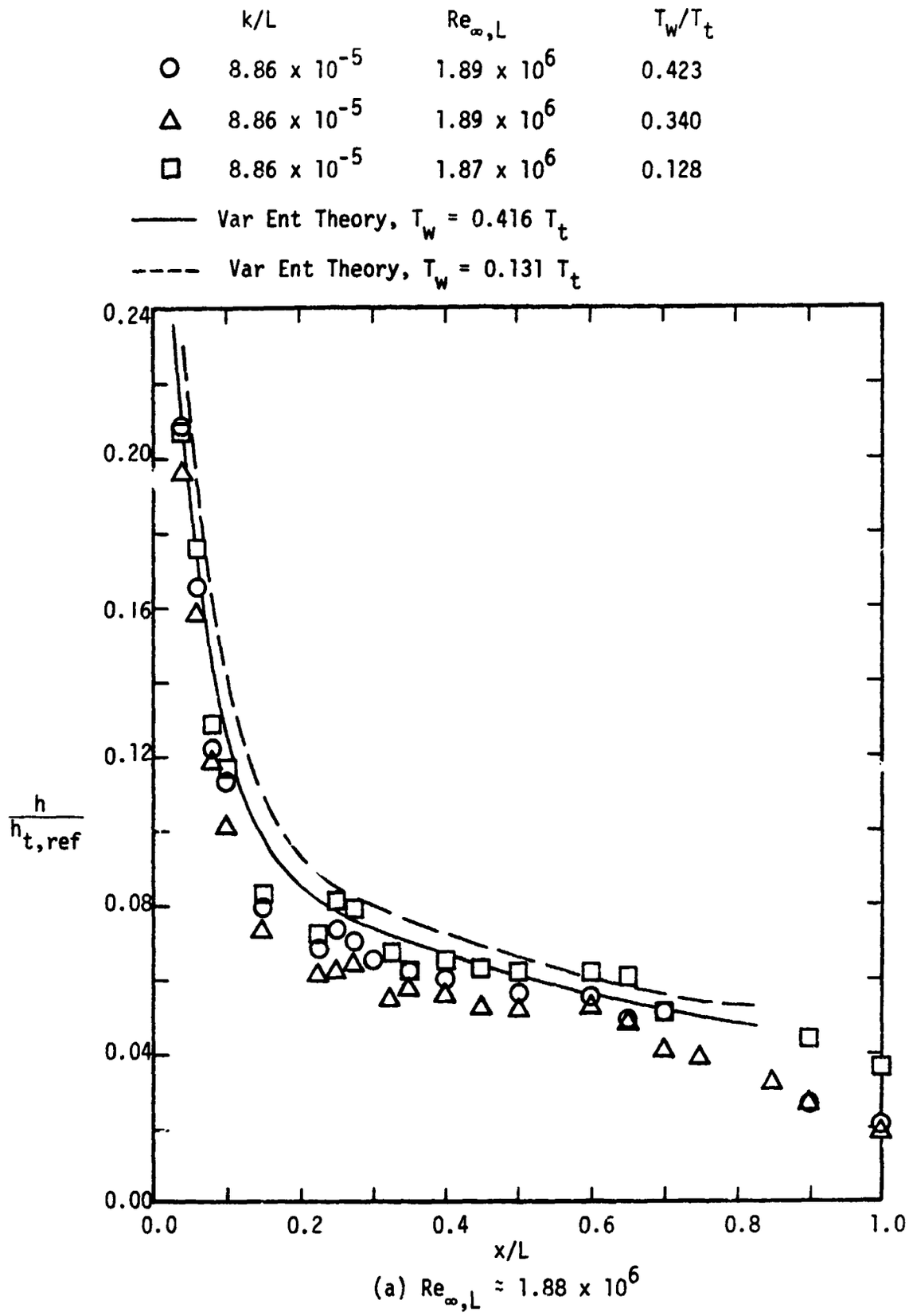

Figure 16. - The effect of surface temperature on the heat-transfer distribution for the MH2B at $\alpha = 30°$.

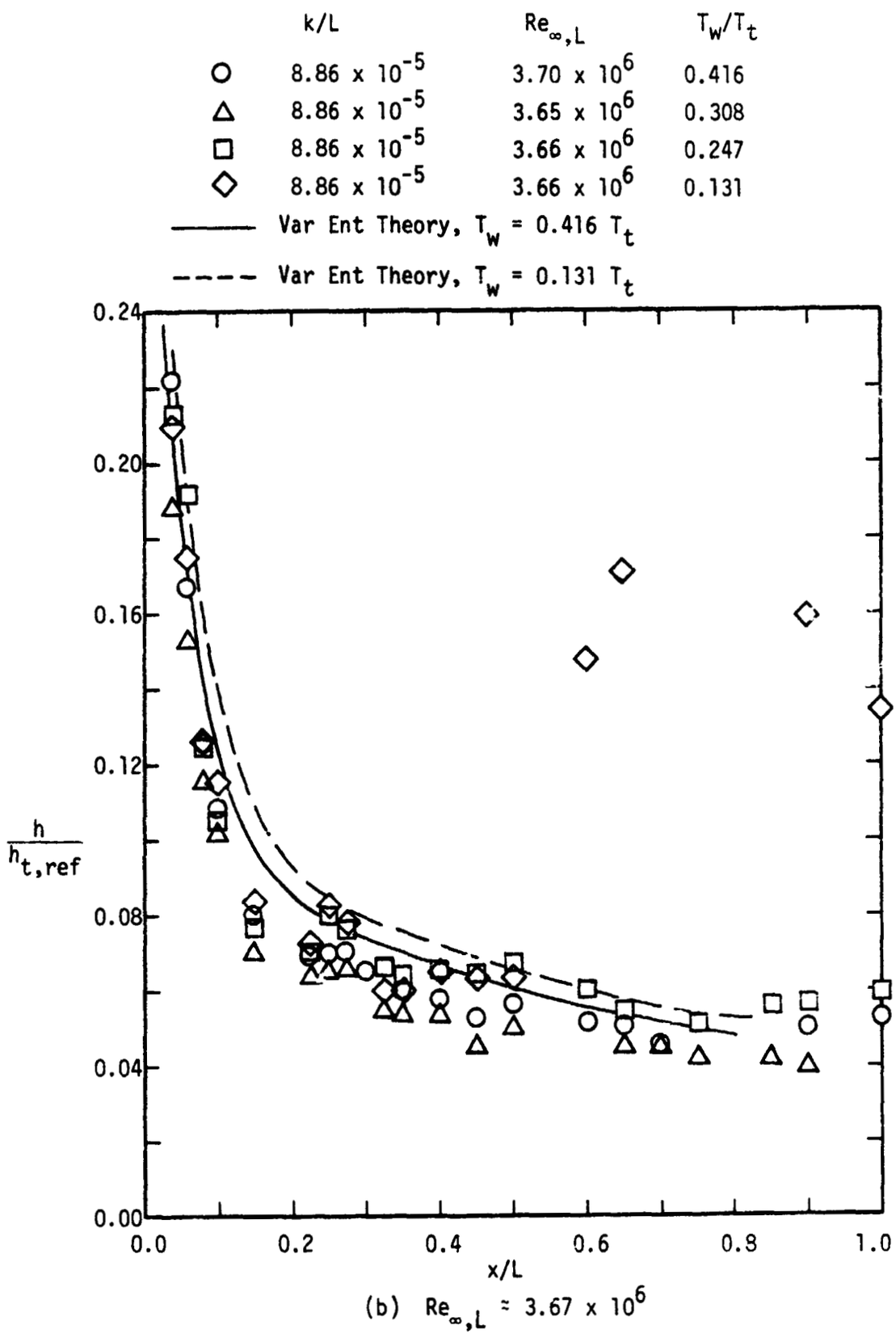

(b) $Re_{\infty,L} \approx 3.67 \times 10^6$

Figure 16. - Continued.

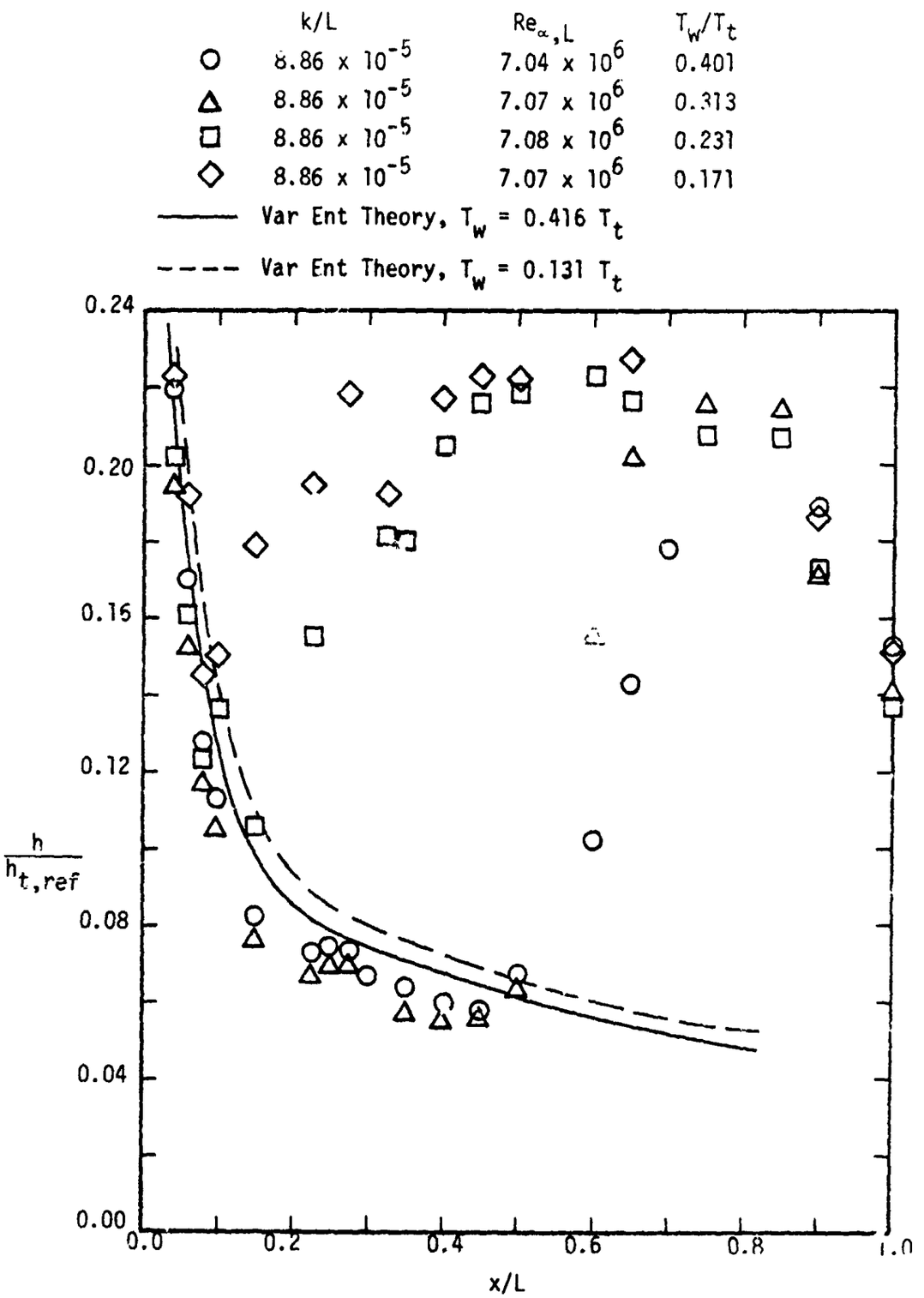

(c) $Re_{\infty,L} = 7.07 \times 10^6$

Figure 16. - Concluded.

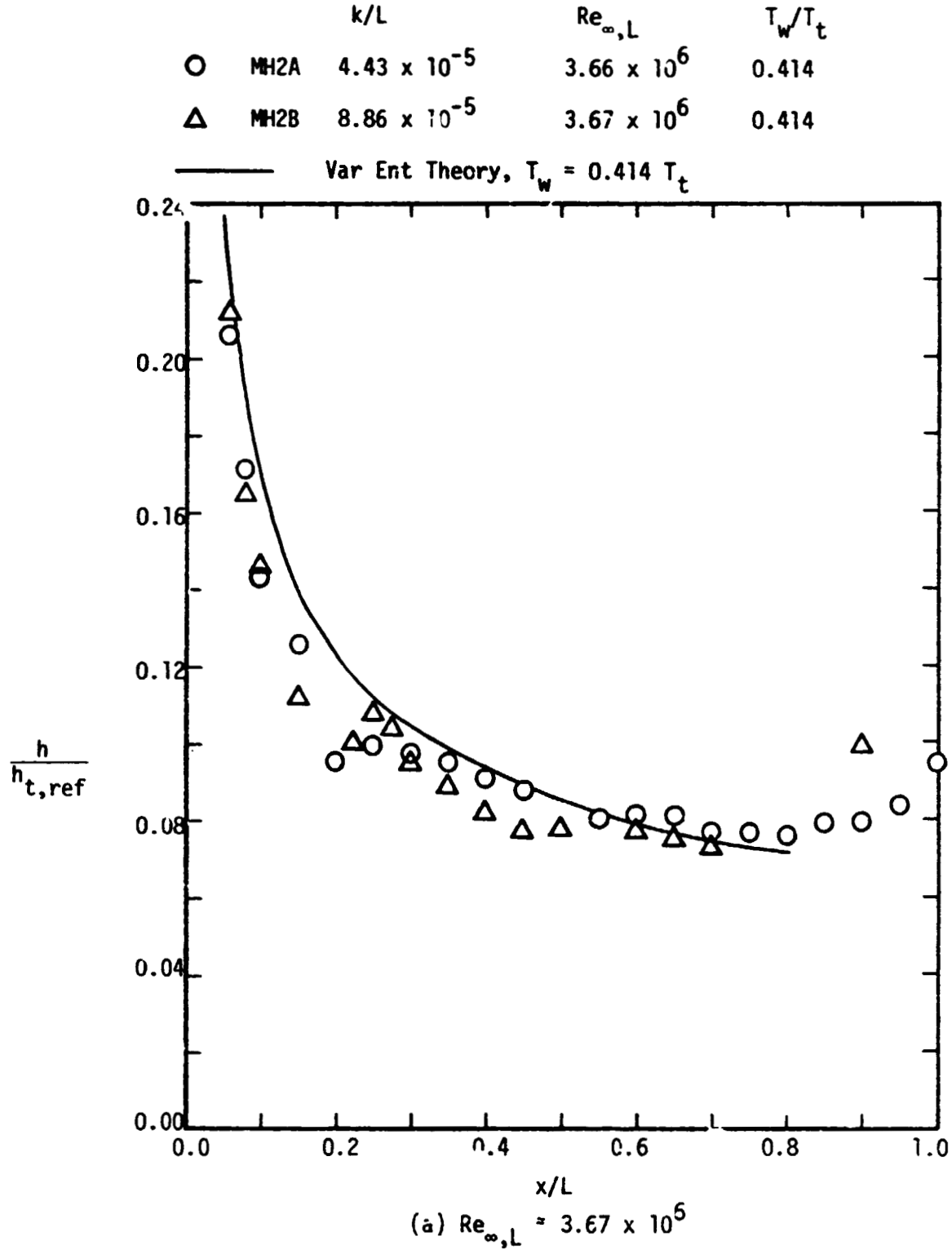

Figure 17. - The effect of tile misalignment height on the heat-transfer distribution for α = 40°.

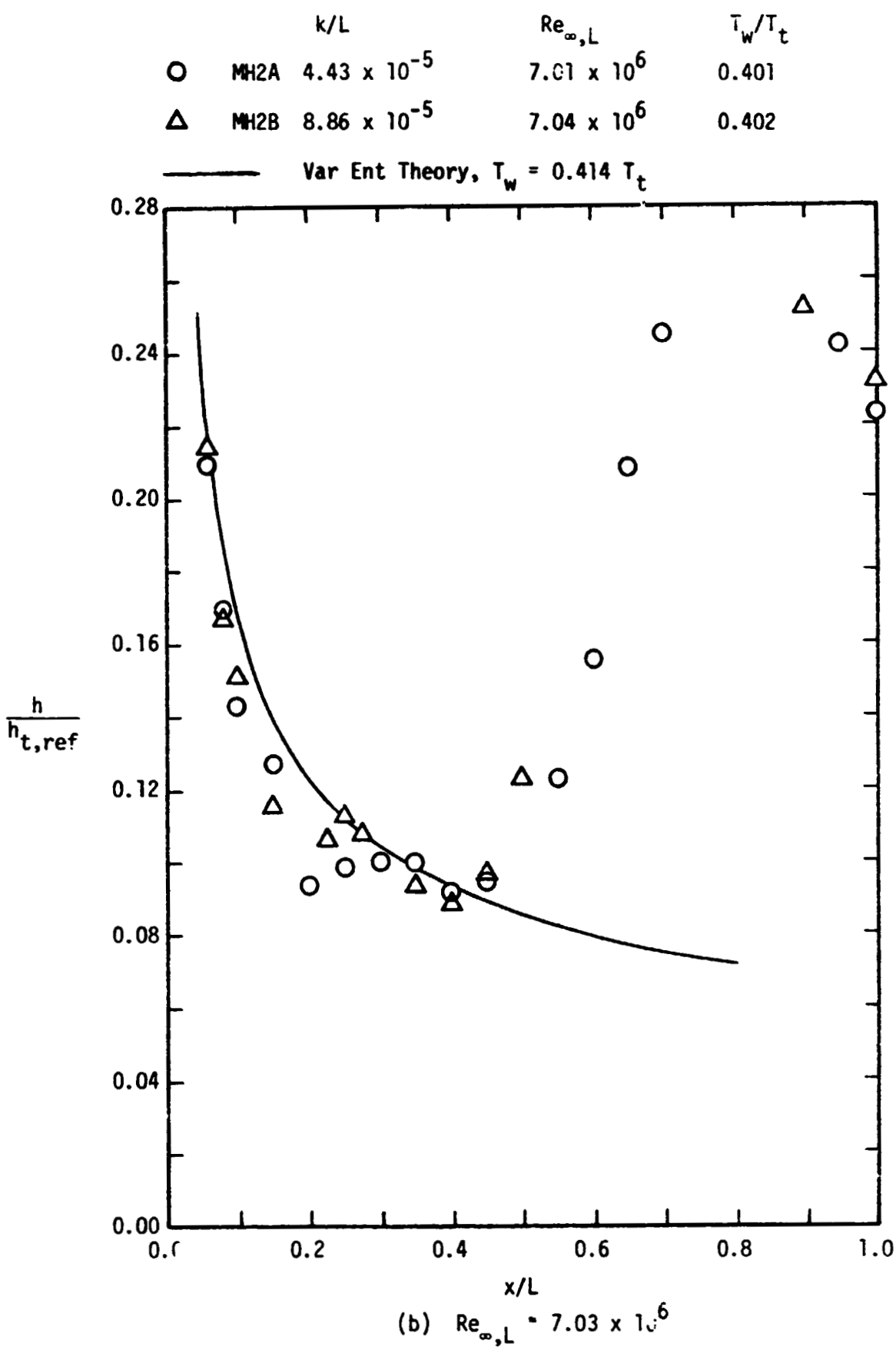

(b) $Re_{\infty,L}$ = 7.03 x 10^6

Figure 17. - Concluded.

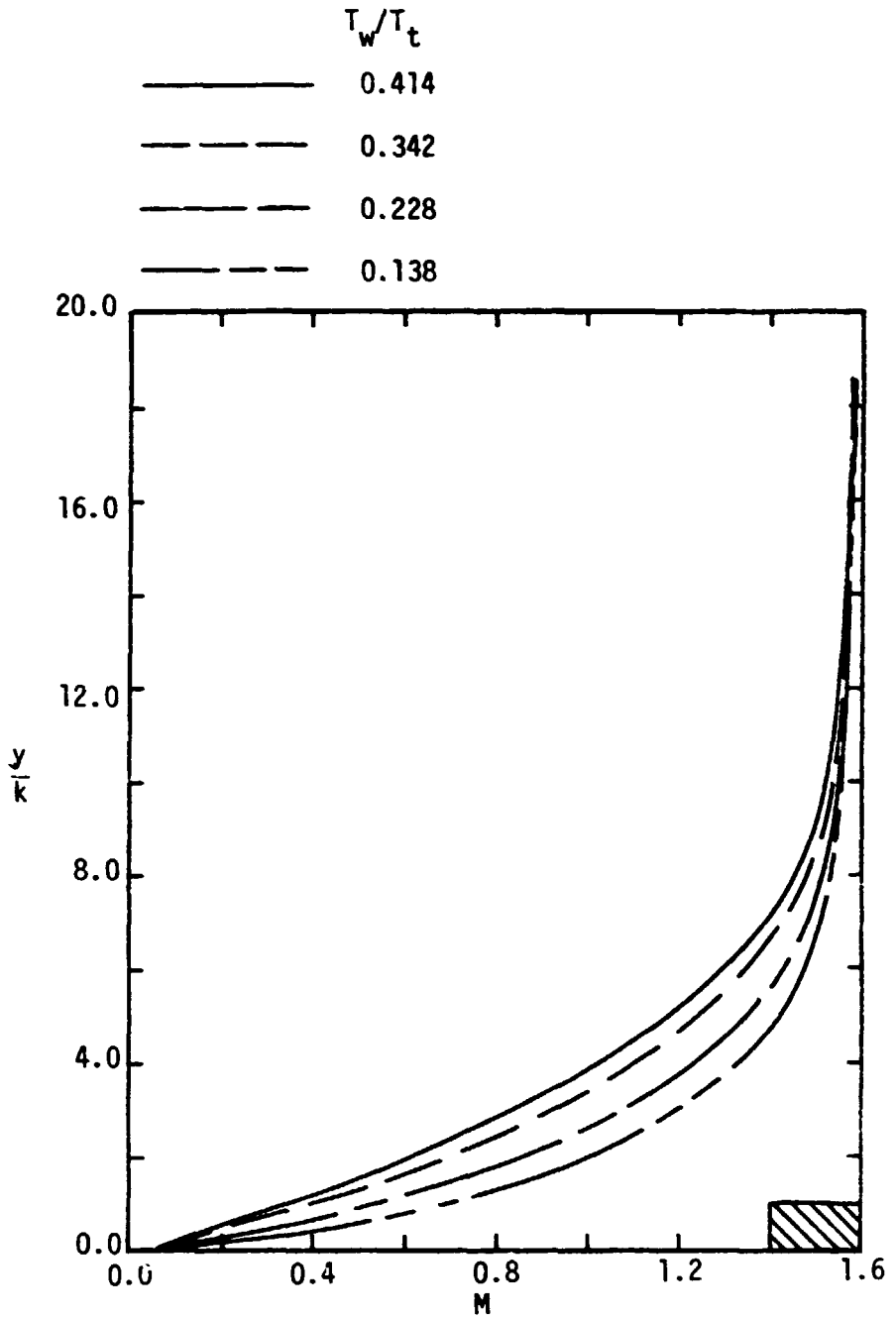

Figure 18. - The effect of surface temperature on the theoretical Mach-number distribution in a laminar boundary layer at $\alpha \approx 40°$ for $Re_{\infty,L} \approx 3.8 \times 10^6$ at $x = 0.255L$

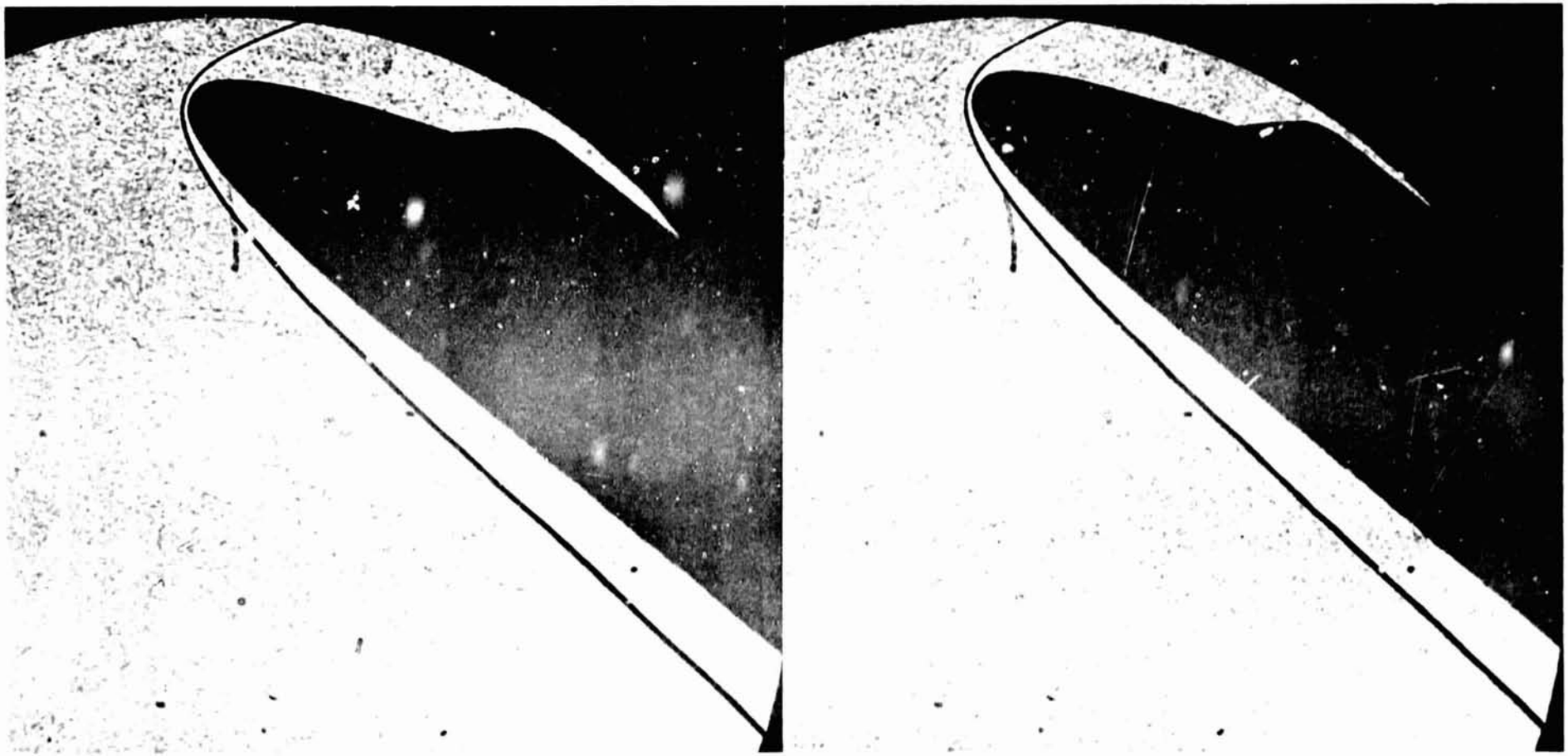

(a) $T_w = 0.414\ T_t$

(b) $T_w = 0.342\ T_t$

Figure 19. - Shadowgraphs for the MH2B Orbiter (i.e, $k = 8.86 \times 10^{-5} L$ at $\alpha = 40°$, $Re_{\infty,L} = 3.66 \times 10^6$.

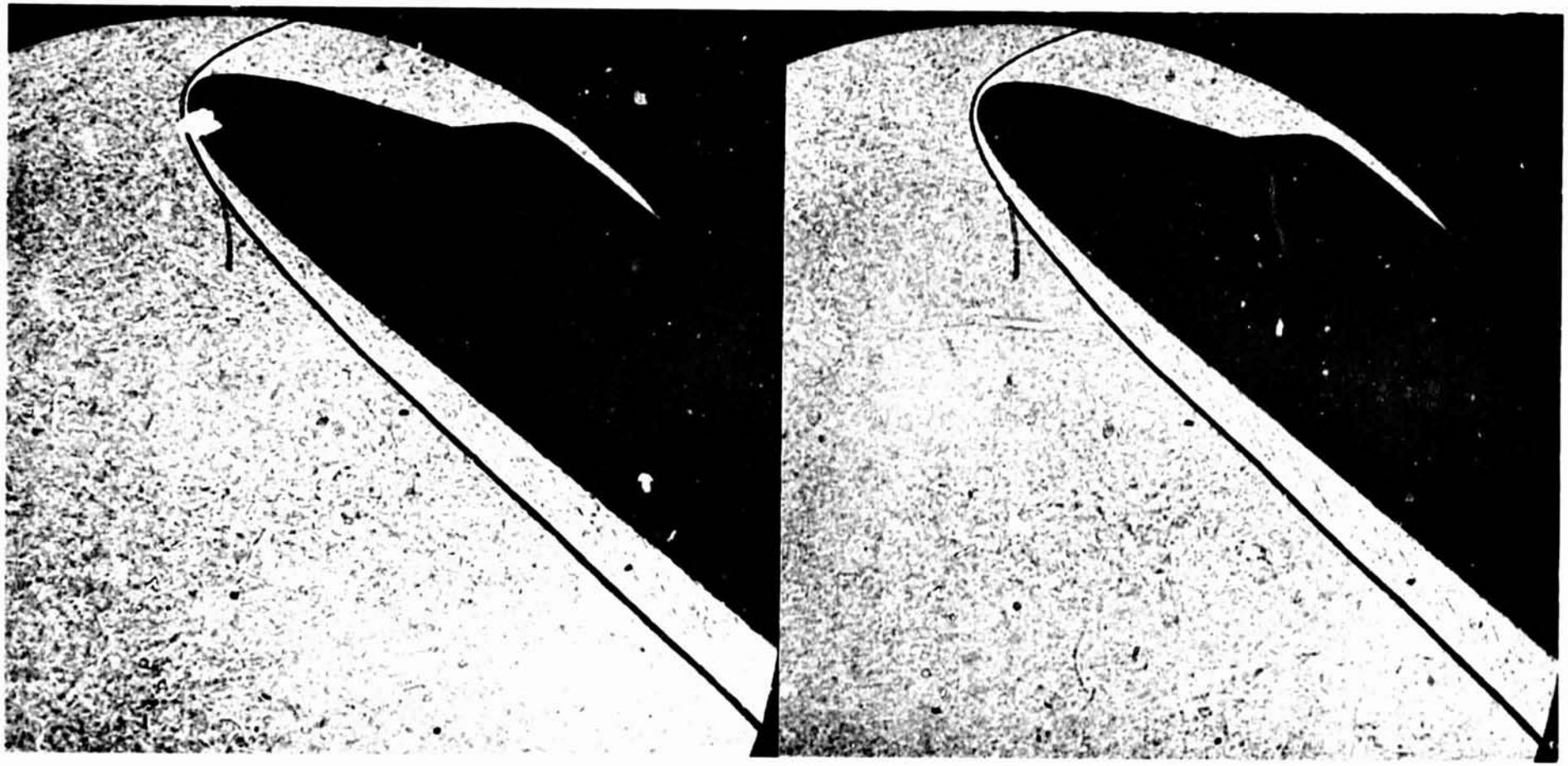

(c) $T_w = 0.228\ T_t$

(d) $T_w = 0.138\ T_t$

Figure 19. - Concluded.

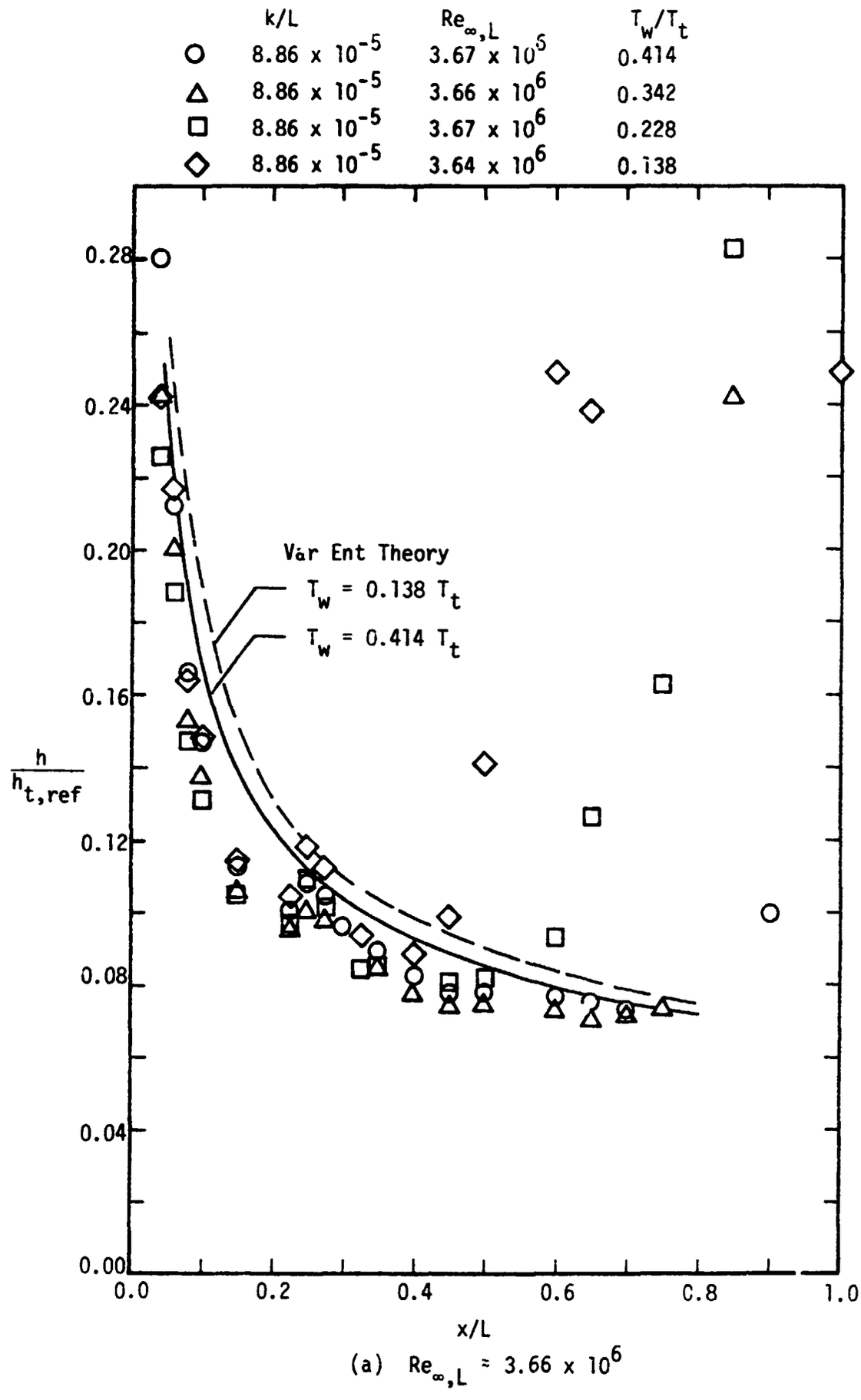

Figure 20. - The effect of surface temperature on the heat-transfer distribution for the MH2B at $\alpha = 40°$.

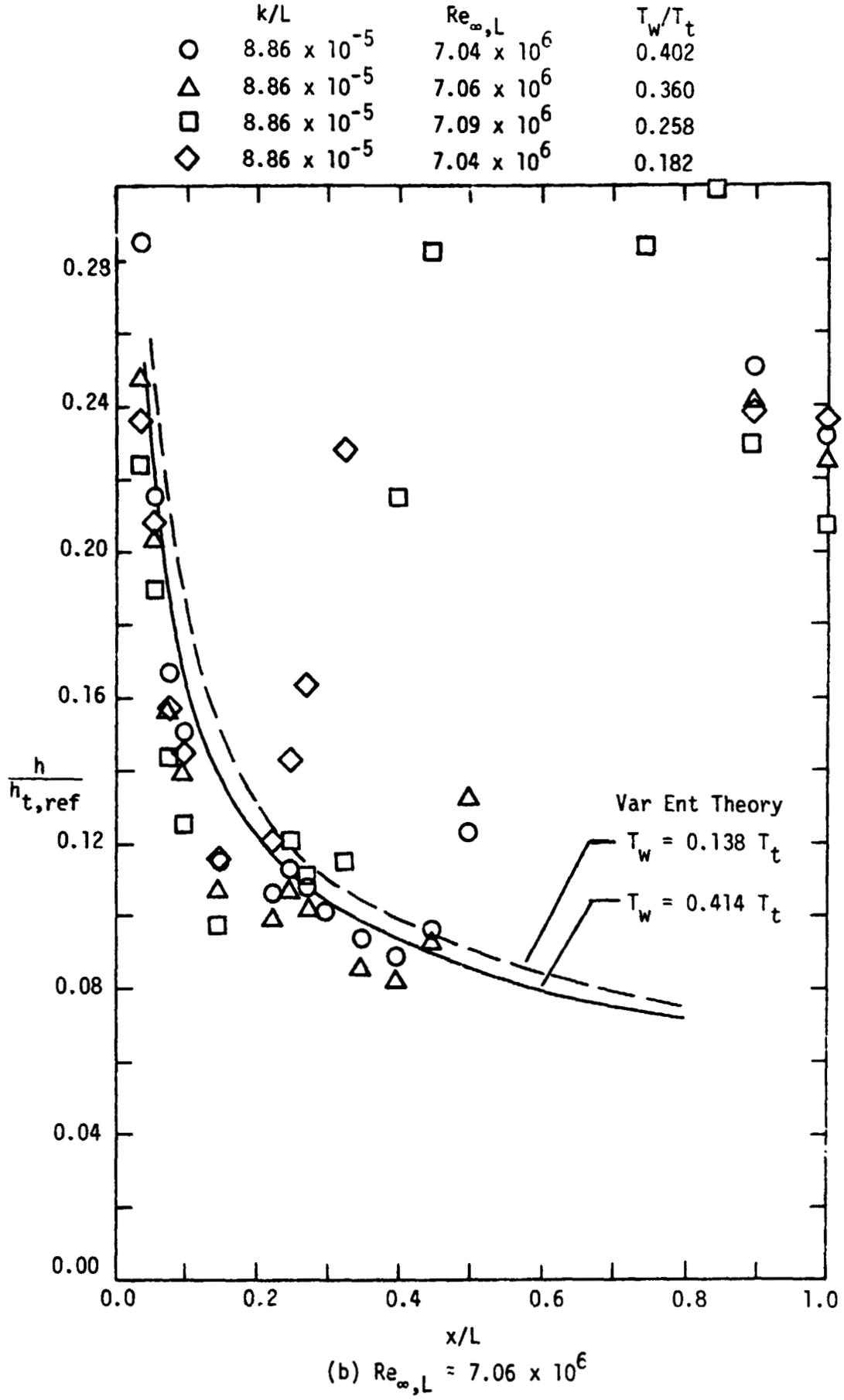

(b) $Re_{\infty,L} = 7.06 \times 10^6$

Figure 20. - Concluded.

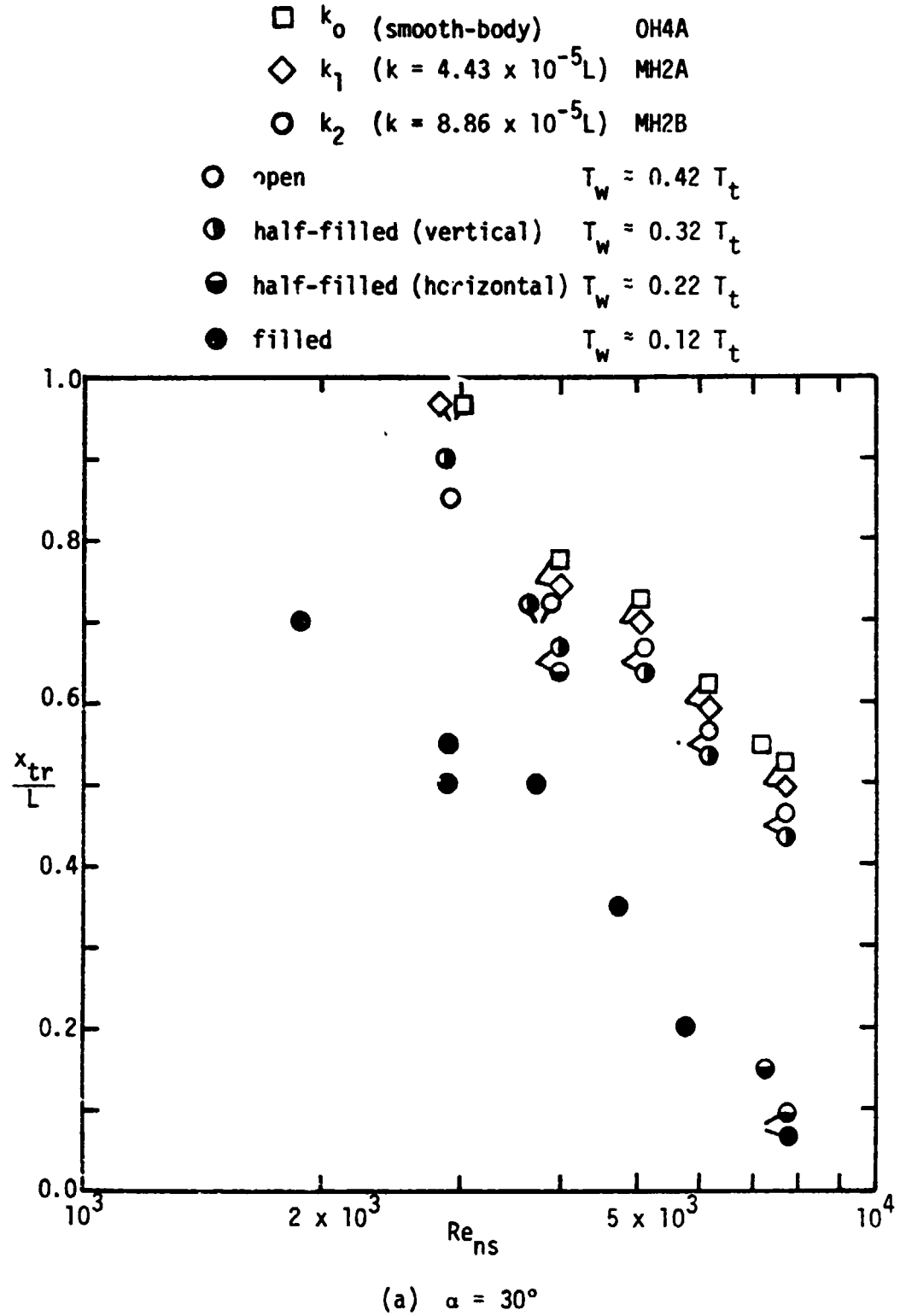

(a) $\alpha = 30°$

Figure 21. - Transition locations as a function of the Reynolds number behind a normal shock wave, data from Tunnel B.

◇ k_1 ($k = 4.43 \times 10^{-5} L$) MH2A

○ k_2 ($k = 8.86 \times 10^{-5} L$) MH2B

○ open $T_w \approx 0.42\ T_t$

◑ half-filled (vertical) $T_w \approx 0.32\ T_t$

◒ half-filled (horizontal) $T_w \approx 0.22\ T_t$

● filled $T_w \approx 0.12\ T_t$

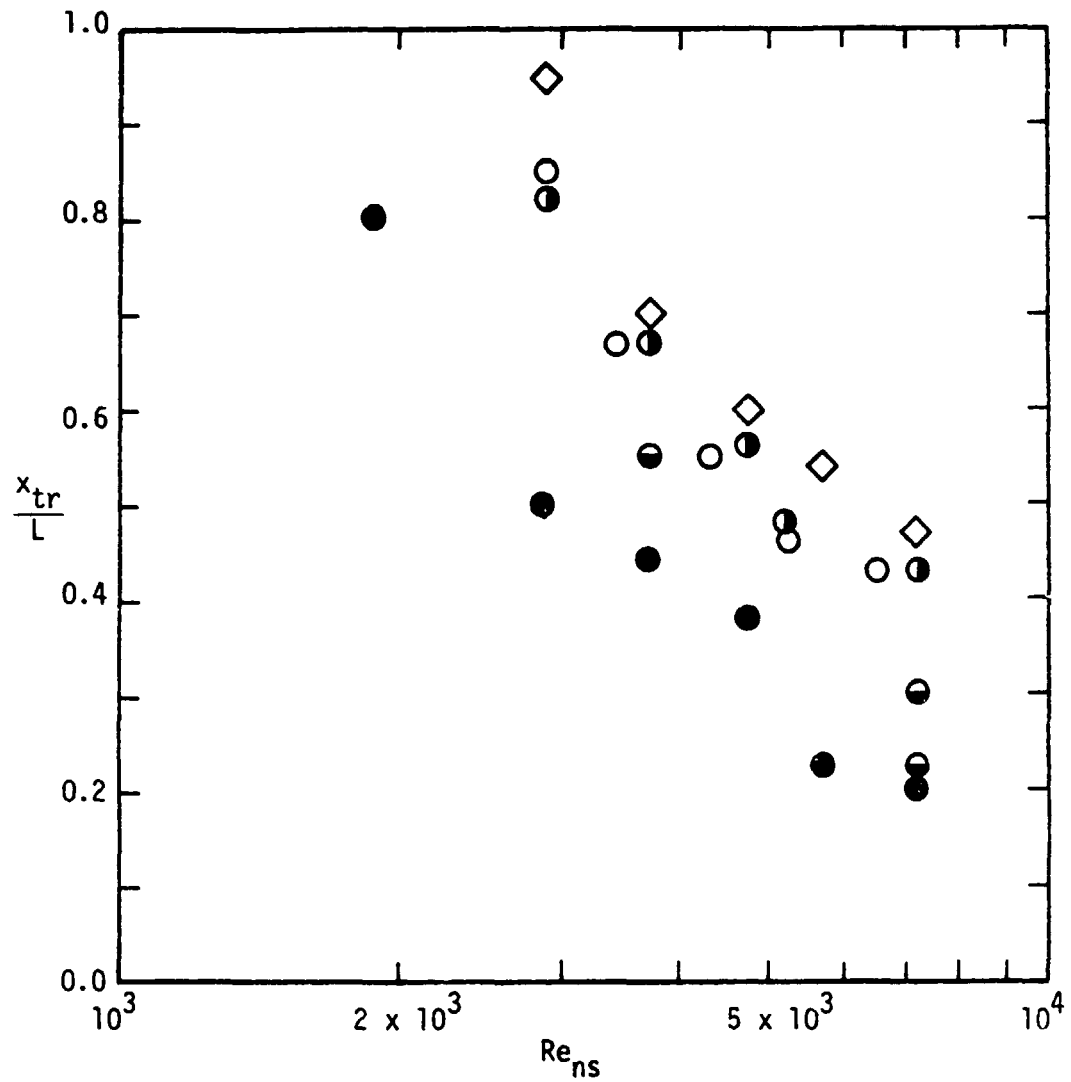

(b) $\alpha = 40°$

Figure 21. - Concluded.

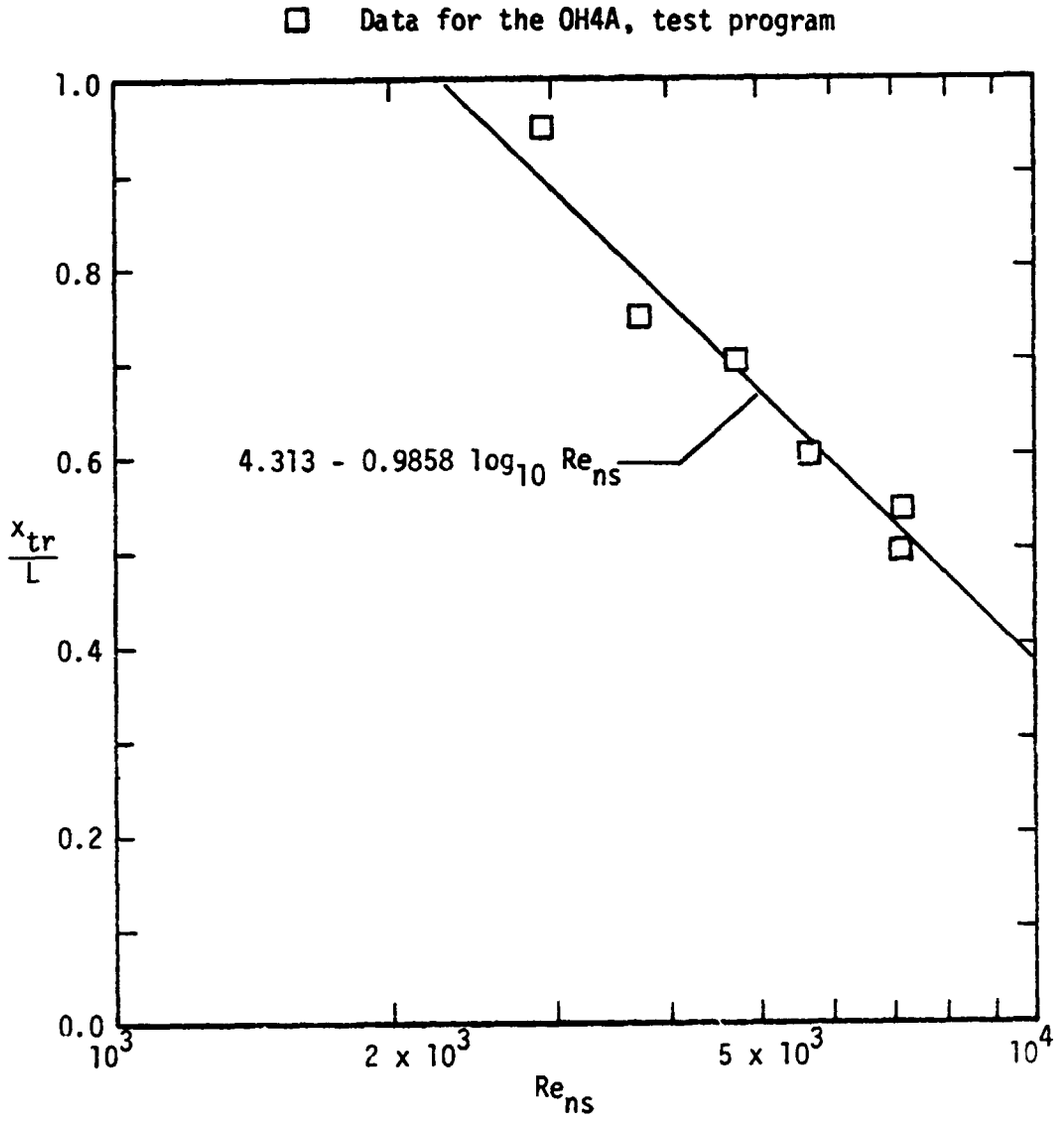

Figure 22. - Correlation of the smooth-body transition locations, $\alpha = 30°$, $T_w \approx 0.42\ T_t$.

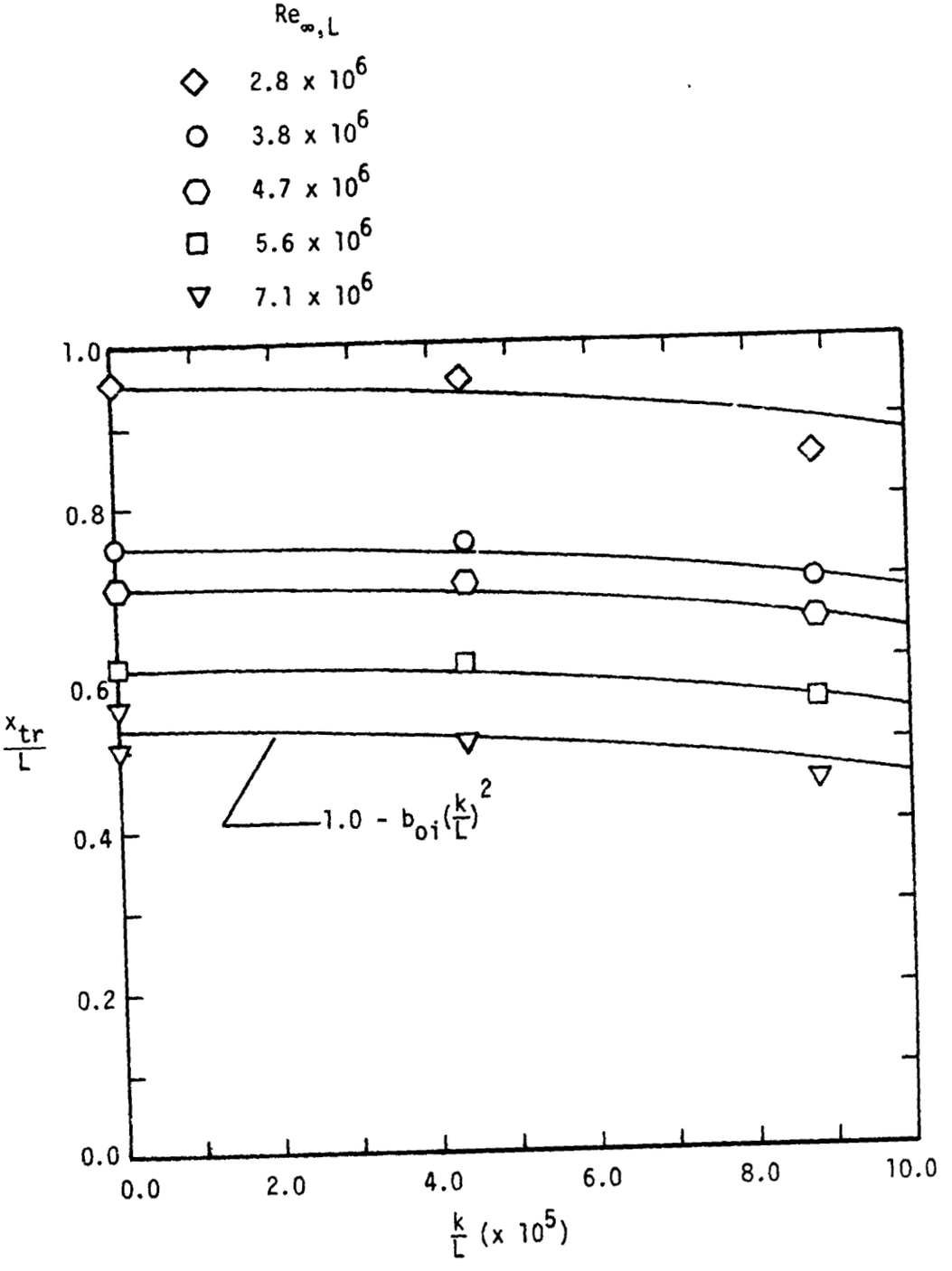

Figure 23. - The effect of misaligned-tile height on the t ansition location, $\alpha = 30°$, $T_w = 0.42\ T_t$.

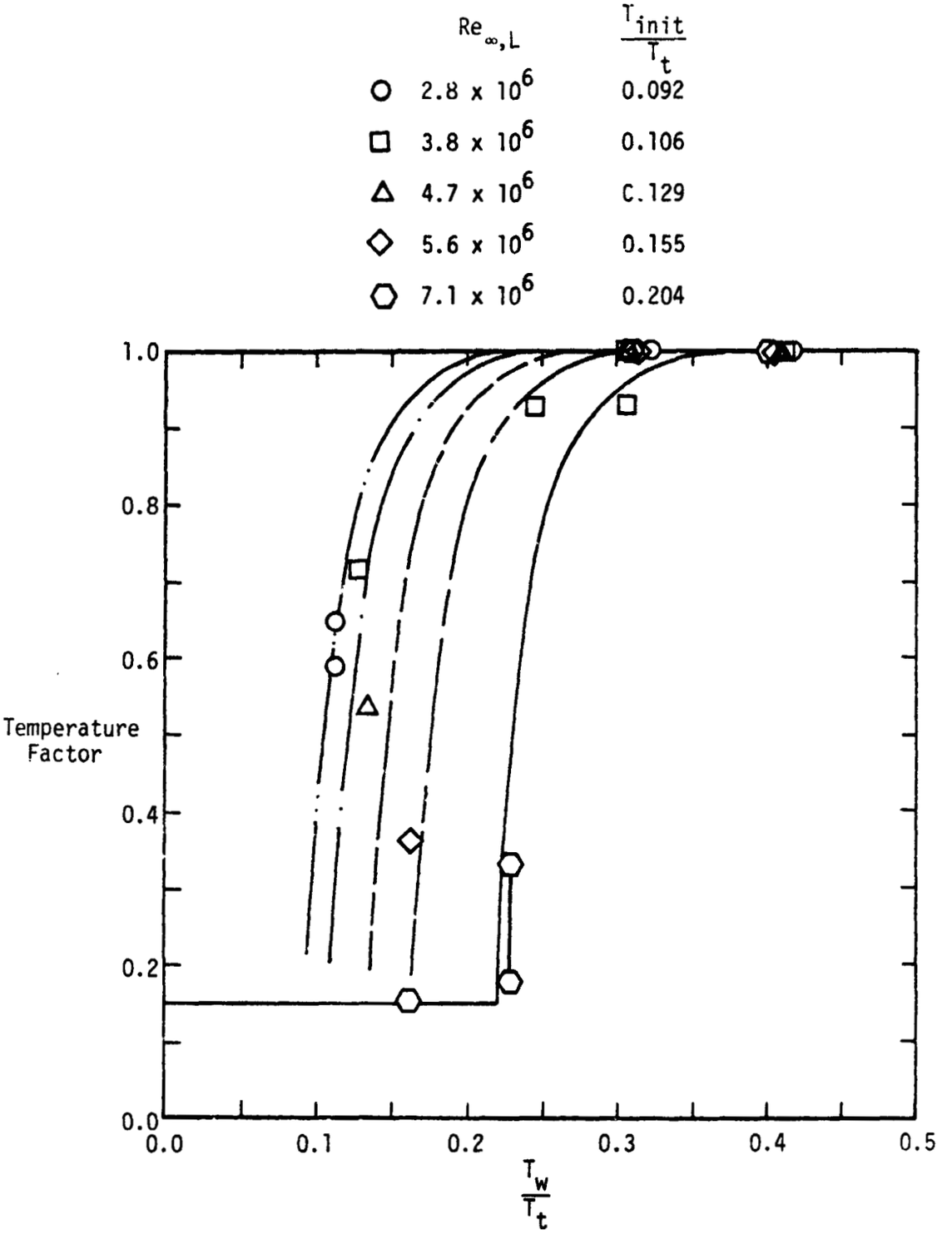

Figure 24. - The effect of the surface temperature on the transi-transition location, $\alpha = 30°$, for k_2 misaligned-tile height (i.e., $k = 8.86 \times 10^{-5}L$).

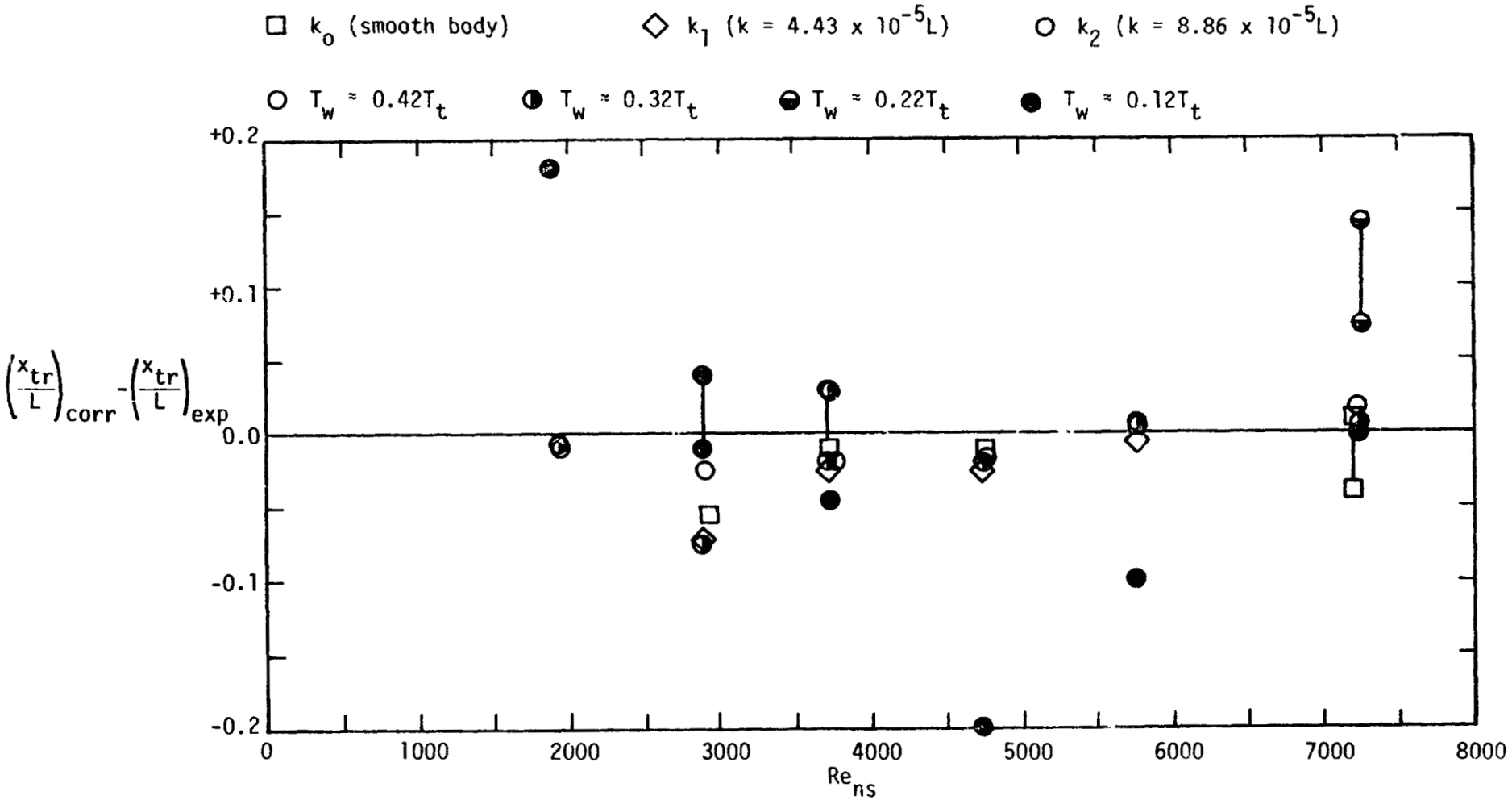

Figure 25. - A comparison of the transition locations calculated using the empirical correlation with the experimentally-determined locations for $\alpha = 30°$, Tunnel B data.

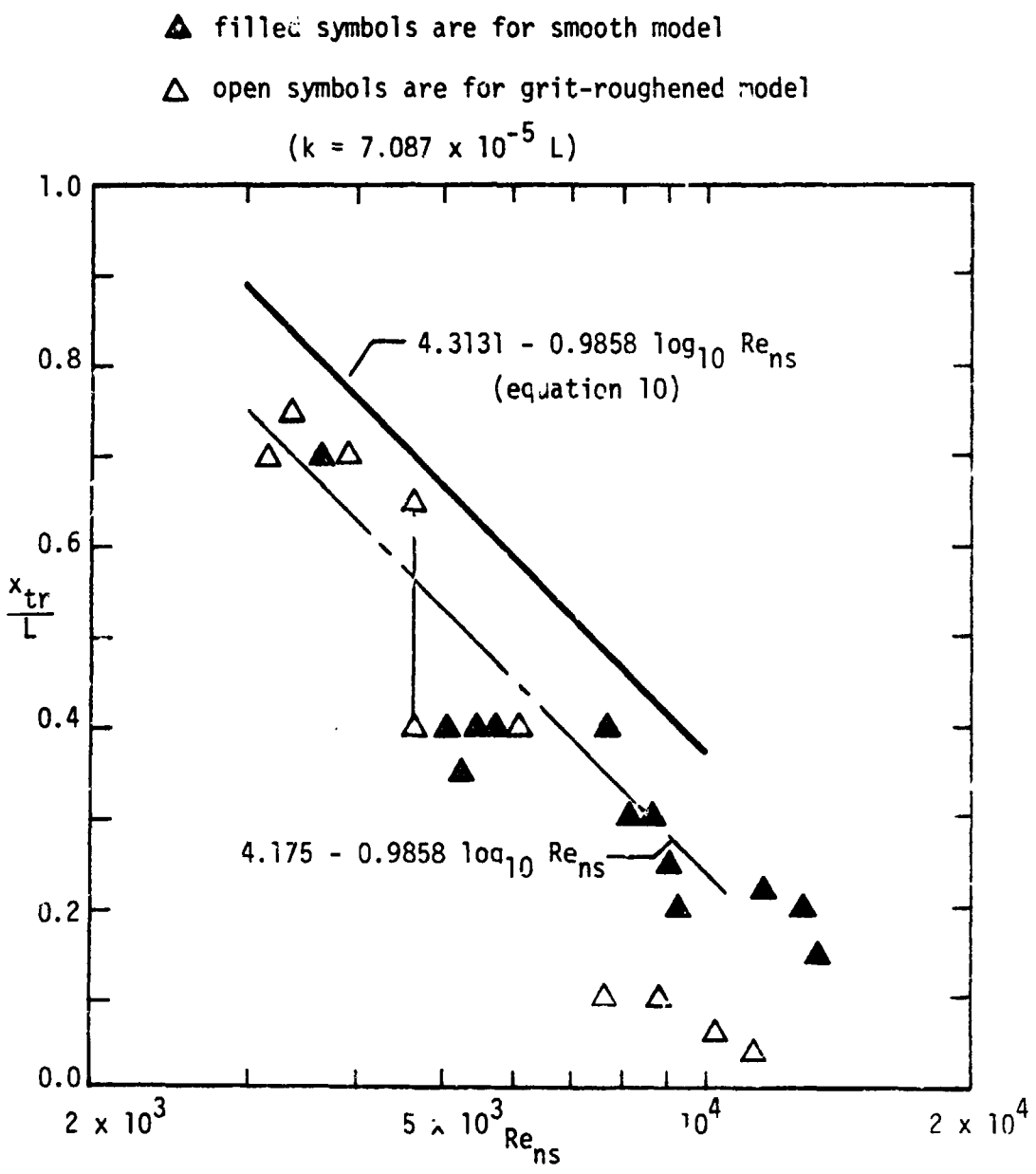

Figure 26. - Transition locations as a function of the Reynolds number behind a normal shock wave. data from Tunnel F, $\alpha = 30°$, $0.16\ T_t < T_w < 0.27\ T_t$ (data from refs. 27 and 28).

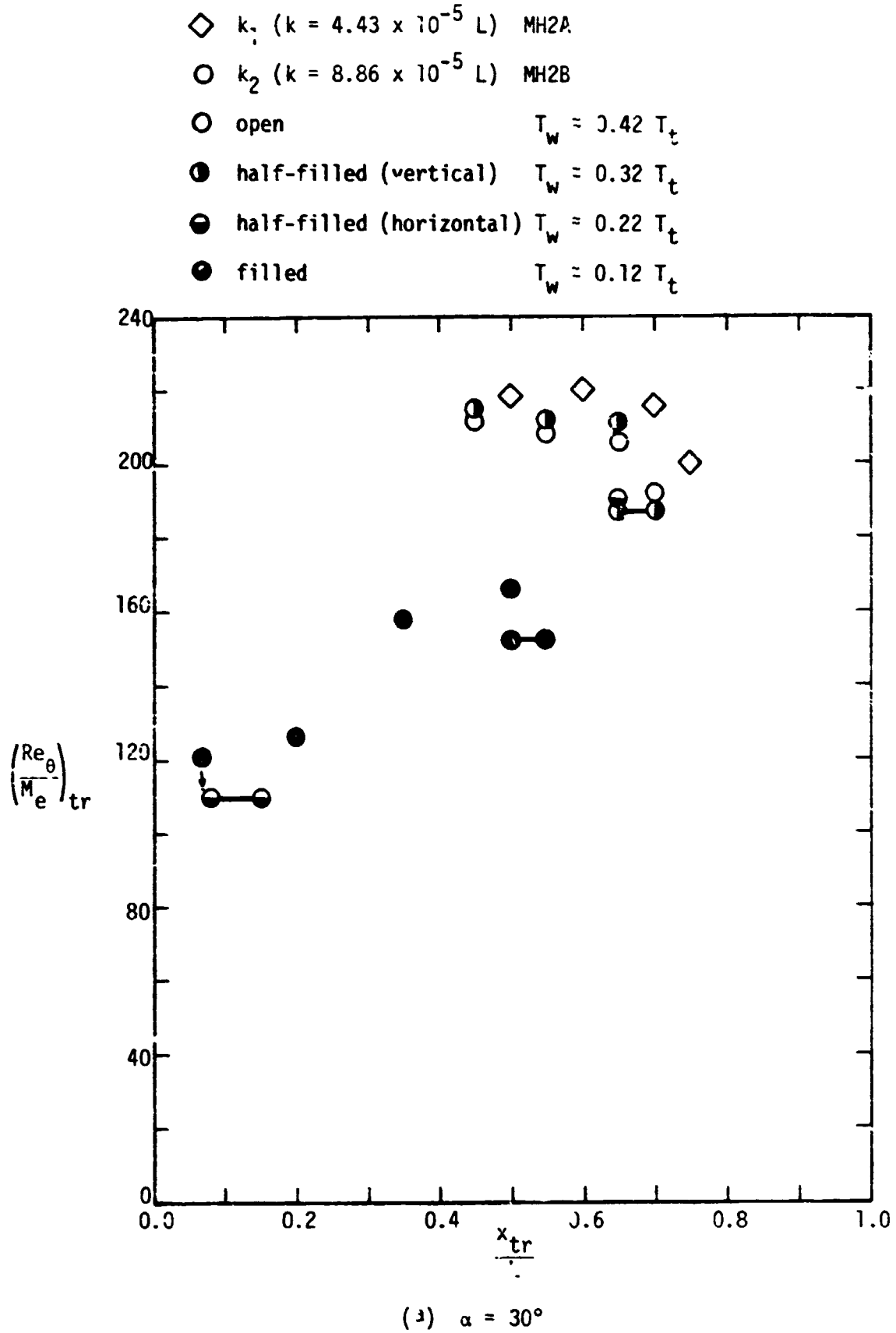

(a) $\alpha = 30°$

Figure 27. - The theoretical values of $(Re_\theta/M_e)_{tr}$ using the Var Ent flow model.

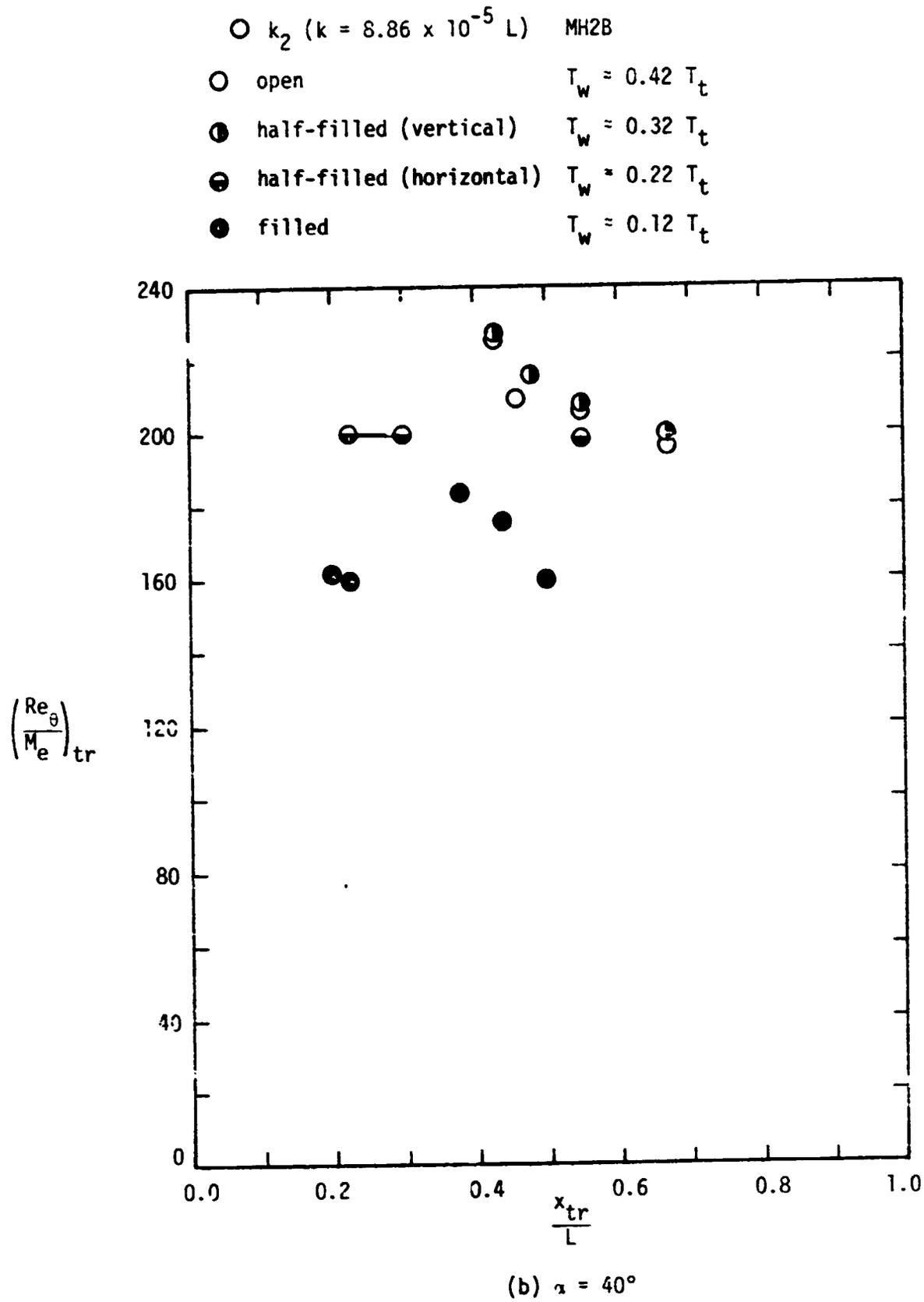

(b) $\alpha = 40°$

Figure 27. - Concluded.

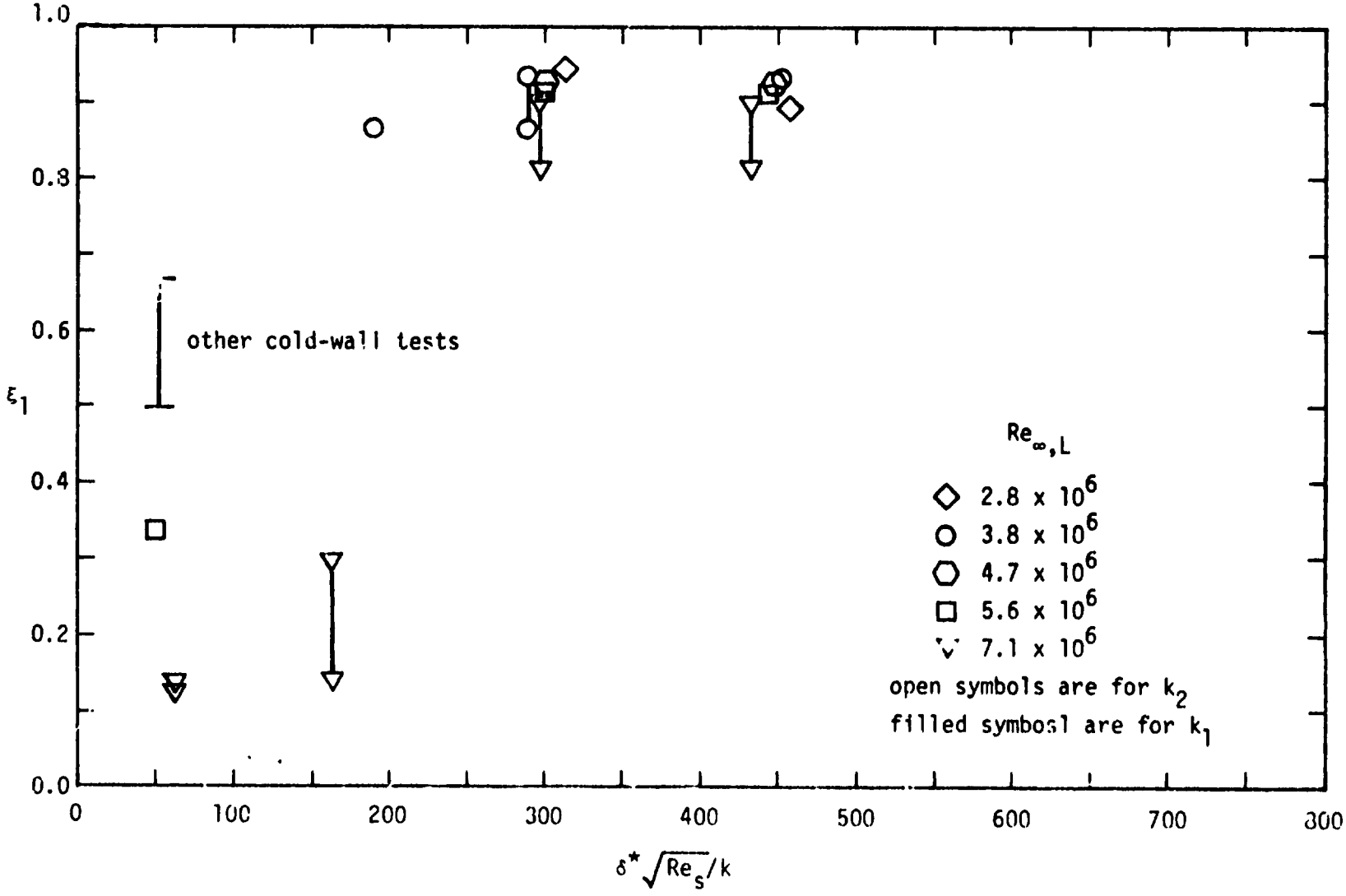

(a) x = 0.096L

Figure 28. - The relative transition location ξ_1 as a function of $\delta^* \sqrt{Re_s}/k$ for Mod Newt NSE Theory, $\alpha = 30°$.

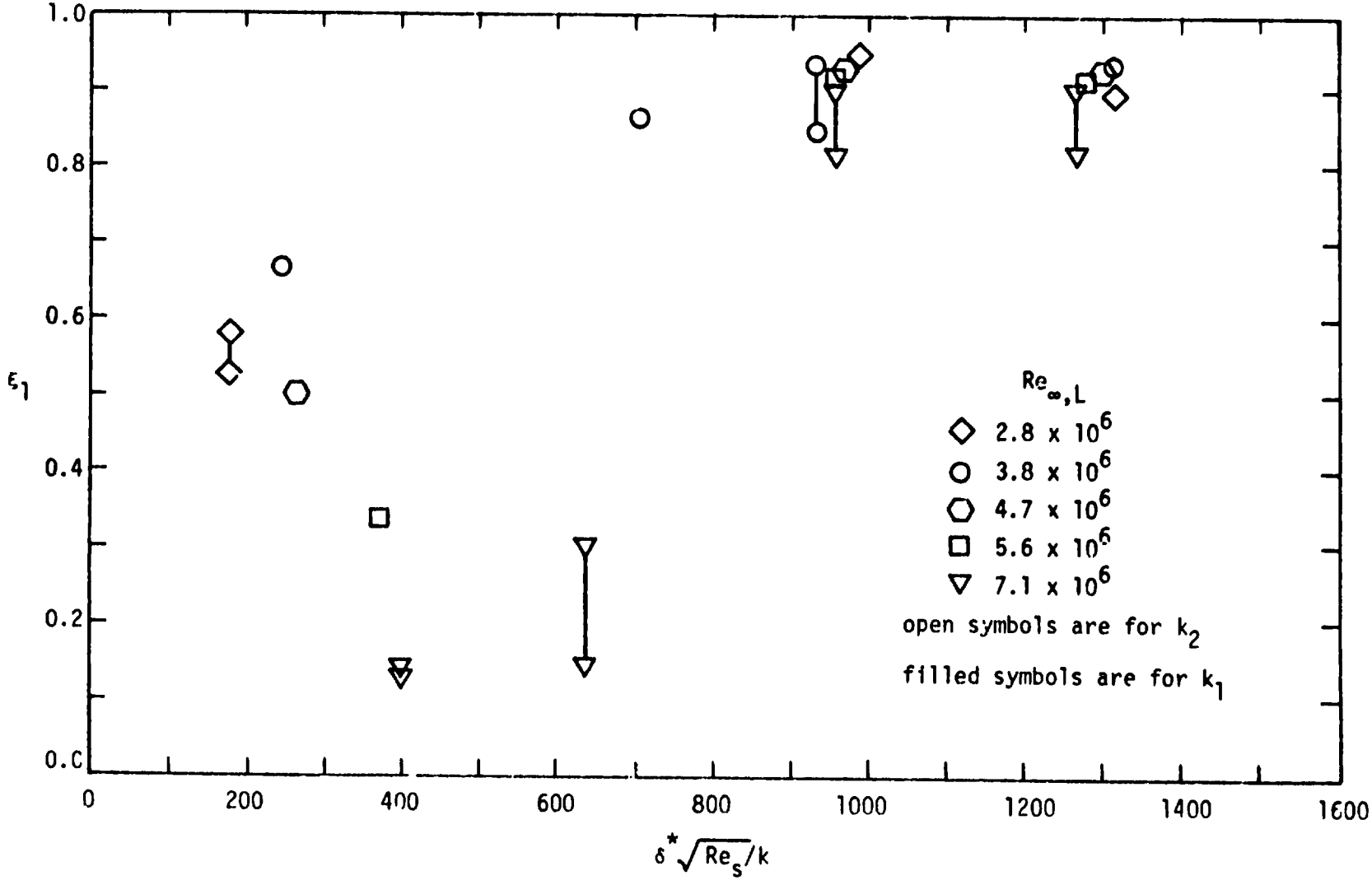

(b) x = 0.189L

Figure 28. - Concluded.

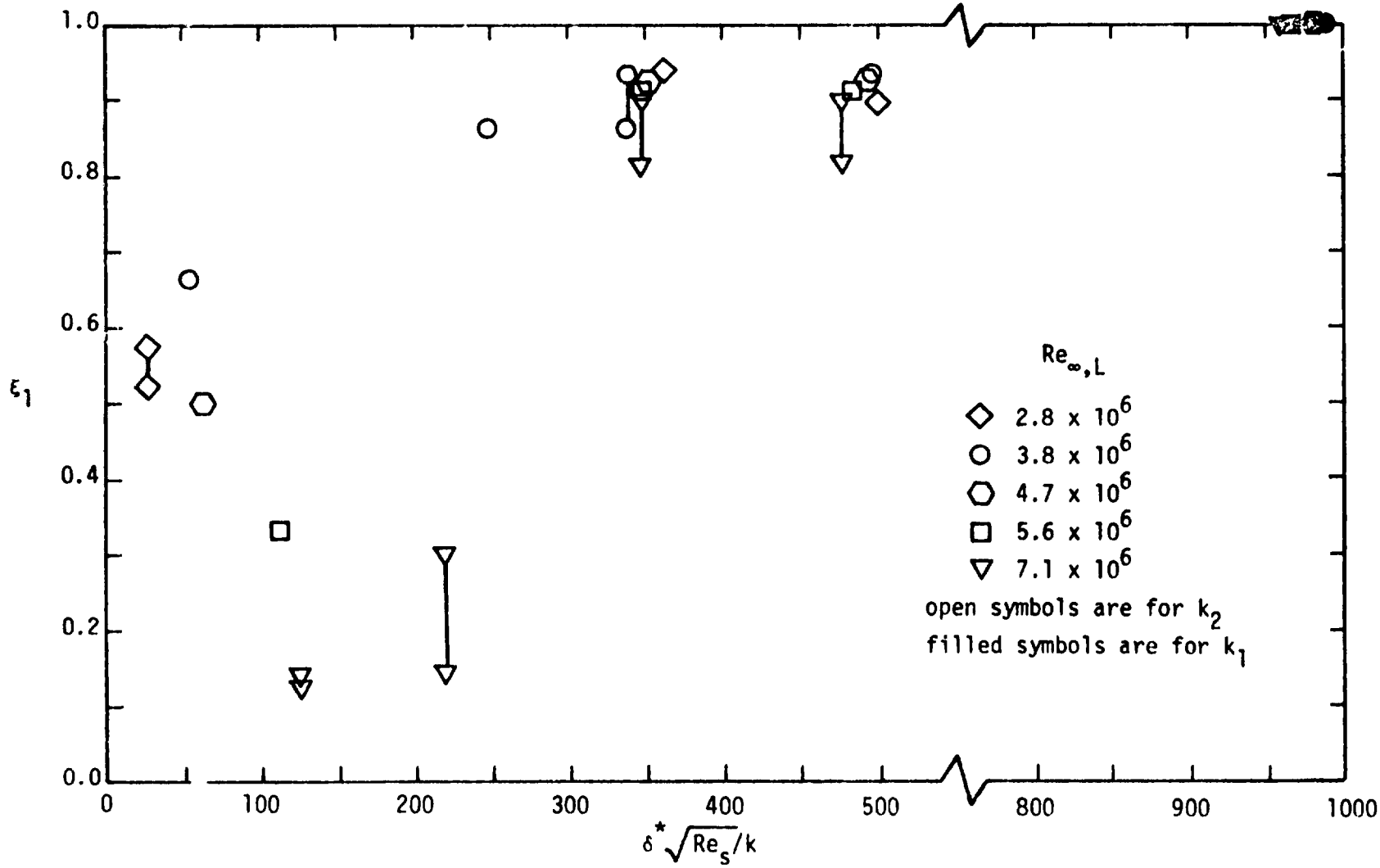

(a) $x = 0.097L$

Figure 29. - The relative transition location ξ_1 as a function of $\delta^* \sqrt{Re_s}/k$ for Var Ent Theory, $\alpha = 30°$.

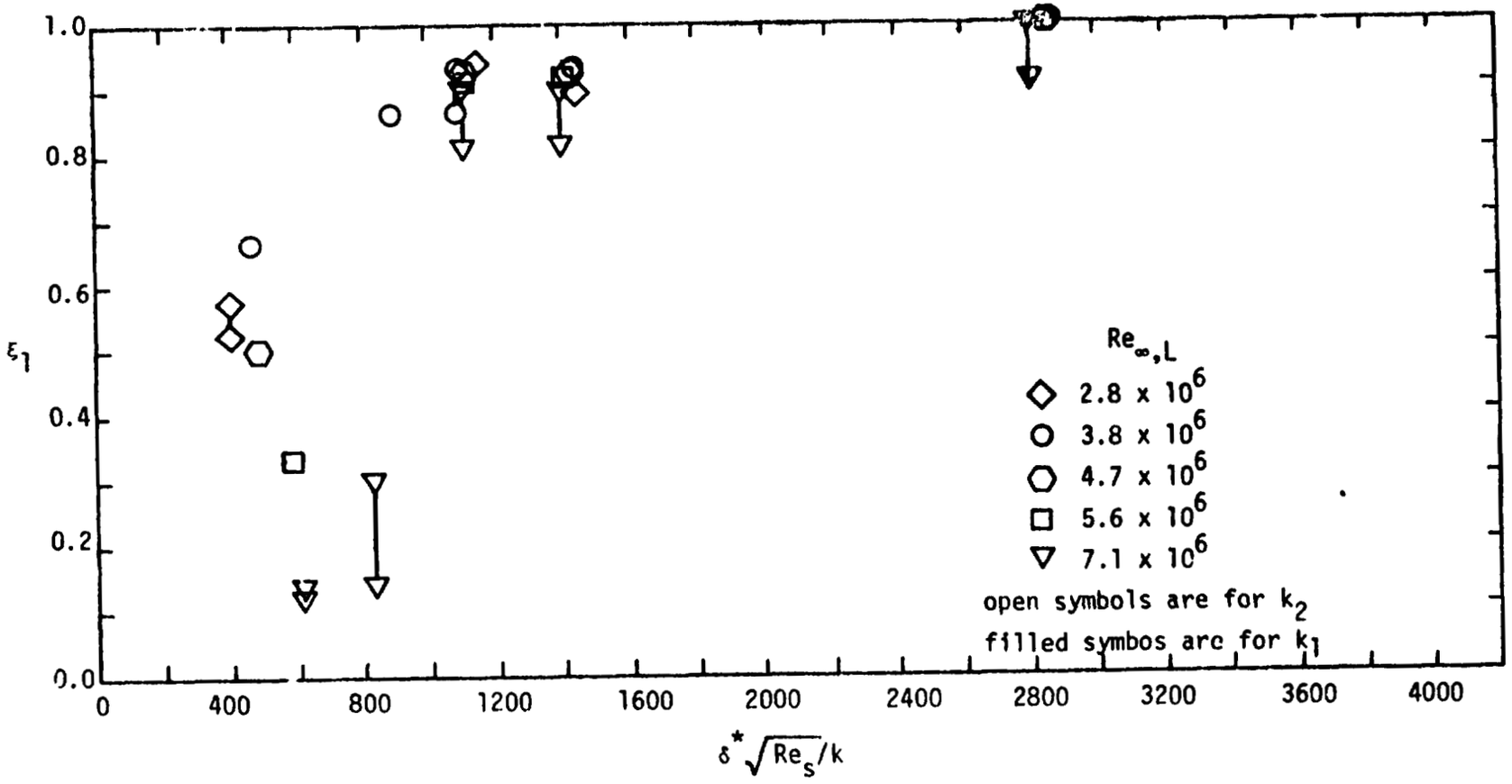

(b) x = 0.182L

Figure 29. - Concluded.

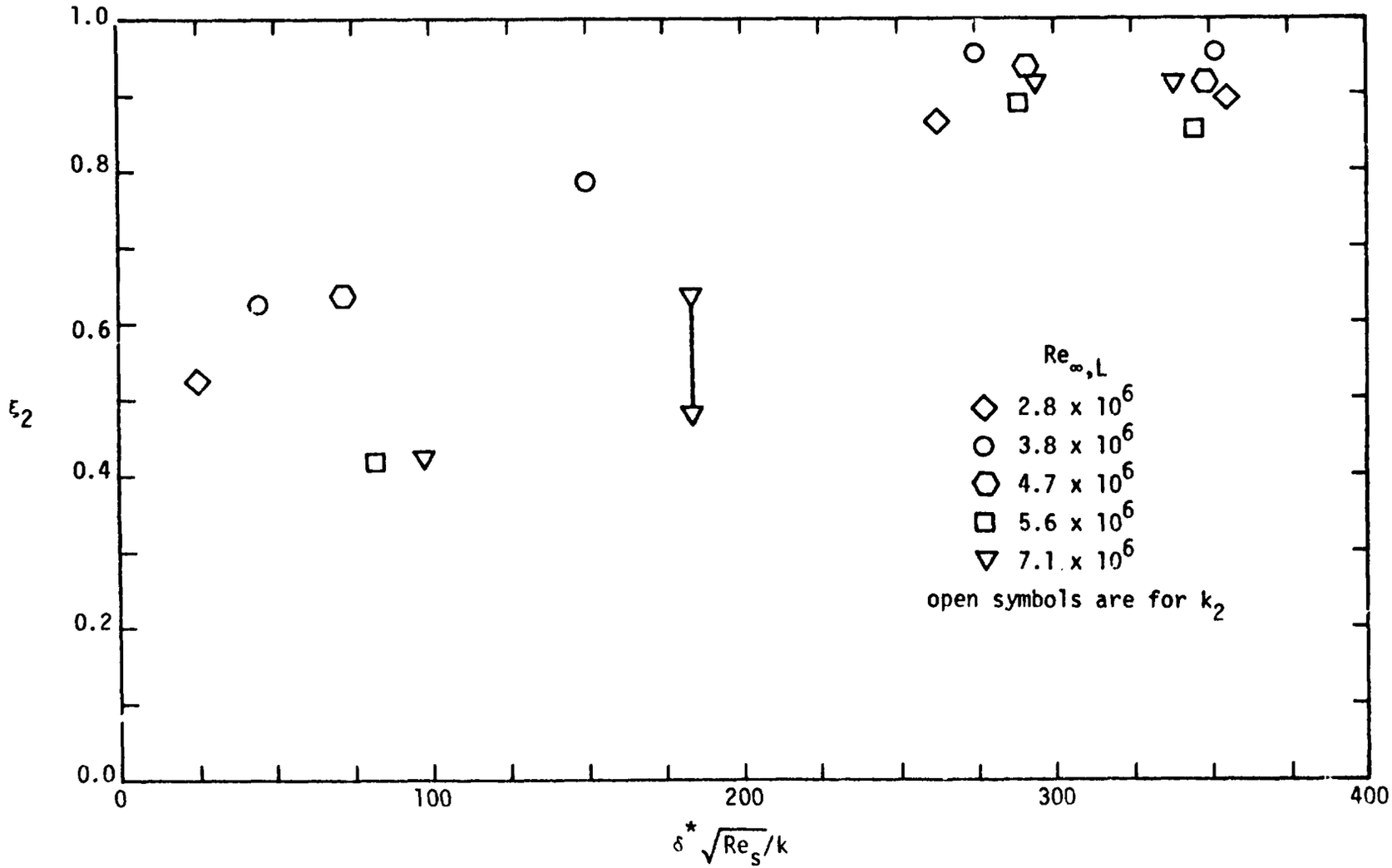

(a) x = 0.098L

Figure 30. - The relative transition location ξ_2 as a function of $\delta^* \sqrt{Re_s}/k$ for Var Ent Theory, α = 40°.

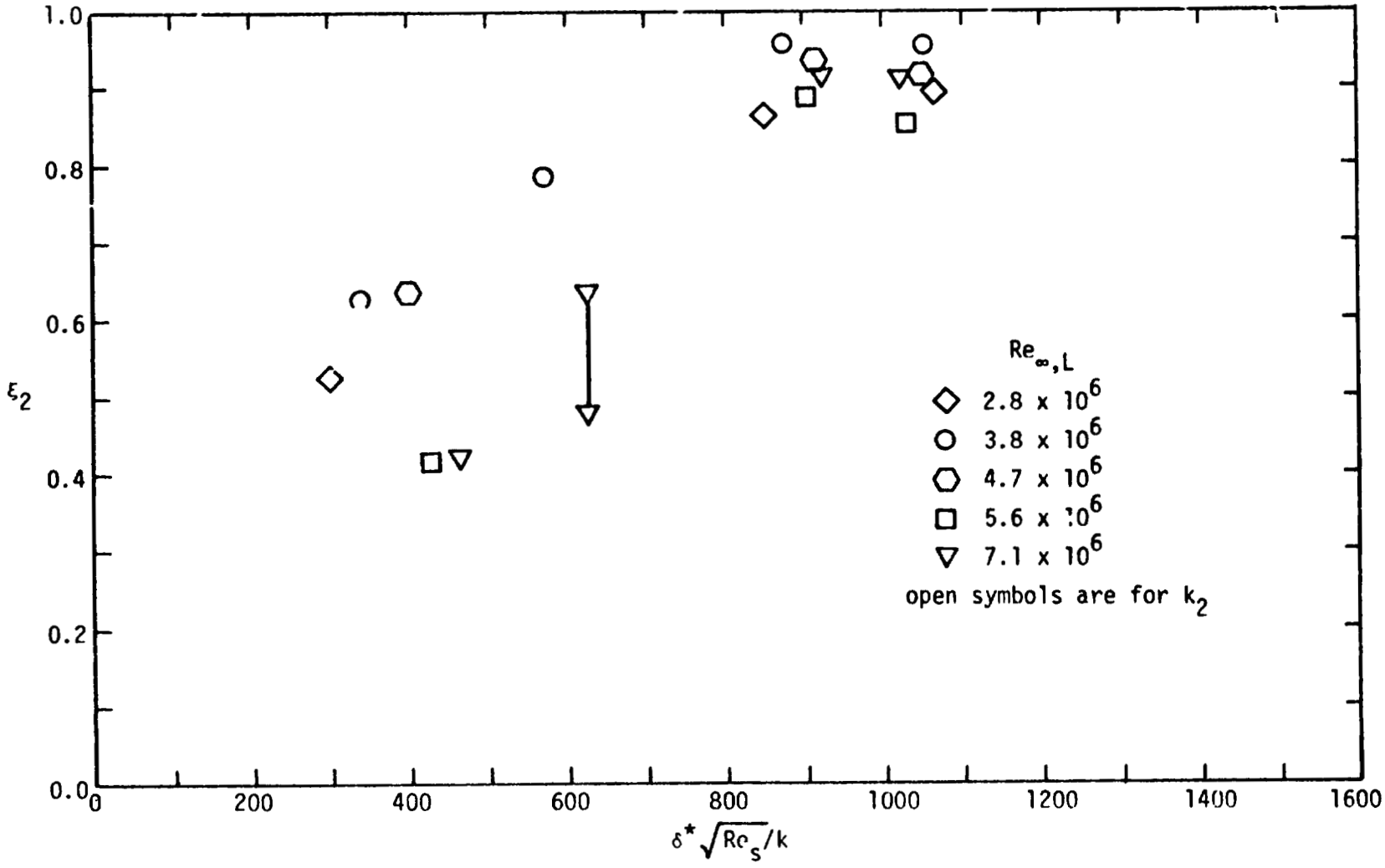

(b) x = 0.182L

Figure 30. - Concluded.

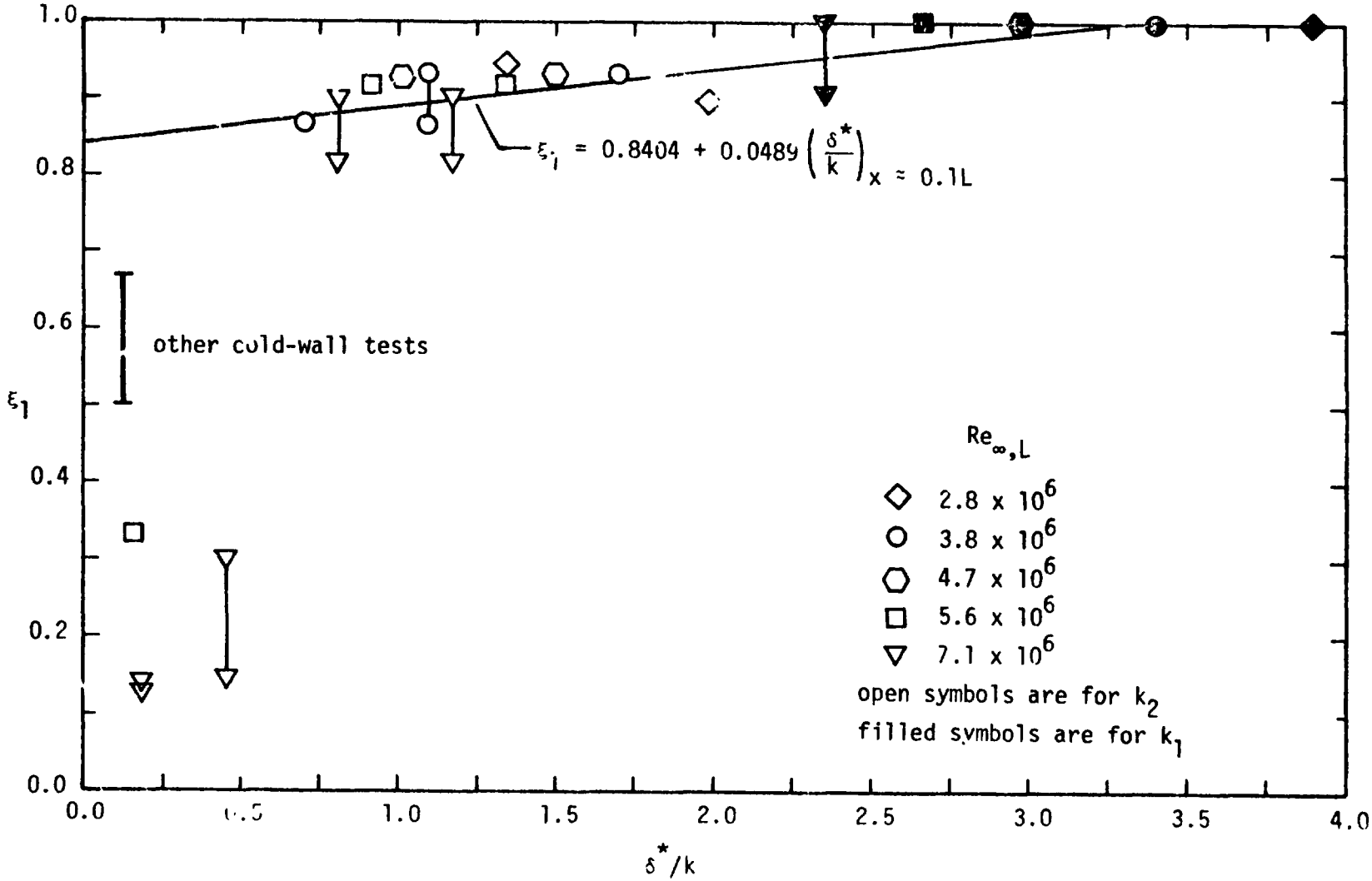

(a) x = 0.096L

Figure 31. - The relative transition location ξ_1 as a function of δ^*/k for Mod Newt NSE theory, $\alpha = 30°$.

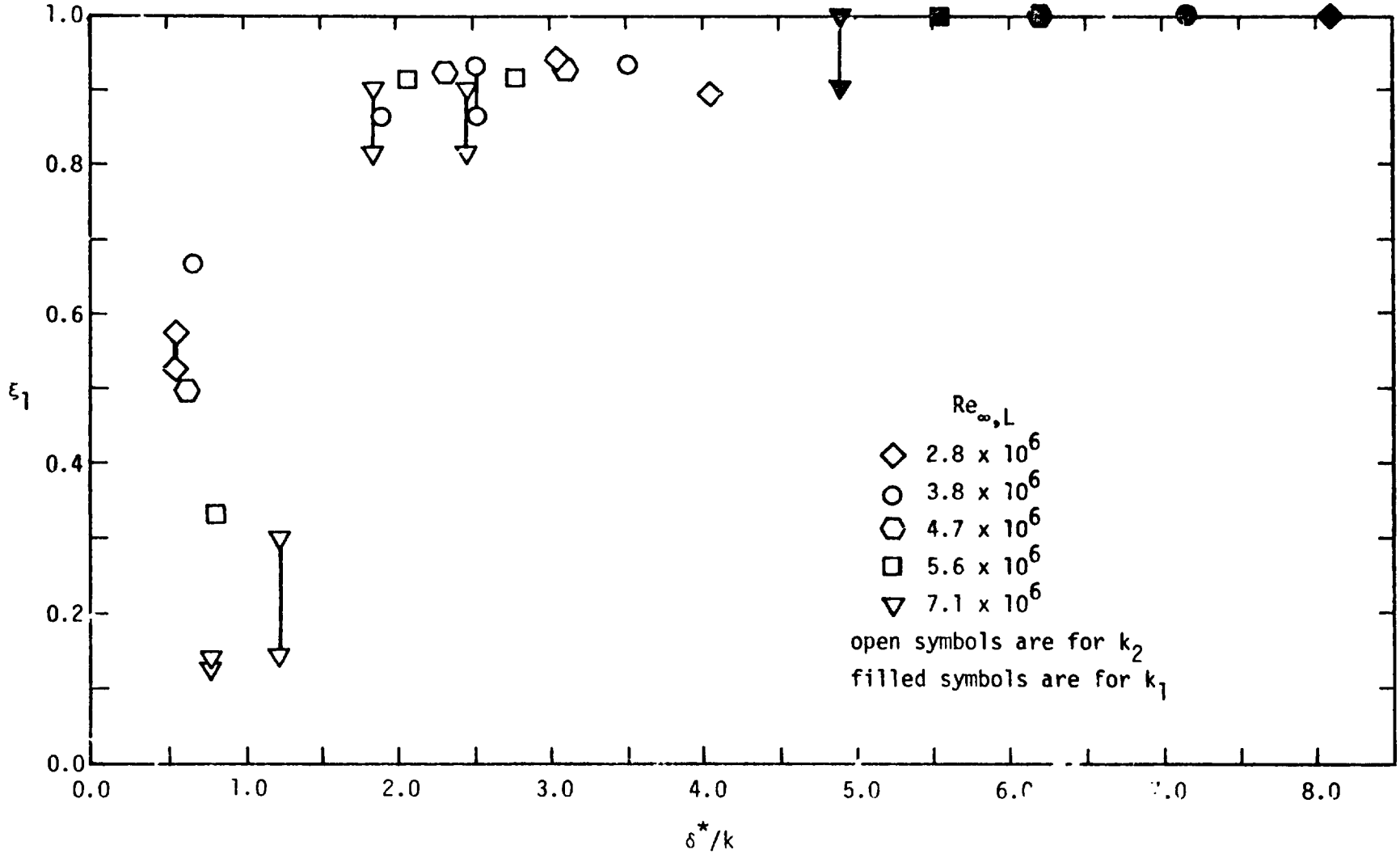

(b) x = 0.189L

Figure 31. - Concluded.

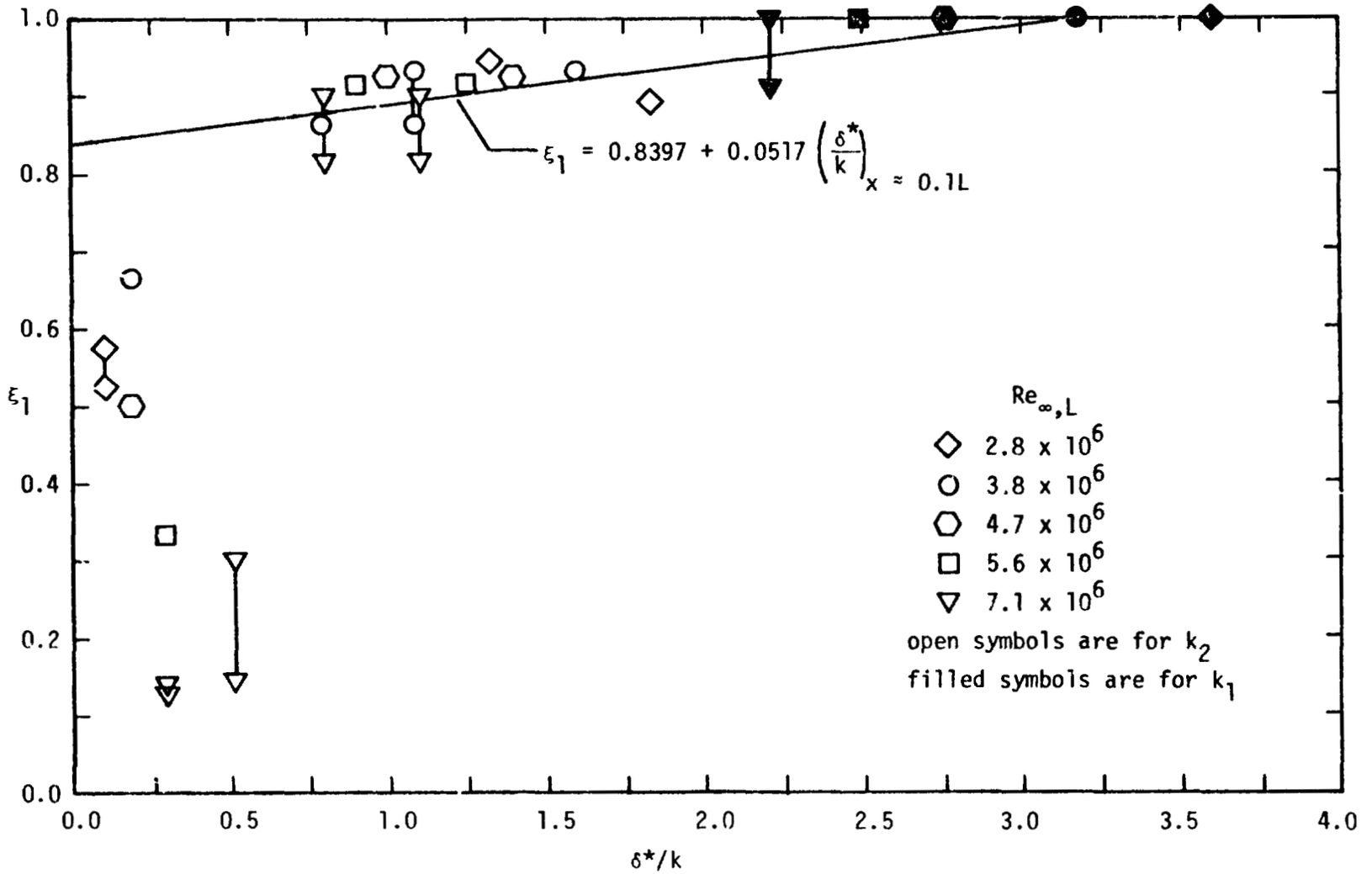

(a) x = 0.097L

Figure 32. - The relative transition location ξ_1 as a function of δ^*/k for Var Ent Theory, $\alpha = 30°$.

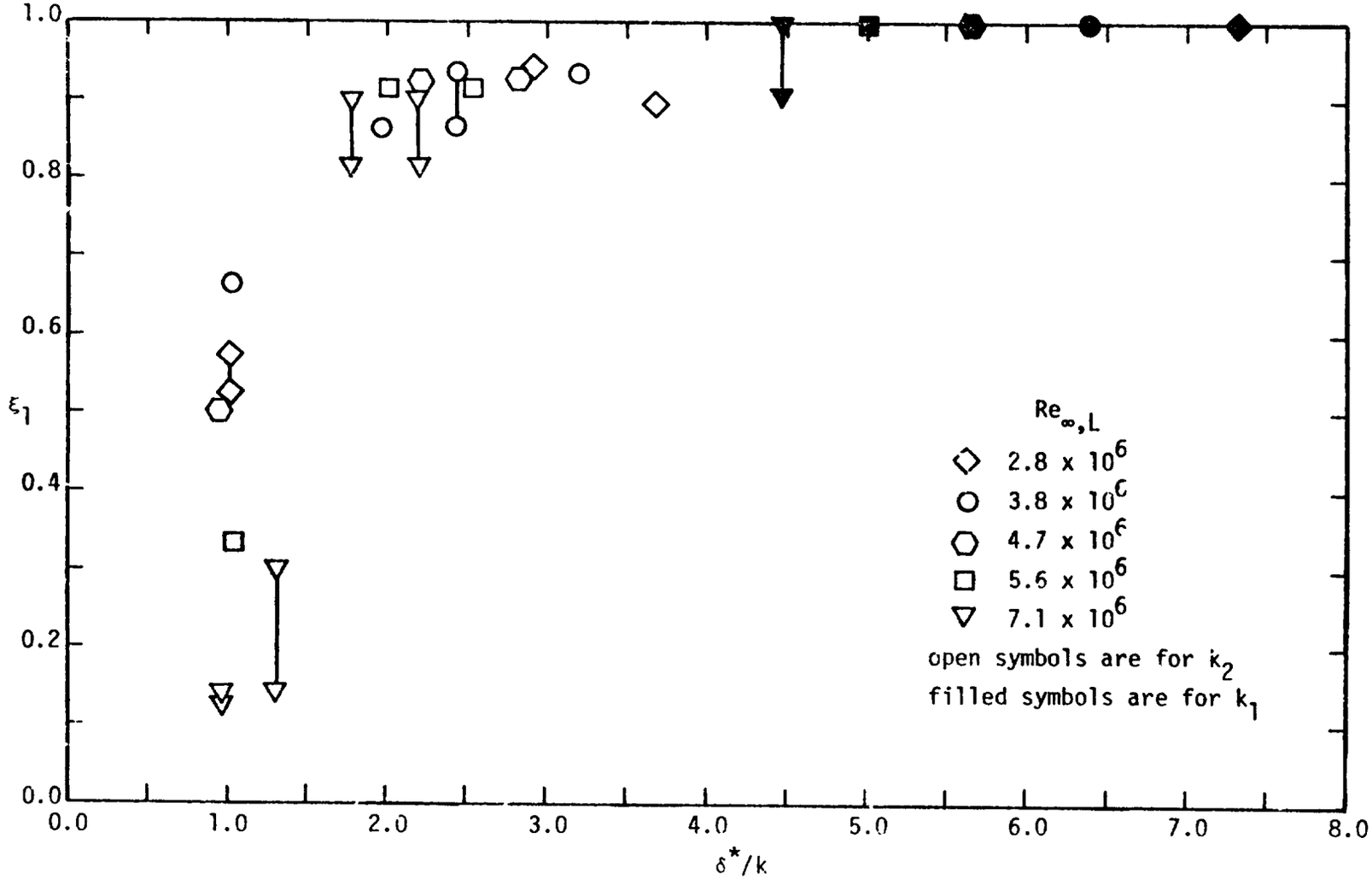

(b) x = 0.182L

Figure 32. - Concluded.

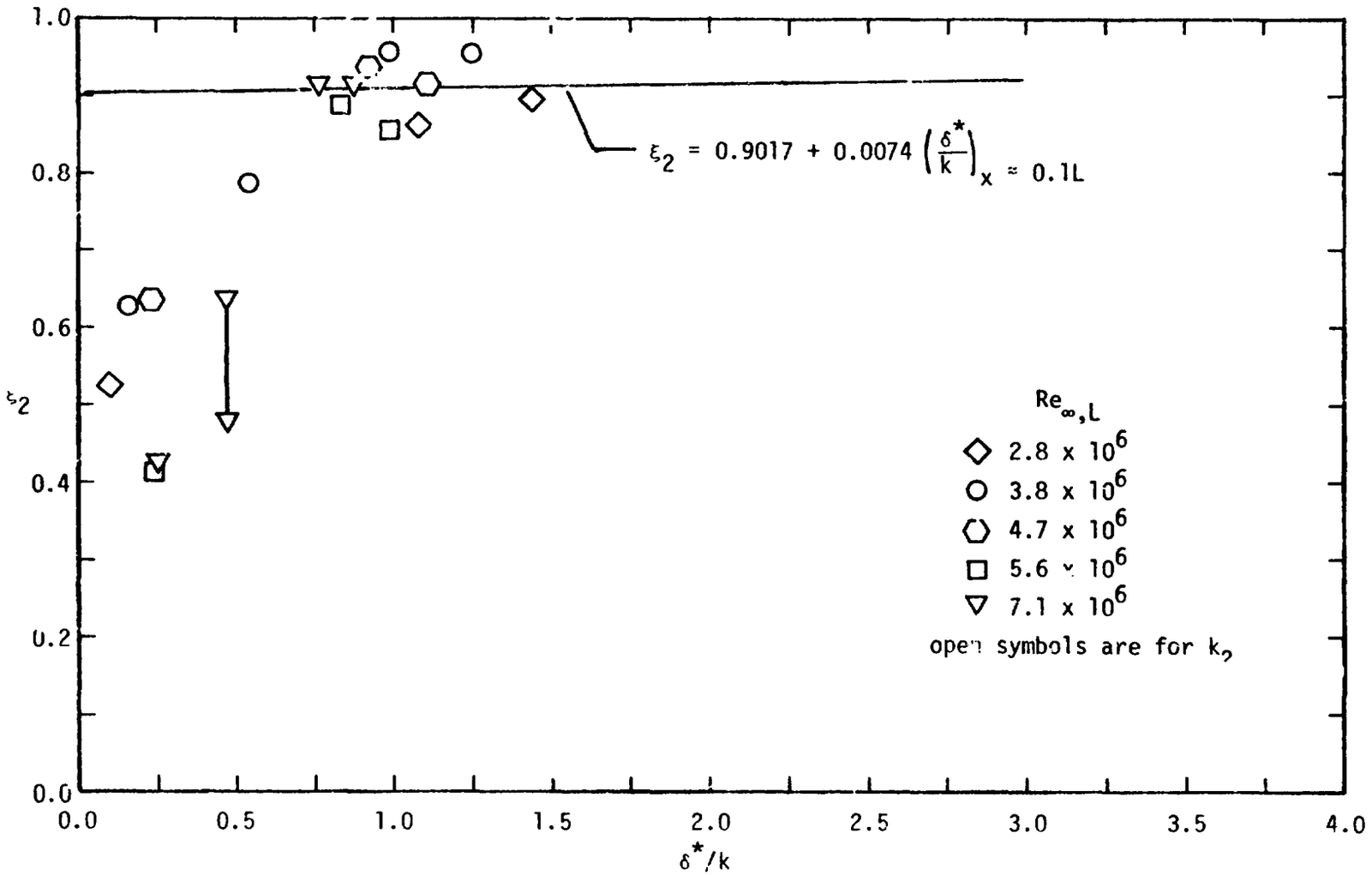

(a) $x = 0.098L$

Figure 33. - The relative transition location ξ_2 as a function of δ^*/k for Var Ent Theory, $\alpha = 40°$.

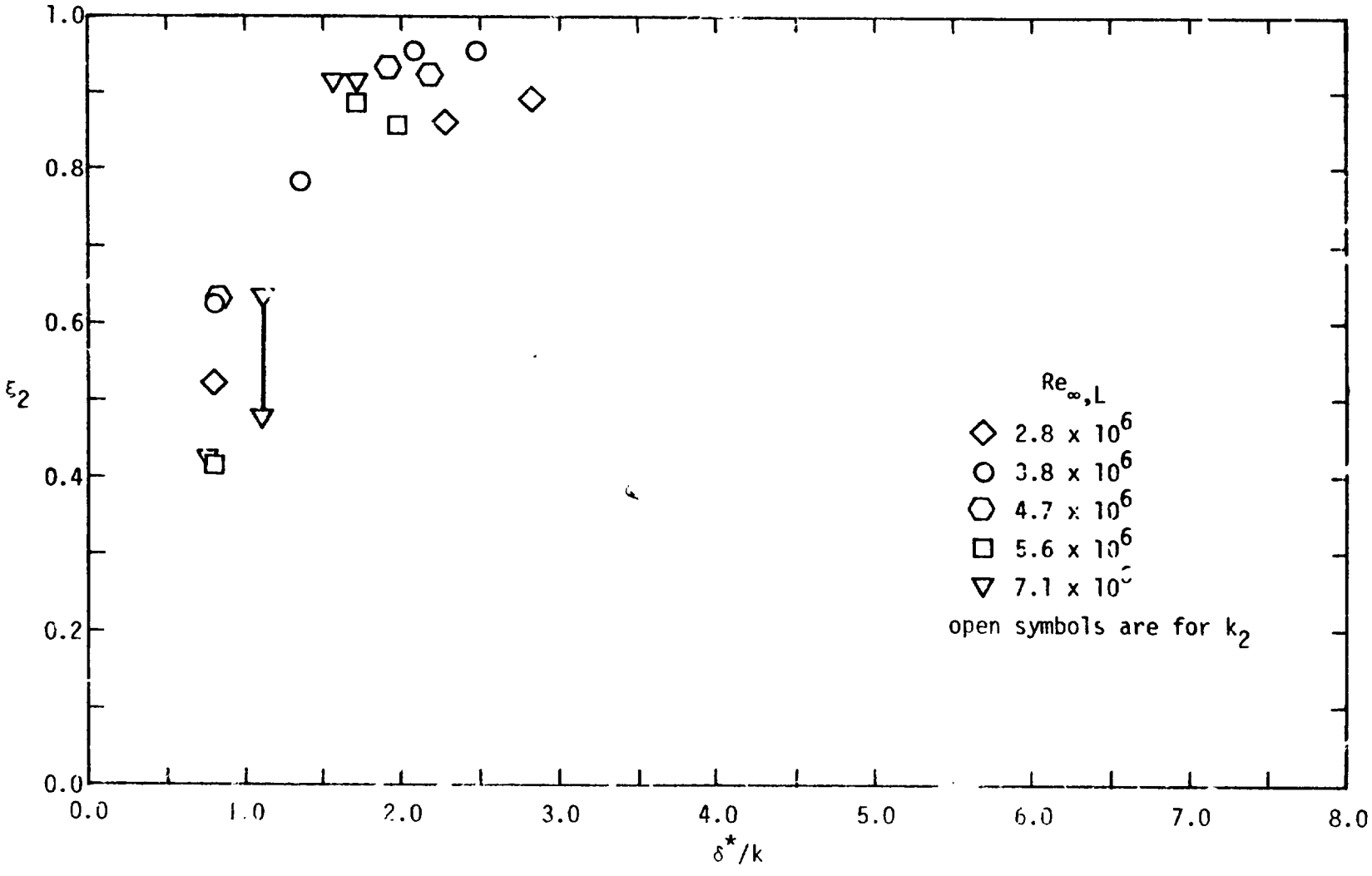

(b) x = 0.182L

Figure 33. - Concluded.

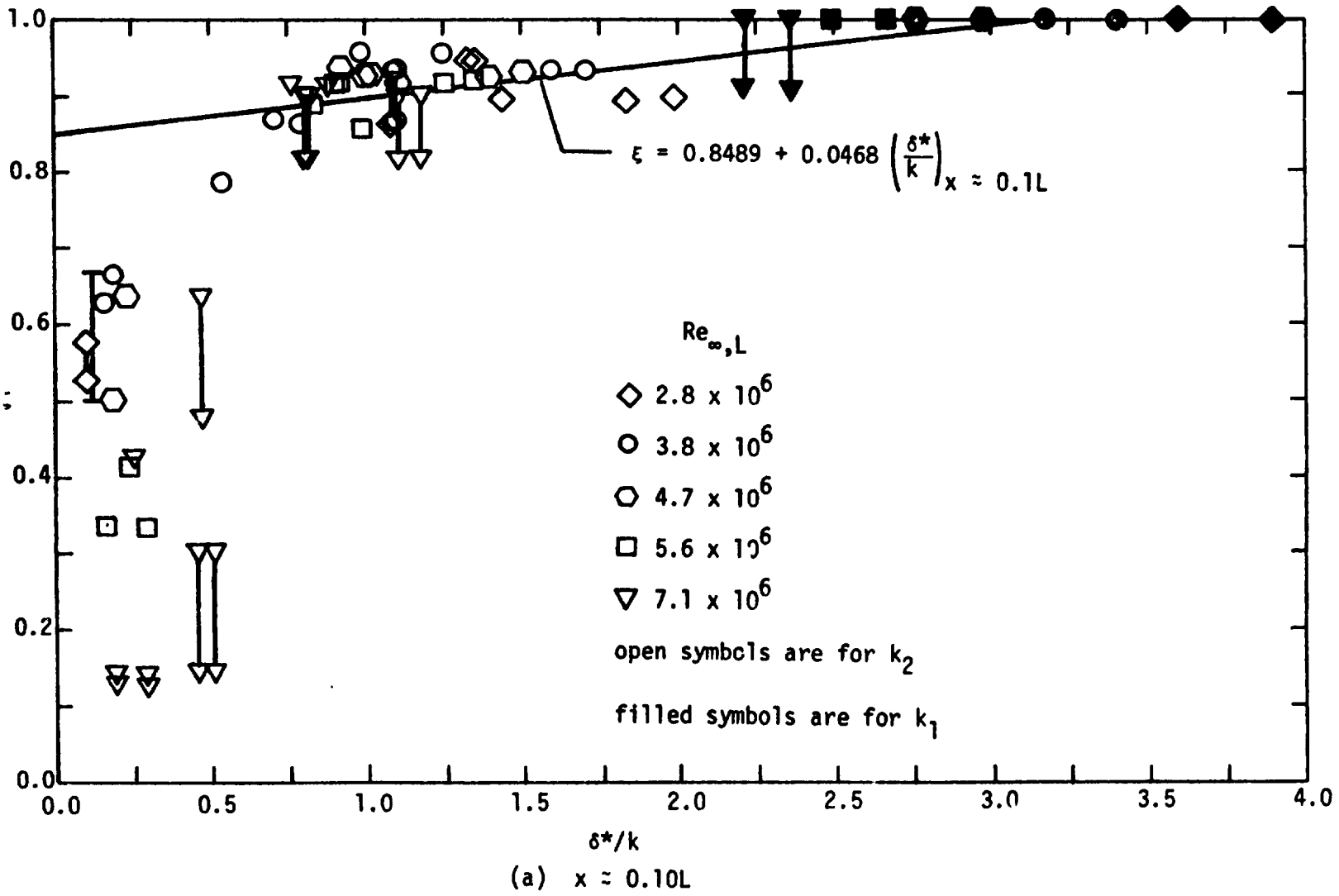

(a) $x \approx 0.10L$

Figure 34. - The relative transition location for both angles-of-attack (ξ) as a function of δ^*/k for both flow models.

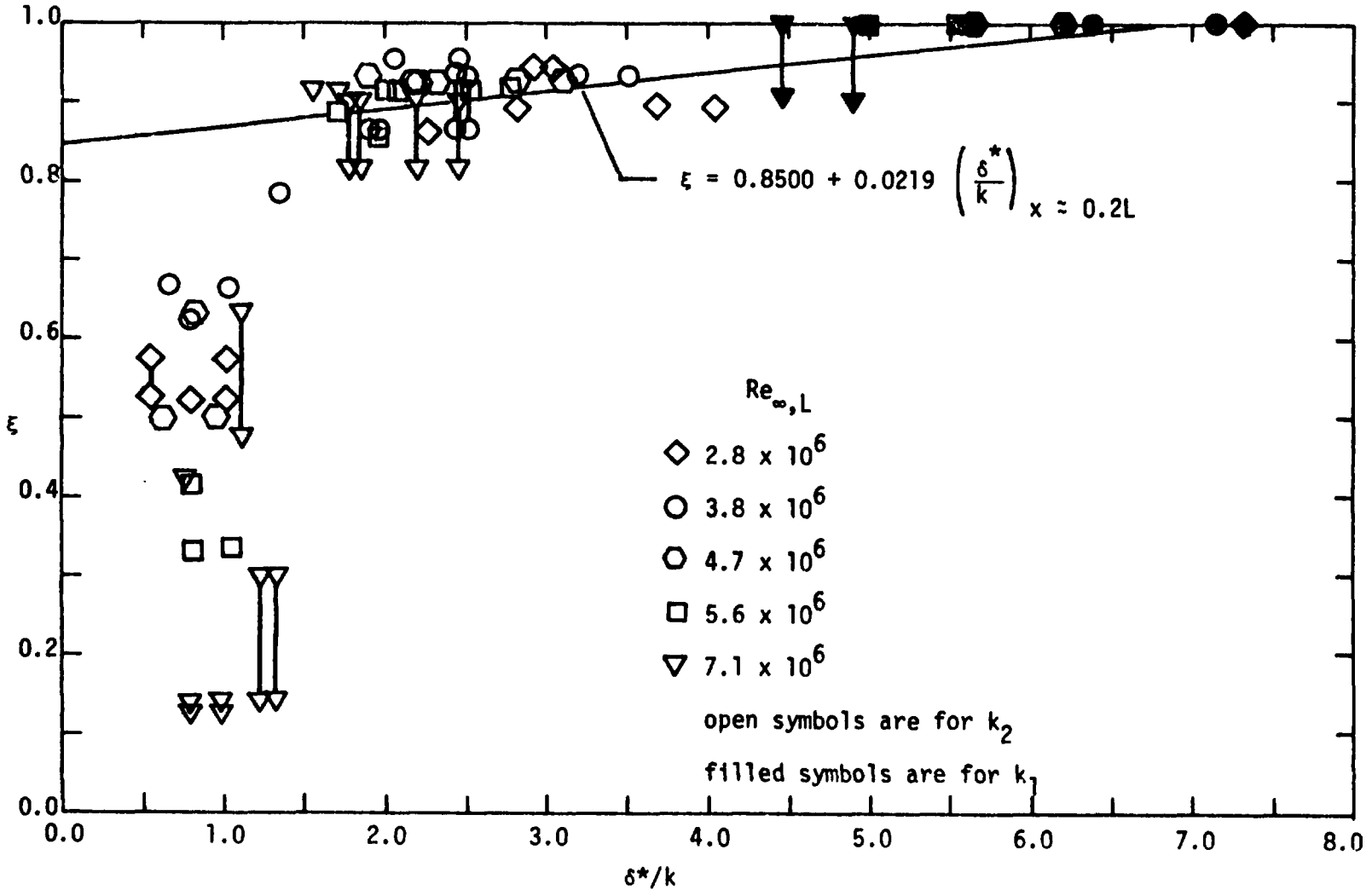

(b) $x \approx 0.20L$

Figure 34. - Concluded.

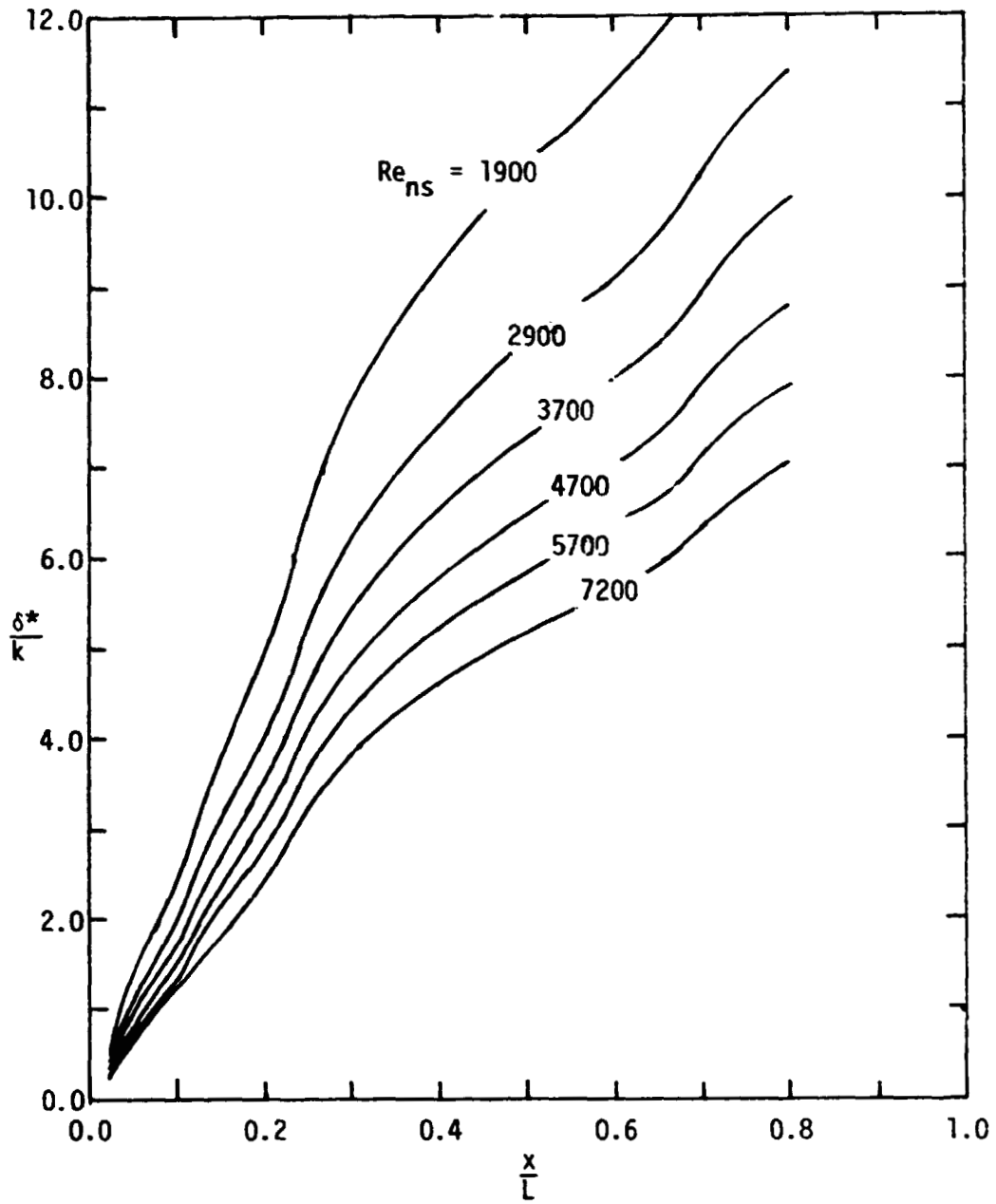

Figure 35. - The theoretical value of the displacement thickness of a nonsimilar, laminar boundary layer as a function of x/L for $T_w \simeq 0.42\ T_t$, $\alpha = 30°$, Var Ent flow model.